VAPOR BUBBLE GROWTH IN HETEROGENEOUS BOILING

By

WEN-CHIN CHEN

A DISSERTATION PRESENTED TO THE GRADUATE SCHOOL
OF THE UNIVERSITY OF FLORIDA IN PARTIAL FULFILLMENT
OF THE REQUIREMENTS FOR THE DEGREE OF
DOCTOR OF PHILOSOPHY

UNIVERSITY OF FLORIDA

1995

TO MY PARENTS, MY WIFE YI-YU, AND MY SON ERIC

ACKNOWLEDGMENTS

I would like to thank Dr. Klausner, chairman of the supervisory committee, for all the support and encouragement during this research. His enthusiasm and great scholarly attainments have contributed substantially to this work.

I also want to express my deepest gratitude to Dr. Mei, cochairman of the supervisory committee, for his patience, invaluable guidance, and editing comments during this study. Without his great scholarly achievements this dissertation would not have been possible.

I would like to express my appreciation to other committee members, Dr. Hsieh, Dr. Kurzweg, and Dr. Sherif.

I also want to thank Dr. Hongjun Li and fellow graduate students and friends for their valuable help.

Finally, my deepest gratitude goes to my parents and to my wife, Yi-Yu, especially for her love, patience, and understanding.

TABLE OF CONTENTS

ACKNOWLEDGMENTS iii

NOMENCLATURE vii

ABSTRACT x

CHAPTERS

1 INTRODUCTION 1

2 VAPOR BUBBLE GROWTH IN SATURATED POOL BOILING --PART I. FORMULATION 8

2.1 Background 8
2.2 Formulation 10
2.2.1 Assumption, Governing Equations, and Boundary and Initial Condition . . 10
2.2.2 Non-dimensionalization and Coordinate Transformation 19
2.3 Results and Discussions 27
2.3.1 Determination of the Empirical Constant C and C_1 27
2.3.2 Comparison of the Predicted and Measured Growth Rate 35
2.4 Summary 41

3 VAPOR BUBBLE GROWTH IN SATURATED POOL BOILING --PART II. GROWTH RATE AND THERMAL FIELDS . . 43

3.1 Background 43
3.2 Effect of Ja, Fo, κ and α on $\bar{R}(\tau)$ . . . 45
3.3 Thermal Field of the Liquid Microlayer . . 51
3.4 Thermal Field of the Solid Heater 57
3.4.1 Effect of Ja 62
3.4.2 Effect of Fo 66
3.4.3 Effect of κ 68
3.4.4 Effect of α 71
3.5 Summary 74

4 A SIMPLIFIED MODEL FOR PREDICTING VAPOR BUBBLE GROWTH RATE IN HETEROGENEOUS BOILING 77

4.1 Background 77
4.2 Analytical Formulation 79
4.2.1 Vapor Bubble and Liquid Microlayer 79
4.2.2 Lumped Analysis for the Solid Heater 82
4.2.3 Non-dimensionalization 83
4.3 Results and Discussion 85
4.3.1 Results for Fo>1; Determination of the Empirical Constant C_2 85
4.3.2 Results for Fo>1; Modified Fourier Number (Fo_m) 92
4.4 Summary 95

5 VAPOR BUBBLE GROWTH IN SUBCOOLED HETEROGENEOUS BOILING 96

5.1 Background 96
5.2 Theoretical Formulation 98
5.2.1 Vapor Bubble and Liquid Microlayer 98
5.2.2 Subcooled Bulk Liquid 100
5.2.3 Solid Heater 103
5.2.4 Non-dimensionalization and Grid Generation 104
5.3 The Asymptotic Analysis of $\theta_{b\ell}$ 109
5.4 Results and Discussion 114
5.4.1 Validation of the Model by the Comparison of Growth Rate 115
5.4.2 Behavior of the Heat Transfer Rate to the Bubble during Growth . . . 119
5.4.3 Thermal Field in the Solid Heater during the Growth 119
5.4.4 Thermal Field of the Bulk Liquid . 122
5.4.5 Asymptotic Behavior of $\theta_{b\ell}$ during Rapid Growth 125
5.4.6 Velocity Field of the Bulk Liquid 127
5.5 Summary 129

6 CONCLUSIONS AND RECOMMENDATION FOR FUTURE RESEARCH 131

6.1 Achievements 131
6.2 Suggestions for Future Work 133

REFERENCES 135

BIOGRAPHICAL SKETCH 140

NOMENCLATURE

A_m	area of microlayer wedge
A_b	surface area of vapor bubble dome
C	bubble shape parameter
C_1	microlayer wedge angle parameter
C_2	to described the region of the heating solid influenced by the microlayer evaporation
$C_{p\ell}$	liquid specific heat
C_{ps}	solid specific heat
f(C)	bubble volume factor
Fo	Fourier number
Fo_m	modified Fourier number
h	vertical distance form the center of bubble to the wall
$\dot{h}$	bubble vertical velocity
h_{fg}	liquid latent heat of vaporization
H	solid heater thickness
k_ℓ & k_s	liquid and solid thermal conductivity
Ja	Jacob number
L(r)	the liquid microlayer thickness
Pr_ℓ	liquid Prandtl number
$\dot{q}_{evap}$	the rate of heat removal from the heating surface due to microlayer evaporation
q''	heat supply from the bottom of the heater
q'''	the internal heat generation per unit volume

r	radial coordinate
$\bar{r}_s$	dimensionless coordinate in the solid heater
$\bar{r}_{b\ell}$	dimensionless coordinate in the bulk liquid
R'	radial direction in the spherical moving coordinate
$R(t)$	bubble radius
$R_b(t)$	radius of the liquid microlayer underneath the bubble
$R_c(t_c)$	bubble radius for a constant wall superheat
$\bar{R}(t)$	dimensionless bubble growth rate
t	time
t_d	one-g boiling vapor bubble departure time estimate
t_c	vapor bubble growth and collapse time scale
$T_{b\ell}$	bulk liquid temperature
T_ℓ & T_s	liquid and solid temperature
T_{sat}	saturated temperature
T_{sub0}	initial bulk liquid temperature
T_w	average temperature of boiling surface
u_r	bulk liquid velocity in the r direction
u_z	bulk liquid velocity in the z direction
V_b	the bubble volume
z	coordinate in the direction normal to the heating surface
$\bar{z}_s$	dimensionless coordinate in the solid heater
$\bar{z}_{b\ell}$	dimensionless coordinate in the bulk liquid
$\bar{z}_h$	grid parameter (=h/R)

Greek symbols

α	liquid-to-solid thermal diffusivity ratio ($=\alpha_\ell/\alpha_s$)

α_ℓ & α_s liquid and solid thermal diffusivity

δ extrapolated superheat-layer thickness

ΔT_{sat} wall superheat

ΔT_{sat0} initial superheat at incipience ($=T_w-T_{sat0}$)

ϕ microlayer wedge angle

Φ velocity potential

κ liquid-to-solid thermal conductivity ratio ($=k_\ell/k_s$)

σ surface tension

ψ spherical angle measured from the axis of symmetry

ν_ℓ liquid kinematic viscosity

θ dimensionless wall superheat ($=\Delta T_{sat}(t)/\Delta T_{sat0}$)

θ_s dimensionless temperature of wall superheat

$\theta_{b\ell}$ dimensionless temperature of bulk liquid

ρ_ℓ & ρ_v liquid and vapor density

τ dimensionless time ($=t/t_d$ or t/t_c)

ξ & η computational coordinates in the bulk liquid

ζ & ϵ computational coordinates in the solid

Abstract of Dissertation Presented to the Graduate School of the University of Florida in Partial Fulfillment of the Requirements for the Degree of Doctor of Philosophy

VAPOR BUBBLE GROWTH
IN HETEROGENEOUS BOILING

By

Wen-Chin Chen

May, 1995

Chairman: James F. Klausner
Cochairman: Renwei Mei
Major Department: Mechanical Engineering

A numerical analysis is carried out to study vapor bubble growth in saturated heterogeneous boiling. The bubble growth rate is determined by considering the simultaneous energy transfer between the vapor bubble, the liquid microlayer which resides beneath the bubble, and the solid heater. Finite difference solutions for the temperature fields in the microlayer and heater are obtained on expanding coordinates as the bubble grows. The predicted bubble growth rate compares very well with the reported experimental data over a wide range conditions. Dimensional analysis subsequently reveals four relevant parameters. A systematic investigation on the dependence of the bubble growth rate and the solid temperature on these parameters is presented. The numerical study for the solid thermal field

elucidates the detailed energy transfer beneath a rapidly growing bubble.

A simplified model, based on heat transfer through a wedge shaped liquid microlayer and a lumped thermal analysis for a solid heater, is developed for predicting the vapor bubble growth rate in heterogeneous pool boiling. A first order ordinary differential equation is obtained for the bubble growth rate. The present bubble growth model compares well with the available experimental data for intermediate and moderately wetting fluids.

In subcooled heterogeneous boiling, detailed theoretical and computational analyses are carried out to investigate the vapor bubble growth process. Vapor bubble growth process is considered to be controlled by the unsteady energy transfer process among four regions. The unsteady energy equation in the subcooled liquid is strongly coupled with the momentum equation, which is approximated with the Laplace equation by assuming an inviscid flow. The bubble radius R(t) is determined by simultaneously solving the temperature fields in the solid and the subcooled liquid. Close agreement between the predicted and measured bubble radius requires specification of the ratio of the microlayer base radius to the bubble radius. The computational study for the solid and the subcooled bulk liquid thermal fields elucidates the energy transfer process.

CHAPTER 1
INTRODUCTION

Many industrial process, utilize nucleate boiling heat transfer due to its highly efficient heat transport mechanism. The requirement for economic heat exchanger designs and concern for safety necessitates both a quantitative and qualitative understanding of the boiling process. Although intensive fundamental research has been conducted over the past five decades in pursuit of the basic mechanisms governing nucleate boiling heat transfer, many uncertainties remain unresolved. In general, the nucleate boiling process consists of incipience, growth, and departure of vapor bubbles. Thus, the understanding of vapor bubble growth is essential to the heat transfer mechanisms associated with nucleate boiling.

Over the past four decades, the rate of vapor bubble growth in heterogeneous boiling systems has been the subject of numerous experimental and theoretical investigations due to its governing influence on heat transfer. A number of theoretical investigations on bubble growth rate have been conducted for uniformly superheated liquids (Dergarabedian, 1953; Plesset and Zwick, 1954; Forster and Zuber, 1954; and Scriven, 1959) and nonuniformly superheated liquids

(Griffith, 1958; Zuber 1961; Skinner and Bankoff, 1964; Han and Griffith, 1965; Van Stralen, 1967; and Mikic et al., 1969), and various closed-form expressions for the growth rate have been proposed. Extensive experimental data exist which demonstrate that such expressions do not accurately predict the vapor bubble growth rate in heterogeneous boiling. In particular, the inadequacy of such expressions have been clearly shown in Cole and Shulman (1966) and Van Stralen et al. (1975) for high Jacob number, Staniszewski (1959) and Akiyama et al. (1969) for low Jacob number, and Keshock and Siegel (1964) for low gravity.

Labunstov (1963) recognized that the majority of heat transfer to a growing vapor bubble occurs in a liquid microlayer which resides beneath its base; he derived a vapor bubble growth expression by assuming a constant wall temperature. Cooper (1983) also developed a microlayer bubble growth model by assuming a constant wall temperature. Dzakowic and Frost (1970) calculated the vapor bubble growth rate using a constant wall temperature evaporating microlayer model in which the transient microlayer thermal field is accounted for. Srinivas and Kumar (1984) proposed a microlayer bubble growth model which accounts for the bubble shape as well as natural convection and assumes a constant wall temperature. However, these models do not agree well with available experimental data (Cole and Shulman, 1966; Van Stralen et al., 1975; Staniszewski, 1959;

Akiyama et al., 1969; and Keshock and Siegel, 1964). Cooper and Vijuk (1970) and Van Stralen et al. (1975) have considered the heat transfer to a growing vapor bubble from both the microlayer and the liquid surrounding the vapor dome. Asymptotic expressions for the vapor bubble growth rate were derived by combining Rayleigh's solution for the initial stage of growth with the heat transfer controlled solution. The growth model of Van Stralen et al. (1975) appears to agree better with the high Jacob number data than that of Cooper and Vijuk (1970). However, its usefulness is limited due to the required specification of a dimensionless bubble growth parameter for which little guidance was provided on how it should be calculated. Fyodorov and Klimenko (1989) recently proposed a microlayer bubble growth rate model in which spatial variations in the wall temperature were included, but the temporal variations were ignored. Their growth rate model predicts that the bubble radius is proportional to the square root of time, $t^{1/2}$. However, the data of Akiyama et al. (1969) clearly demonstrate that the exponent on t can be as small as 1/5 at very low Jacob number.

In their model for predicting the growth and detachment of a vapor bubble attached to a heating surface, Lee and Nydhal (1989) incorporated the effect of hydrodynamics surrounding the dome of the growing bubble. They assumed a constant wall temperature, modelled the bubble as consisting

of a wedge-shaped microlayer and a hemisphere, and carried out detailed numerical computations for the momentum and energy equations for the liquid phase surrounding the vapor bubble. However, their predictions for the bubble growth rate and the detachment radius are not satisfactory when compared against experimental data.

Despite the importance of predicting the bubble growth rate in heterogeneous boiling and continuous research efforts covering the subject, no satisfactory theory has been formulated to cover a wide range of conditions. In the recent works for predicting the vapor bubble detachment diameter for pool boiling (Zeng et al.,1993) and that for flow boiling (Zeng et al., 1993), a successful model was developed based on first principles of mechanics. The predictions for the detachment radius agree quite well with the data over a wide range of conditions; however, the agreement was obtained only after using the actual bubble growth rate reported for each experiment. Clearly, without a reliable, physically sound bubble growth rate model, the utility of the bubble detachment models (Zeng et al., 1993a and 1993b) is limited.

Vapor bubble growth and collapse in subcooled boiling were experimentally studied by Gunther and Kreith (1950), Ellion (1954), and Cochran and Aydelott (1966). Theoretical studies were investigated by Plesset and Zwick (1954), Bankoff and Mikesel (1958), and Zuber (1961). In their

model for predicting bubble growth and collapse in highly subcooled nucleate boiling, Bankoff and Mikesell (1958) considered the effects of liquid inertia only. Plesset and Zwick (1954) studied vapor bubble collapse in a uniformly subcooled liquid. They suggested that the thermal effects may be unimportant for the collapse rate. From Ellion's experimental data, Zuber (1961) considered bubble growth and collapse separately. Zuber extended the Bosnjakovic-Jakob theory for bubble growth and used Rayleigh's solution for bubble collapse. Rayleigh's equation is only applicable when heat transfer is negligible.

In the present work, detailed numerical analyses are carried out to study vapor bubble growth in saturated and subcooled heterogeneous boiling. In the study of saturated heterogeneous pool boiling, the energy transfer process is considered to be among three phases: the vapor bubble, the liquid microlayer, and the solid heater. The unsteady energy equations in the solid heater and the liquid microlayer are solved by using finite difference method. Finite difference solutions for the temperature fields are obtained on expanding coordinates as the bubble grows. The bubble growth rate is obtained simultaneously with the thermal fields at every time step. The predicted bubble radius compares very well with the reported experimental data over a wide range of conditions. The current analysis, together with the experimental bubble growth rate data,

indicates that the liquid Prandtl number has little effect on the bubble growth rate. Through dimensional analysis, four relevant dimensionless parameters have been found. They are Jacob number Ja, Fourier number Fo, the liquid-to-solid conductivity ratio κ, and the liquid-to-solid thermal diffusivity ratio α. Systematic investigation on the dependence of the bubble growth rate and the solid temperature is conducted to assist in the basic understanding of the bubble growth mechanism. Although the above two-dimensional axisymmetric unsteady bubble growth model is accurate for predicting bubble growth rate, it is impractical to use as a design tool. Thus, a simplified model, based on heat transfer through a wedge shaped liquid microlayer and a lumped thermal analysis for a solid heater is developed for predicting the vapor bubble growth rate. A first order ordinary differential equation is obtained for predicting the bubble growth rate. The present bubble growth model compares well with the available experimental data. In the study of subcooled heterogeneous pool boiling, the energy transfer process is considered to be among four regions: a vapor bubble whose shape is assumed to be a truncated sphere, a liquid microlayer, a subcooled bulk liquid, and a solid heater. Due to the strong effect of subcooling and rapid bubble growth and collapse, the unsteady energy equation in the subcooled liquid is coupled with the momentum equation; the momentum equation is

approximated by the Laplace equation. A grid generation technique has been used in solving the temperature field of the subcooled bulk liquid. To ensure the accurancy of the present numerical results in the subcooled bulk liquid, an asymptotic solution for small time has been obtained. The numerical results in the subcooled liquid compare well with the asymptotic solution. The computational study for the subcooled liquid and the solid heater elucidates the energy transfer. In the computation two parameters, ϕ and μ_s, need to be specified in order to obtain good agreement between the predicted and measured bubble radius. The numerical results show that only one combination for these two parameters is possible to obtain the best fit.

This work is divided into six chapters. The formulation for vapor bubble growth in saturated pool boiling is given in Chapter 2. In Chapter 3, systematic investigations on the growth rate and thermal fields are considered. A simplified model for predicting the vapor bubble growth rate is developed in Chapter 4. Vapor bubble growth in subcooled heterogeneous boiling is studied in chapter 5. Finally, conclusions and recommendations for future work are discussed in Chapter 6.

CHAPTER 2
VAPOR BUBBLE GROWTH IN SATURATED POOL BOILING --PART I. FORMULATION

2.1 Background

In the previous work considering the growth rate of a bubble attached to a heating surface (heterogeneous boiling), the simultaneous spatial and temporal changes of the heating surface temperature were not considered. However, the temperature distribution in the neighborhood of a heater wall has long been believed by Westwater (1963) to be important to the mechanics of bubble growth. The growth of a vapor bubble requires a certain amount of energy from the heating surface to vaporize the surrounding liquid. In saturated boiling, this energy must come from the microlayer which resides beneath the base of the bubble and in turn withdraws energy from the solid heater (Moore and Mesler, 1961). Typically, the growth and departure of a vapor bubble involves a very short period of time (Hospeti and Mesler, 1969). Although energy is continuously supplied to the solid, the time scale required for the solid to adjust its temperature into a uniform distribution for most boiling systems is much longer than the bubble departure time. Consequently, the local solid temperature directly beneath the microlayer will decrease, both in space and in time,

because the local rate of energy removal due to the bubble growth is typically much larger than that added. The rapid decrease of the heating surface temperature directly beneath a growing vapor bubble has been experimentally demonstrated by Moore and Mesler(1961) and Hospeti and Mesler (1969). As the local solid wall temperature decreases with time during the bubble growth period, the temperature gradient across the microlayer is reduced and in turn directly reduces the rate of energy transferred to the bubble. Therefore, the actual bubble growth rate should be smaller than that predicted by assuming a constant wall temperature. This prognosis is in qualitative agreement with the existing data which show that the growth rate R(t) is less than or equal to $\beta t^{1/2}$ in which β is a constant.

In this saturated pool boiling investigation, the bubble growth process is considered to be controlled by the simultaneous unsteady energy transfer process among three phases: the vapor bubble, the liquid microlayer, and the solid heater. The bubble is assumed to have a uniform temperature at saturated conditions, T_{sat0}; the liquid microlayer is assumed to be very thin; and the temperature field in the solid is assumed to be axisymmetric with respect to (w.r.t.) the axis drawn through the center of the bubble. In section 2.2.1, the pertinent assumptions are made and the equations, the boundary conditions, and the initial conditions governing the unsteady energy transfer

from the solid layer through the microlayer to the bubble are presented. In section 2.2.2, non-dimensionalization and coordinate transformations are presented, which lead to necessary simplifications of the governing equations. The solution procedure for the microlayer and solid temperature fields and the bubble radius is also described. The parameters characterizing the bubble shape and the microlayer wedge angle during the growth are determined by matching the predicted growth rate with the existing experimental data. In section 2.3 The predicted bubble growth rate is compared with the available experimental data over a wide range of boiling conditions ; very good agreement is obtained. Notably, it is found that the Prandtl number has little or no effect on the bubble growth rate for the experimental conditions considered. To assist the basic understanding of bubble growth in heterogeneous boiling, the results of a systematic study considering the dependence of the bubble growth rate and the thermal fields of the liquid microlayer and the solid heater on the dimensionless parameters are presented in Chapter 3 of this investigation.

2.2 Formulation

2.2.1 Assumptions, Governing Equations, and Boundary and Initial Conditions

2.2.1.1 On the vapor bubble

A rigorous description of the vapor bubble growth and heat transfer processes among three phases requires a complete account for the hydrodynamics around the rapidly growing bubble in addition to the complex thermal energy transfer. The most difficult part, perhaps, is the exact determination of the bubble shape which is a moving interface between the vapor and liquid. The numerical analysis by Lee and Nydahl (1989) still relied on an assumed shape for the bubble, although the hydrodynamics based on the assumed bubble shape is properly accounted for. The discussion in the Introduction suggests that the thermal coupling between the liquid microlayer and the solid heater is perhaps more important than hydrodynamics. Therefore, in order to simplify the problem, the hydrodynamics of the liquid motion induced by the growing bubble is not pursued in this analysis. The determination of the bubble shape thus relies on empirical evidence. Furthermore, it is assumed that energy transfer to the bubble occurs only through the microlayer, and energy transfer to the bubble dome is small. Thus, the current analysis is only applicable to saturated boiling.

In this study, the liquid microlayer between the vapor bubble and the solid heating surface is assumed to have a simple wedge shape with an angle $\phi \ll 1$. The interferometry measurements of Koffman and Plesset (1983) demonstrate that a wedge shaped microlayer is a good approximation. There

exists ample experimental evidence (Van Stralen et al.; 1975; Akiyama et al., 1969; and Moore and Mesler, 1961) suggesting that, as the bubble grows, the bubble dome has approximately a spherical shape with a radius R(t). Thus, the bubble is modelled as a truncated sphere on a wedge shaped microlayer as depicked in Figure 2.1. Using cylindrical coordinates, the local microlayer thickness is denoted by L(r). The radius of the wedge-shaped interface is denoted by $R_b(t)$, which is typically not equal to R(t). Let

$$C = R_b(t)/R(t) \tag{2.1}$$

and the vapor bubble volume $V_b(t)$ can be expressed approximately as

$$V_b(t) = \frac{4\pi}{3} R^3(t) f(C) \tag{2.2}$$

with

$$f(C) \approx 1 - \frac{3}{4}(1-\sqrt{1-C^2})^2 + \frac{1}{4}(1-\sqrt{1-C^2})^3 \qquad for\ \phi \ll 1. \tag{2.3}$$

In the limit C→1, the bubble is a hemisphere and $V_b(t) = \frac{2}{3}\pi R^3(t)$. In the limit C→0, the bubble approaches a sphere and $V_b(t) \rightarrow \frac{4\pi}{3} R^3(t)$. The dependence of C on other parameters will be determined from measurements of the bubble shape reported under various conditions. In this study, C is assumed to be independent of time for simplicity.

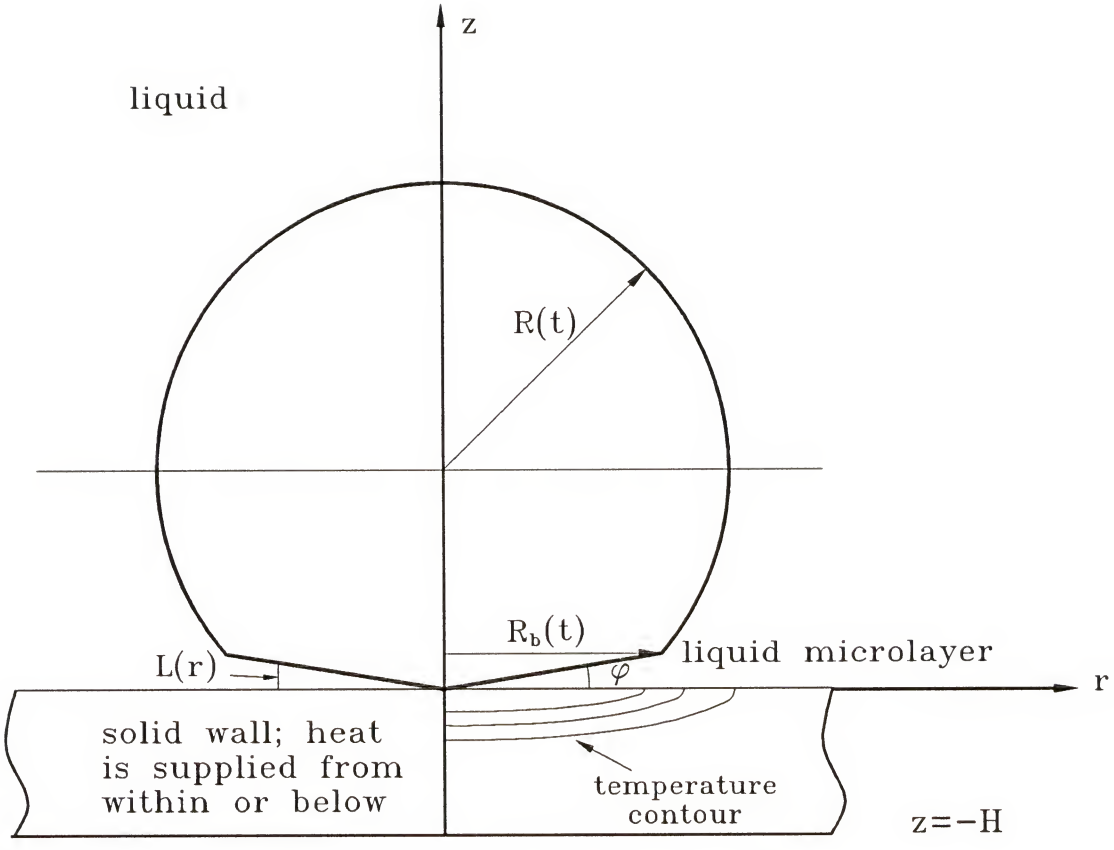

Figure 2.1 Sketch for the growing bubble, microlayer and the heating solid.

An energy balance for the growing bubble at the microlayer liquid-vapor interface depicted in Fig. 2.1 is described as

$$\rho_v h_{fg} 4\pi R^2 f(C) \frac{dR}{dt} = \int_A -k_\ell \left(\frac{\partial T_\ell}{\partial Z}\right)_{z=L(r)} dA, \qquad for\ \phi \ll 1 \tag{2.4}$$

where ρ_v is the vapor density, h_{fg} the latent heat, k_ℓ the liquid thermal conductivity, T_ℓ the liquid temperature, and A the surface area of the wedge at the liquid-vapor interface. With axisymmetry and $\phi \ll 1$, $dA \sim 2\pi r dr$ and $A \sim \pi R_b^2(t)$ at a given instant. Equation (2.4) simply states that the energy conducted from the liquid to the bubble through the microlayer is used to vaporize the surrounding liquid and thus expands the bubble. The initial condition for R(t) will be discussed later.

2.2.1.2 <u>On the microlayer</u>

The microlayer is assumed to be a wedge centered at r=0 with local thickness L(r). Because the hydrodynamics are not considered, the wedge angle ϕ cannot be determined as part of the solution. In Cooper and Lloyd (1969), the angle ϕ was related to the viscous diffusion length of the liquid as $R_b(t)\tan\phi = C_1\sqrt{\nu_\ell t}$ in which ν_ℓ is the kinematic viscosity of the liquid. Hence for small ϕ, one has

$$\phi = \frac{C_1\sqrt{\nu_\ell t}}{R_b(t)} = \frac{C_1\sqrt{\nu_\ell t}}{CR(t)}. \tag{2.5}$$

Cooper and Lloyd (1969) estimated C_1 to be within 0.3 to 1.0

for the conditions under their consideration. It is postulated here that the behavior of ϕ is insensitive to whether or not the wall temperature is constant. Thus the above form of equation (2.5) for ϕ is adopted. The constant C_1 will be determined from matching the predicted growth rate R(t) with experimentally measured growth rate. The two dimensionless constants, C and C_1, constitute the only empiricism of the present analysis. They arise because the hydrodynamics around the bubble are not taken into account in the analysis which follows.

For both the microlayer and the solid, the temperature fields are assumed to be axisymmetric. The energy balance for the liquid within the microlayer is

$$\frac{\partial T_\ell}{\partial t} = \alpha_\ell \left[\frac{1}{r}\frac{\partial}{\partial r}\left(r\frac{\partial T_\ell}{\partial r} \right) + \frac{\partial^2 T_\ell}{\partial z^2} \right], \quad for\ 0 \le r \le R_b(t),\ 0 \le z \le L(r) \tag{2.6}$$

where α_ℓ is the liquid thermal diffusivity. The boundary conditions are given as follows

$$T_\ell = T_{sat} \qquad at\ z = L(r), \tag{2.7}$$

$$T_\ell = T_s \quad and \quad k_\ell \frac{\partial T_\ell}{\partial z} = k_s \frac{\partial T_s}{\partial z} \qquad at\ z = 0, \tag{2.8a\&b}$$

$$\frac{\partial T_\ell}{\partial r} = 0 \qquad at\ r = 0, \tag{2.9}$$

$$\frac{\partial T_\ell}{\partial r} = 0 \qquad at\ r = R_b(t). \tag{2.10}$$

In the above, T_s is the solid temperature. Equations

(2.8a&b) simply ensure the continuity of the temperature and heat flux on the liquid-solid interface. Equation (2.10) is only an approximation in which radial heat conduction at the edge of the microlayer is neglected. Equation (2.9) guarantees that T_ℓ is finite as r→0. The initial condition for T_ℓ is discussed later.

2.2.1.3 <u>On the solid heater</u>

The energy equation for the solid is

$$\frac{\partial T_s}{\partial t} = \alpha_s\left[\frac{1}{r}\frac{\partial}{\partial r}\left(r\frac{\partial T_s}{\partial r}\right) + \frac{\partial^2 T_s}{\partial z^2}\right] + \frac{\alpha_s}{k_s}q''', \quad for\ 0 \le r < \infty,\ -H \le z \le 0 \tag{2.11}$$

where α_s and k_s are the thermal diffusivity and conductivity of the solid, and q''' is the volumetric heating and H is the thickness of the heater. The boundary conditions are

$$\frac{\partial T_s}{\partial r} = 0 \qquad at\ r=0 \quad and \quad r\to\infty, \tag{2.12a&b}$$

$$\frac{\partial T_s}{\partial z} = -q''/k_s \qquad at\ z=-H, \tag{2.13}$$

$$T_s = T_\ell \quad and \quad k_\ell\frac{\partial T_\ell}{\partial z} = k_s\frac{\partial T_s}{\partial z} \qquad at\ z=0, \quad 0 \le r \le R_b(t), \tag{2.14a&b}$$

$$T_s = T_\ell \quad and \quad \frac{\partial T_s}{\partial z} = 0 \qquad at\ z=0 \quad r \ge R_b(t). \tag{2.15a&b}$$

In the above, two possible mechanisms for heat supply are incorporated: a heat supply on the lower surface at z=-H, q'', or a volummetric heat supply (on average) within the solid layer, q'''. For $r>R_b(t)$ at z=0, the heat transfer due to natural convection of the liquid is neglected. Whether

or not the heat removal from the solid due to natural convection is included, it has virtually no influence on the solution because it is so small compared with latent heat removed due to bubble growth. The condition at $r\to\infty$ reflects the uniformity of the temperature far away from the bubble. Because of the continuous energy supply, it is not quit correct to specify, for all times, $T_s=T_{sat}+\Delta T_{sat0}$ as $r\to\infty$ in which ΔT_{sat0} is the initial superheat at incipience. If there exists strong thermal interaction among adjacent nucleation sites, as might occur in the coalesced bubble regime, the present analysis needs to be modified. Hence, the present analysis is restricted, strictly speaking, to the isolated bubble regime.

2.2.1.4 <u>On the initial conditions</u>

It must be noted that the above formulation requires a well established microlayer at the beginning of the solution. This implies that the solution must start at some finite but small time $t_0 \ll t_d$ in which t_d is the depart time of the bubble and is the time scale of interest for the present problem. It is assumed here that at $t=t_0$ the microlayer has formed and the bubble has a radius R_0. But since R_0 is small, the bubble has withdrawn little energy from the solid at $t=t_0$. Thus, the solid temperature T_s is practically constant everywhere,

$$T_s = T_{sat} + \Delta T_{sat0} \qquad at\ t = t_0 \ll t_d. \tag{2.16}$$

This assumption is justified because the initial stage of the growth is governed by hydrodynamics considerations as is the case for Rayleigh's solution. The present study focuses on the coupling of the solid temperature with that of the liquid and the rate of bubble growth. However, this coupling becomes important only after a significant amount of energy is transferred from the solid to the bubble through the microlayer. Therefore, a reasonable initial condition for T_ℓ is

$$T_\ell(t=t_0, r<R_0, z) = T_{sat} + \Delta T_{sat0}\left[1 - \frac{z}{L(r)}\right] \qquad at\ t=t_0 \ll t_d. \tag{2.17}$$

Consistent with equations (2.16) and (2.17), the initial bubble radius at $t=t_0$ can be obtained by assuming a constant wall temperature. This is appropriate because the solid temperature is not affected yet by the growth of the bubble at very small t_0. Integrating equation (2.4) by assuming a time independent $\frac{\partial T_\ell}{\partial z}$, one obtains

$$R_c(t) = \frac{C^2}{f(C)} \frac{Ja}{C_1 Pr_\ell^{1/2}} (\alpha_\ell t)^{1/2} \tag{2.18}$$

for the growth rate with a constant wall temperature. In the above

$$Ja = \frac{\rho_\ell C_{p\ell} \Delta T_{sat0}}{\rho_v h_{fg}} \tag{2.19}$$

and

$$Pr_\ell = \frac{\nu_\ell}{\alpha_\ell} \tag{2.20}$$

are, respectively, the Jacob number and Prandtl number, and

$C_{p\ell}$ is the specific heat of the liquid. Hence R_0 can be found as $R_0=R_c(t_0)$. In equation (2.18), the relation between ϕ and R(t) given by equation (2.5) has been used. Equations (2.16-2.18) complete the specification of the initial conditions. Although the actual initial growth is governed by hydrodynamics, this assumed initial radius has little effect on the later growth as long as $t_0 \ll t_d$. It is noted that the liquid Prandtl number Pr_ℓ results from Cooper and Lloyd's model for the microlayer wedge angle ϕ given by equation (2.5), and using equation (2.18) ϕ may be expressed as

$$\phi = \frac{f(C)\, C_1^2\, Pr_\ell}{C^3\, Ja}. \tag{2.21}$$

2.2.2 Non-dimensionalization and Coordinate Transformation

2.2.2.1 Non-dimensionalization and further simplification

To gain an understanding of the important physics and to efficiently solve the energy equations, the following dimensionless variables are introduced,

$$\tau = t/t_d, \quad \bar{r} = r/R_b(t), \quad \bar{z}_\ell = z/L(r), \quad \bar{z}_s = z/H,$$

$$\bar{R}(\tau) = R(t)/R_c(t_d), \quad \theta_\ell = (T_\ell - T_{sat})/\Delta T_{sat0}, \quad \theta_s = (T_s - T_{sat})/\Delta T_{sat0}, \tag{2.22}$$

where t_d is the bubble departure time scale. An accurate determination of t_d is not necessary because only the time scale is relevant. The length scale in the z-direction for the solid is the thickness of the heater. However, this is

not the correct length scale if H is very large or the solid conductivity is very small. Thus another transformation is expected for $\bar{z}_s$ in carrying out the computation. The utilization of H is sufficient for the purpose of dimensional analysis.

Upon substitution of equation (2.22) into equation (2.4), the normalized bubble growth rate is governed by

$$\frac{d\bar{R}^2(\tau)}{d\tau} = -\int_0^1 \left(\frac{\partial\theta_\ell}{\partial\bar{z}_\ell}\right)_{\bar{z}_\ell=1} d\bar{r}. \tag{2.23}$$

For constant wall temperature, the right-hand-side of equation (2.23) is one and $\bar{R}(\tau)=\tau^{1/2}$. Hence, any mechanism that causes $\left|\left(\frac{\partial\theta_\ell}{\partial\bar{z}_\ell}\right)_{\bar{z}_\ell=1}\right|$ to decrease with time will yield a growth rate $\bar{R}(\tau)<\tau^{1/2}$.

Substituting the above dimensionless variables into the governing equations, one obtains for the microlayer

$$\frac{\partial\theta_\ell}{\partial\tau} - \frac{t_d\dot{R}_b}{R_b}\bar{r}\frac{\partial\theta_\ell}{\partial\bar{r}} = \frac{\alpha_\ell t_d}{R_b^2}\frac{1}{\bar{r}}\frac{\partial}{\partial\bar{r}}\left(\bar{r}\frac{\partial\theta_\ell}{\partial\bar{r}}\right) - \frac{\alpha_\ell t_d}{R_b}\frac{L'(\bar{r})}{L(\bar{r})}\frac{\bar{z}_\ell}{\bar{r}}\frac{\partial\theta_\ell}{\partial\bar{z}_\ell} + \frac{\alpha_\ell t_d}{L^2(\bar{r})}\frac{\partial^2\theta_\ell}{\partial\bar{z}_\ell^2} \tag{2.24}$$

for $0\le\bar{r}\le1$, $0\le\bar{z}_\ell\le1$. In the above,

$$L'(r)=\frac{dL}{dr}=\phi\ll1, \quad \dot{R}_b=\frac{dR_b}{dt}, \quad and \quad L(\bar{r})\le L(1)=\phi R_b(\tau)\ll R_b(\tau).$$

For very small ϕ, the right-hand-side (RHS) of equation (2.24) reduces to

$$\frac{\alpha_\ell t_d}{L^2(\bar{r})}\left[\phi^2\frac{\partial}{\partial\bar{r}}\left(\bar{r}\frac{\partial\theta_\ell}{\partial\bar{r}}\right) - \phi^2\frac{\bar{z}_\ell}{\bar{r}}\frac{\partial\theta_\ell}{\partial\bar{z}_\ell} + \frac{\partial^2\theta_\ell}{\partial\bar{z}_\ell^2}\right] \sim \frac{\alpha_\ell t_d}{L^2(\bar{r})}\frac{\partial^2\theta_\ell}{\partial\bar{z}_\ell^2}$$

and consequently equation (2.24) becomes, to the leading

order for small ϕ

$$\frac{\partial\theta_\ell}{\partial\tau} - \frac{\bar{R}'}{\bar{R}}\bar{r}\frac{\partial\theta_\ell}{\partial\bar{r}} = \frac{1}{C_1^2 Pr_\ell}\frac{1}{\bar{r}^2\bar{R}^2}\frac{\partial^2\theta_\ell}{\partial\bar{z}_\ell^2} \quad for\ 0\le\bar{r}\le1,\ 0\le\bar{z}_\ell\le1, \tag{2.25}$$

where the prime denotes the time derivative w.r.t. τ. If $C_1^2Pr_\ell \ll 1$, the conduction term dominates and a quasi-steady heat conduction problem results. Only for some cases, such as low Jacob number boiling, it is found that $C_1^2Pr_\ell \ll 1$ is possible. Hence all three terms on equation (2.25) must be retained for numerical accuracy.

It is also noted that since the second order derivative wrt $\bar{r}$ disappears following the foregoing scaling analysis, only one boundary condition in the $\bar{r}$-direction is required. Because $\bar{R}'(\tau)>0$, the first order derivative w.r.t $\bar{r}$ acts as a convection term with a negative speed in the $\bar{r}$-direction. Thus the condition at $\bar{r}=0$ given by equation (2.9) is dropped. The advantage of solving equation (2.25) over equation (2.24) is that equation (2.25) is parabolic, instead of elliptic, and marching from $\bar{r}=1$ to $\bar{r}=0$ for equation (2.25) is relatively simple.

For the solid layer, the energy equation in dimensionless form is

$$\frac{\partial\theta_s}{\partial\tau} - \frac{\bar{R}'}{\bar{R}}\bar{r}\frac{\partial\theta_s}{\partial\bar{r}} = \frac{\alpha_s t_d}{R_b^2(\tau)}\frac{1}{\bar{r}}\frac{\partial}{\partial\bar{r}}\left(\bar{r}\frac{\partial\theta_s}{\partial\bar{r}}\right) + \frac{\alpha_s t_d}{H^2}\frac{\partial^2\theta_s}{\partial\bar{z}_s^2} + \frac{\alpha_s t_d q'''}{k_s\Delta T_{sat0}} \tag{2.26}$$

for $0\le\bar{r}<\infty$, $-1\le\bar{z}_s\le0$. For the first term on the RHS of equation (2.26), the ratio $(R_b(\tau)/H)^2$ is small at the early

stage of growth but can be large at a later time if a thin heater is used. Thus unlike the liquid microlayer case, both the derivatives wrt $\bar{r}$ and $\bar{z}_s$ are important in equation (2.26). Using equations (2.1), (2.18), and (2.22), equation (2.26) can be expressed as

$$\frac{\partial\theta_s}{\partial\tau} - \frac{\bar{R}'}{\bar{R}}\bar{r}\frac{\partial\theta_s}{\partial\bar{r}} = \frac{1}{\alpha}\frac{f^2(C)C_1^2 Pr_\ell}{C^6 Ja}\frac{1}{\bar{R}^2}\frac{1}{\bar{r}}\frac{\partial}{\partial\bar{r}}\left(\bar{r}\frac{\partial\theta_s}{\partial\bar{r}}\right) + Fo\frac{\partial^2\theta_s}{\partial\bar{z}_s^2} + \frac{\alpha_s t_d q'''}{k_s\Delta T_{sat0}} \qquad (2.27)$$

where

$$\alpha = \frac{\alpha_\ell}{\alpha_s}, \qquad Fo = \frac{\alpha_s t_d}{H^2}. \qquad (2.28)$$

Fo is the solid Fourier number. The last term in equation (2.27) is usually insignificant in most boiling systems. In all the data analyzed, when neglected, the last term causes at most 10% error for $\bar{R}(\tau)$ in a worst case with large t_d. Although this term is kept in the computation to obtain better values for C_1; no particular attention will be given to its effect on the growth rate.

It is emphasized here that the introduction of the bubble departure time scale, t_d, in the computation of the growth rate is an artifact. The growth rate R(t) in dimensional form is independent of t_d. However, t_d is a useful quantity to characterize the effective thickness of the heater in defining Fo and to scale the growth time. If t_d is quite small so that $Fo \ll 1$, the heater is considered to

be very thick and the temperature at the bottom of the heater is not affected by the time the bubble departs. If Fo~O(1) or larger the temperature on the bottom of the heater will be influenced by the bubble growth on a time scale of t_d. The thermal interaction between the bubble and the heater, which determines the bubble growth rate, thus depends strongly on Fo. From another perspective, the actual physical process does depend on t_d because after departure the solid temperature field will rise again. An estimate for t_d can be obtained, for example, from the balance of the buoyancy force with the growth force as discussed in Zeng et al. (1993a). In estimating t_d and calculating the growth force, the bubble growth rate, which is the solution to be sought here, is needed. This dilemma can be easily solved since we do not need the exact value of t_d in equations (2.25) and (2.27), and the growth rate can be estimated by using the constant wall temperature solution for R(t) given by equation (2.18). Hence the estimate used here for t_d is

$$t_d \sim \left[\frac{C^2}{f^2(C)}\,\frac{Ja}{C_1 Pr_\ell^{1/2}}\,\frac{\alpha_\ell^{1/2}}{g}\right]^{2/3} \tag{2.29}$$

which gives

$$Fo = \frac{\alpha_s \alpha_\ell^{1/3}}{g^{2/3} H^2}\,\frac{Ja^{2/3}}{C_1^{2/3} Pr_\ell^{1/3}}\,\frac{C^{4/3}}{f^{4/3}(C)}\,. \tag{2.30}$$

It is noted that the above choice for t_d is adopted.

Non-dimensionalization of the boundary condition (2.14b) on the liquid-solid interface results in

$$\frac{\partial\theta_\ell}{\partial\bar{z}_\ell} = \frac{k_s}{k_\ell}\frac{L(\bar{r})}{H}\frac{\partial\theta_s}{\partial\bar{z}_s}.$$

Using $L(\bar{r})=\phi r$, $r=CR(t)\bar{r}=R_c(t_d)C\frac{R(t)}{R_c(t_d)}\bar{r}$, equation (2.21) for ϕ and equation (2.18) for $R_c(t)$, the above can be expressed as

$$\frac{\partial\theta_\ell}{\partial\bar{z}_\ell} = \frac{\alpha^{1/2}}{\kappa} Fo^{1/2} C_1 Pr_\ell^{1/2} \bar{R}(\tau)\,\bar{r}\frac{\partial\theta_s}{\partial\bar{z}_s} \qquad at\ \bar{z}_s=0 \tag{2.31}$$

where the liquid-to-solid conductivity ratio and thermal diffusivity ratio,

$$\kappa = k_\ell/k_s \tag{2.32}$$

and

$$\alpha = \frac{\alpha_\ell}{\alpha_s} \tag{2.33}$$

are two more independent dimensionless parameters that are important to the bubble growth process in addition to Ja, Pr_ℓ, and Fo. It is noted that κ only appears in the boundary condition, equation (2.31), while α appears in both the boundary condition and the energy equation for the solid. Hence, the effect of α on the growth rate and the solid thermal field is more complicated than that of κ.

2.2.2.2 Coordinate transformations

To apply the boundary condition at large $\bar{r}$ for the solid temperature, the following simple transformations are applied in the $\bar{r}$-direction

$$\bar{r} = \bar{r}_{\infty}\{1 - S_r \tan^{-1}[(1-\zeta)\tan(1/S_r)]\} \qquad for\ 0 \le \zeta \le 1, \tag{2.34}$$

where $\bar{r}_{\infty}$ is the radial position at which equation (2.12b) is applied and the constant S_r determines the percentage of the grid number allocated to the region of $\bar{r} \le 1$. Typically, S_r=0.7 to 0.8 is used and $\bar{r}_{\infty}$ ranges from 5 to 25. To place more grids near $\bar{z}_s$=0 where a large temperature gradient occurs, the following transformation is applied

$$\bar{z}_s = -1 + S_z \tan^{-1}[(1-\varepsilon)\tan(1/S_z)] \qquad for\ 0 \le \varepsilon \le 1 \tag{2.35}$$

where S_z is a constant characterizing the stretching. The clustering of the grids occurs near $\bar{z}_s$=0. For a thicker plate, S_z=0.65 is typically used. For a thin solid layer, a larger value of S_z=1.0 is preferred because the thermal layer will quickly penetrate to the bottom soon after incipience.

The computation must start from some very small but nonzero initial time, τ_0, with the present formulation. Because the error for $\bar{R}(\tau)$ associated with τ_0 is of $O((\tau_0)^{1/2})$, it is desirable to use τ_0 as small as possible. To this end, the following transformation is introduced

$$\tau = \sigma^2 \tag{2.36}$$

with a uniform "time step" $\Delta\sigma$.

The energy equation for the solid heater is transformed to (ζ,ε) coordinates. The equation is

$$\frac{1}{2\sigma}\frac{\partial\theta_s}{\partial\sigma}-\frac{\bar{R}'(\tau)}{\bar{R}(\tau)}\bar{r}_s\frac{\partial\theta_s}{\partial\zeta}\frac{\partial\zeta}{\partial\bar{r}_s}=\frac{f^2(C)C_1^2Pr_\ell}{C^6\alpha Ja^2}\frac{1}{\bar{R}^2(\tau)}\frac{1}{\bar{r}_s}\frac{\partial}{\partial\zeta}\left(\bar{r}\frac{\partial\theta_s}{\partial\zeta}\frac{\partial\zeta}{\partial\bar{r}_s}\right)\frac{\partial\zeta}{\partial\bar{r}_s}$$

$$+Fo\frac{\partial}{\partial\varepsilon}\left(\frac{\partial\theta_s}{\partial\varepsilon}\frac{\partial\varepsilon}{\partial\bar{z}_s}\right)\frac{\partial\varepsilon}{\partial\bar{z}_s}+\frac{\alpha_s t_d q'''}{k_s\Delta T_{sat0}}. \qquad (2.37)$$

It is solved using the ADI method (Anderson et al., 1984) while that for the microlayer is solved by marching from $\bar{r}=1$ to $\bar{r}=0$.

2.2.2.3 Solution procedure

Due to the coupling between the solid and liquid temperature fields through the boundary conditions, θ_s and θ_ℓ must be solved simultaneously at a given instant. However, θ_ℓ needs to be solved only for $\bar{r}\leq 1$ while θ_s should be solved for $\bar{r}\leq\bar{r}_\infty$ with $\bar{r}_\infty\gg 1$. Hence, an iterative solution procedure is adopted which is precisely described.

The solution for θ_s and θ_ℓ are assumed to be known at $\sigma=\sigma^n$ as θ_s^n and θ_ℓ^n. At $\sigma=\sigma^{n+1}=\sigma^n+\Delta\sigma$, the first iteration for θ_s^{n+1} is solved using the ADI scheme by simply marching in time by one time step for the given boundary condition $\theta_s^n(\bar{z}_s=0)$. The liquid temperature θ_ℓ is solved next with $\theta_s^n(\bar{z}_s=0)$. After one sweep, the interface temperature $\theta_s^{n+1}(\bar{z}_s=0)$ is updated by forcing the continuity of the heat flux,

$$\frac{\partial\theta_\ell}{\partial\bar{z}}=\frac{k_s}{k_\ell}\frac{\partial\theta_s}{\partial\bar{z}}.$$

The second iteration for θ_s^{n+1} begins with this updated condition at $\bar{z}_s=0$. Several iterations bring the successive

difference in temperature on the interface down to 10^{-3} (this tolerance is sufficient for the present computation). After the temperature fields converge at σ^{n+1} (or τ^{n+1}) the growth rate $\bar{R}(\tau^{n+1})$ is updated by integrating equation (2.23) using Euler's explicit scheme. The information for $\bar{R}(\tau^{n+1})$ is a necessary input in equations (2.25) and (2.27). Although the solution for $\bar{R}(\tau^{n+1})$ is only first order accurate in $\Delta\sigma$, the $O(\Delta\sigma)$ accuracy is not a concern here because a very small $\Delta\sigma$ has to be used to retain the numerical stability in solving equations (2.23), (2.25) and (2.27). Typically, $n=10^4$ is needed for $\tau \leq 1$ to achieve the convergence of the solution with a moderate and large Ja if 16 to 26 grids are allocated in $0 \leq \bar{r} \leq 1$. For Ja~1, the total number of time steps is on the order of $n=8\times10^4$ for Fo=10, 100 and 1000.

2.3 Results and Discussions

2.3.1 Determination of the Empirical Constants C and C_1

After examining a limited number of photographs for growing vapor bubbles in a saturated pool boiling (Van Stralen et al., 1975, Akiyama, 1969, and Hospeti and Mesler, 1969), the following trend is observed:

(a) For high Jacob number, the bubble shape tends to resemble a hemisphere on top of a wedge (microlayer). Thus C is close to 1.

(b) For low Jacob number, the bubble shape is more

spherical and C is thus small.

The values of C are determined from the vapor bubble profiles and the photographs provided by Van Stralen & Cole (1975), Akiyama et al. (1969) and Hospeti and Mesler (1969). The following correlation for C best fits these data,

$$C = [\,(0.4134\,Ja^{0.1655})^{-6} + (1 - 0.1\,e^{0.0005\,Ja})^{-6}\,]^{-1/6}. \tag{2.38}$$

Fig. 2.2 compares the above fit with the data. It is possible that C may also depend on other parameters such as Pr_ℓ and Fo. For the purpose of developing a model for predicting the bubble growth rate, a simple form for C is adopted and C_1 is allowed to vary with Ja, Pr_ℓ and α. As will be demonstrated, this approach turns out to be quite useful.

The determination of C_1, which describes the microlayer wedge angle as shown by equation (2.5), is crucial to the success of the present study. Because the hydrodynamics are not considered in this analysis, C_1 must be determined empirically. For each experimentally measured R(t), a series of values for C_1 are used in the numerical computation for θ_s, θ_ℓ and R(t). The one that results in the closest agreement between the measured and computed R(t) over a large range of t prior to departure is taken to be the value of C_1 required in the present analysis. The results of such are given in Table 2.1. The data are presented from large to small Ja. Based on these 32 data sets, the following

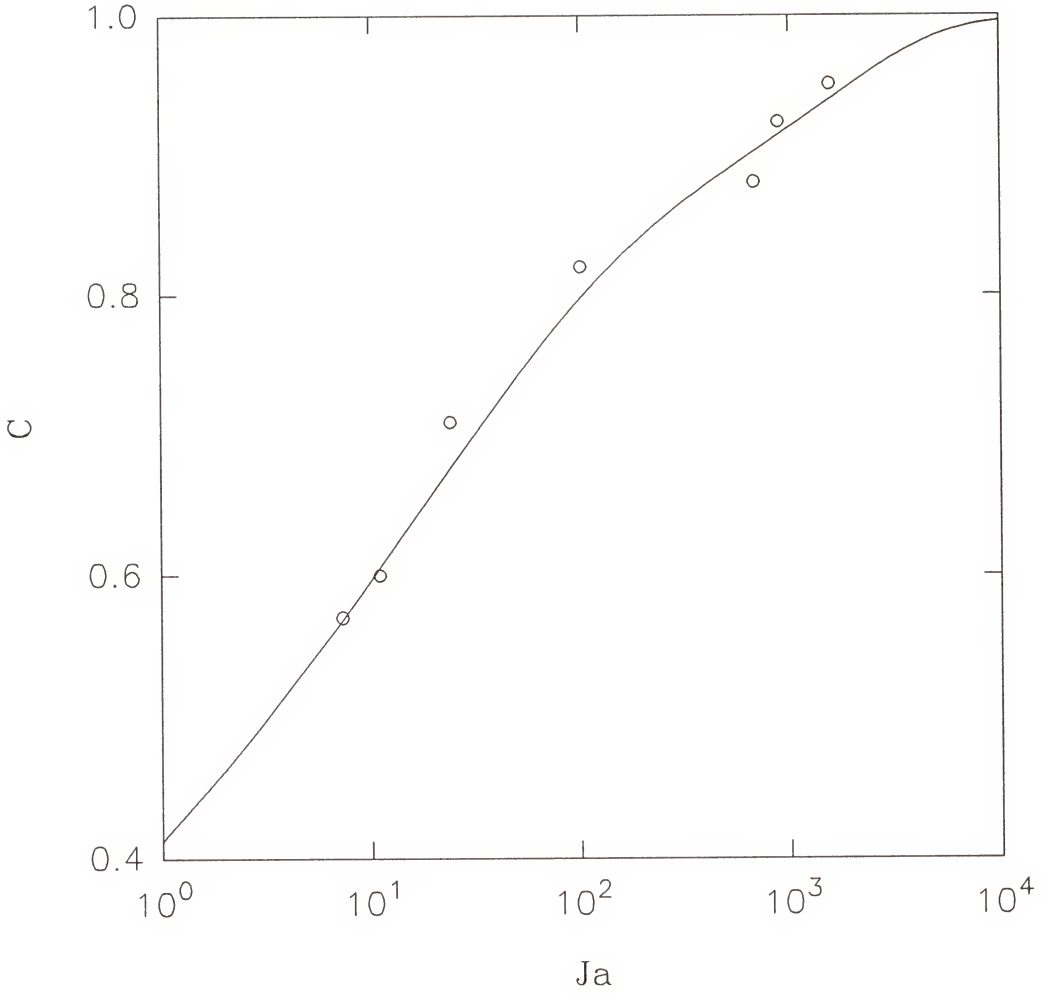

Figure 2.2 Dependence of C on Ja based on the data of Van Stralen et al. (1975), Akiyama et al. (1969), and Hospeti and Mesler (1969).

Table 2.1 Microlayer angle parameter c_1 determined from various sources

No.	Ja	Pr_ℓ	K_ℓ/K_s	α_ℓ/α_s	C_1	P (atm)	Source
1	1973.6	4.65	0.00156	0.00126	3.10	0.040	Van Stralen et al. (1975)
2	887.3	4.22	0.00161	0.00130	1.75	0.079	Van Stralen et al. (1975)
3	766.2	4.54	0.0270	0.01210	1.30	0.066	Cole and Shulman (1966)
4	389.5	3.46	0.00164	0.00133	1.20	0.182	Van Stralen et al. (1975)
5	289.3	3.42	0.02840	0.01260	0.45	0.129	Cole and Shulman (1966)
6	210.0	6.44	0.00577	0.00810	0.33	0.063	Cole and Shulman (1966)
7	201.0	2.97	0.00166	0.00136	0.17	0.203	Van Stralen et al. (1975)
8	178.7	2.70	0.0290	0.01290	0.55	0.257	Cole and Shulman (1966)
9	156.0	6.70	0.00449	0.00604	0.30	0.182	Cole and Shulman (1966)
10	150.5	2.70	0.00168	0.00137	0.45	0.268	Van Stralen et al. (1975)
11	130.0	6.13	0.00870	0.00830	0.20	0.268	Cole and Shulman (1966)
12	90.6	2.17	0.02970	0.01331	0.20	0.474	Cole and Shulman (1966)
13	67.1	5.60	0.00860	0.00815	0.17	0.40	Cole and Shulman (1966)
14	50.6	4.74	0.00508	0.00629	0.30	0.689	Cole and Shulman (1966)
15	50.0	5.14	0.00848	0.00808	0.16	0.522	Cole and Shulman (1966)
16	42.3	1.76	0.00173	0.00144	0.52	1.0	Staniszewski (1959)
17	37.6	4.60	0.00837	0.00806	0.15	0.711	Cole and Shulman (1966)
18	35.8	1.76	0.00173	0.00144	0.38	1.0	Staniszewski (1959)

Table 2.1 (continued)

No.	Ja	Pr_ℓ	K_ℓ/K_s	α_ℓ/α_s	C_1	P (atm)	Source
19	25.3	1.76	0.00173	0.00144	0.25	1.0	Staniszewski (1959)
20	25.0	1.76	0.00173	0.00144	0.30	1.0	Staniszewski (1959)
21	24.5	4.25	0.00493	0.00597	0.10	1.0	Cole and Shulman (1966)
22	23.4	1.76	0.00730	0.00577	0.12	1.0	Hospeti and Mesler (1969)
23	23.0	4.30	0.00048	0.00086	0.12	1.0	Staniszewski (1959)
24	14.9	1.76	0.00730	0.00577	0.10	1.0	Hospeti and Mesler (1969)
25	18.4	1.76	0.00173	0.00144	0.28	1.0	Keshock and Siegel (1964)
26	14.9	1.76	0.00730	0.00577	0.07	1.0	Hospeti and Mesler (1969)
27	11.5	1.43	0.02630	0.02440	0.16	2.0	Akiyama et al. (1969)
28	11.2	1.44	0.00174	0.00146	0.20	1.90	Staniszewski (1959)
29	9.16	1.30	0.00175	0.00148	0.16	2.72	Staniszewski (1959)
30	7.73	4.0	0.00046	0.00068	0.050	1.90	Staniszewski (1959)
31	1.17	1.02	0.02620	0.02470	0.015	8.0	Akiyama et al. (1969)
32	0.52	0.92	0.02560	0.02430	0.007	15.0	Akiyama et al. (1969)

correlation for C_1 is obtained

$$C_1 \sim 0.00643\, Ja^{0.763}\, Pr_\ell^{-0.390}\, \kappa^{0.0746}\, \alpha^{-0.221} \tag{2.39}$$

by requiring the least relative deviation

$$r.d. = \frac{1}{32}\sum_{n=1}^{32} |\, C_{1,n} - C_{1,n}^{*} \,| / C_{1,n}^{*} \tag{2.40}$$

in which $C_{1,n}^{*}$ is the value determined from matching the experimental growth rate data with the present computation. The above expression gives r.d.=0.232. A very similar expression is obtained with a standard deviation of 0.19 for the exponent of Pr_ℓ using a least squares fitting. Hence, within statistical error, the exponent for Pr_ℓ may be taken as -0.5. Requiring the least relative deviation again,

$$C_1\, Pr_\ell^{0.5} \sim 0.00525\, Ja^{0.752}\, \kappa^{-0.113}\, \alpha^{-0.117} \tag{2.41}$$

with a relative deviation of 0.238. Fig. 2.3 compares the above correlation for C_1 with the data presented in Table 2.1; reasonable agreement is observed. An important implication immediately follows when one substitutes (2.41) into (2.21), (2.18), (2.25), and (2.27)-(2.31), which are the only places where Pr_ℓ appears. Since C_1 and Pr_ℓ appear in the form of $C_1 Pr_\ell^{1/2}$, it is obvious that Pr_ℓ is no longer relevant to the present problem. This implies that the liquid viscosity is not important in determining the bubble shape which are characterized by C and C_1 in the present analysis.

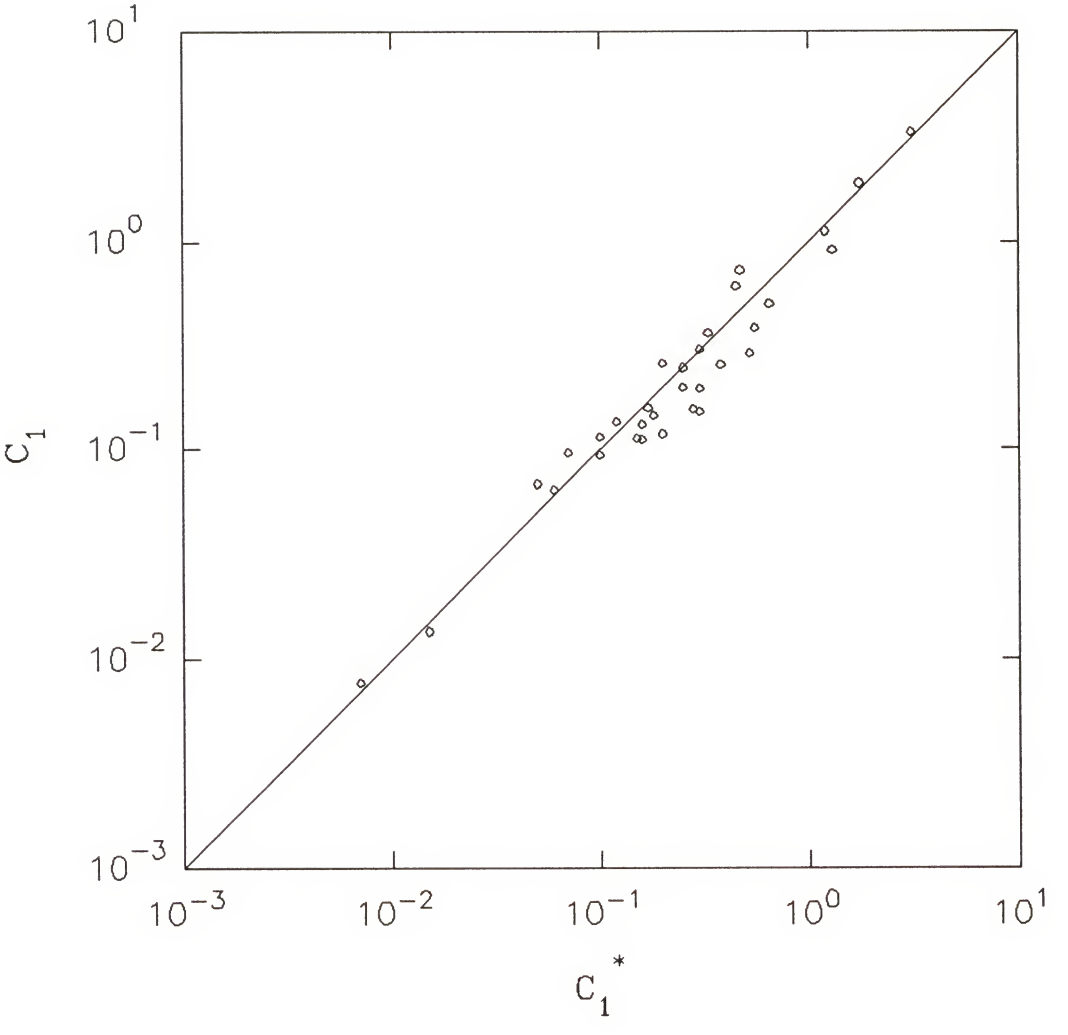

Figure 2.3 Comparison for C_1 based on the correlation and data presented in Table 2.1.

To understand the independence of vapor bubble shape on the liquid viscosity, it is instructive to estimate the Reynolds number of the liquid motion associated with the bubble growth. Using d=2R(t) as the length scale, $\dot{R}(t)$ as the velocity scale, assuming $R(t)\sim\beta t^{1/2}$, the Reynolds number of the liquid flow may be estimated as $Re_d\sim\beta^2/\nu_\ell$. For case No. 3 (Ja=766.2) listed in Table 2.1, using the measured growth rate shown in Fig. 2.4b, it is easily shown that $Re_d\sim12,941$ for $\beta^2\sim8.8$ (mm^2/ms) and $\nu_\ell=6.8x10^{-3}$ (cm^2/s). Hence, the liquid motion induced by the expanding bubble in this case is clearly of inviscid nature. Even for case No. 28 (Ja=11.24) for which $\beta^2\sim0.064$ (mm^2/ms), one obtains $Re_d\sim256$ by taking $\nu_\ell=5x10^{-3}$ (cm^2/s). Typically, $Re_d\sim40$ may be the lower limit above which a uniform liquid flow around a bubble can be treated as inviscid flow. For the present case, the bulk liquid motion is mainly in the radial direction. Because the viscous effect associated with the radial motion is weaker than that in a uniform flow over a sphere, the liquid flow induced by the growing bubble in the present study is mainly of inviscid nature. Therefore the hydrodynamics, which is important to the bubble shape appears to have a universal effect on the bubble growth rate, i.e. independent of the liquid viscosity, for most of the data listed in Table 2.1. The foregoing discussion also, to certain extent, justifies the choice of using Ja alone to correlate c as given by equation (2.38).

2.3.2 Comparison of the Predicted and Measured Growth Rate

To validate the present numerical analysis and also to examine the effect of the Jacob number, Ja, on the growth rate, comparisons are made between the present prediction and the experimentally measured R(t) over a large range of Ja. Fig. 2.4a shows such a comparison in the high Jacob number range, Ja=201~1973.6 at κ=0.00156~0.0016. The data are taken from Van Stralen et al. (1975) who used water as the boiling liquid. The Prandtl number, Pr_ℓ, in Fig. 4a changes from 2.97 to 4.65; but it is not expected that Pr_ℓ will affect the growth rate. Excellent agreement is observed between the prediction and the measurement in this large Ja range. Fig. 2.4b compares the numerical results with the data of Cole & Shulman (1966) in which Ja ranges from 90.6 to 766.2, κ=0.027 to 0.0297 and Pr_ℓ =2.17~4.54. For these intermediate to high values of Ja, excellent agreement for R(t) is again observed. Fig. 2.4c compares the prediction with the data obtained by Cole & Shulman (1966) using methanol as the boiling liquid which has a higher Prandtl number, Pr_ℓ =4.6~6.13. The Jacob number ranges from 37.6 to 130.0 which is considered to be in the intermediate range. Very good agreement is seen between these data and the prediction. While the measurements shown in Figs. 4a-c were obtained under subatmospheric or atmospheric conditions, Fig. 2.4d compares the present prediction with the data of Staniszewski (1959) obtained at p_{sat}=193 and 276 kpa (or 28

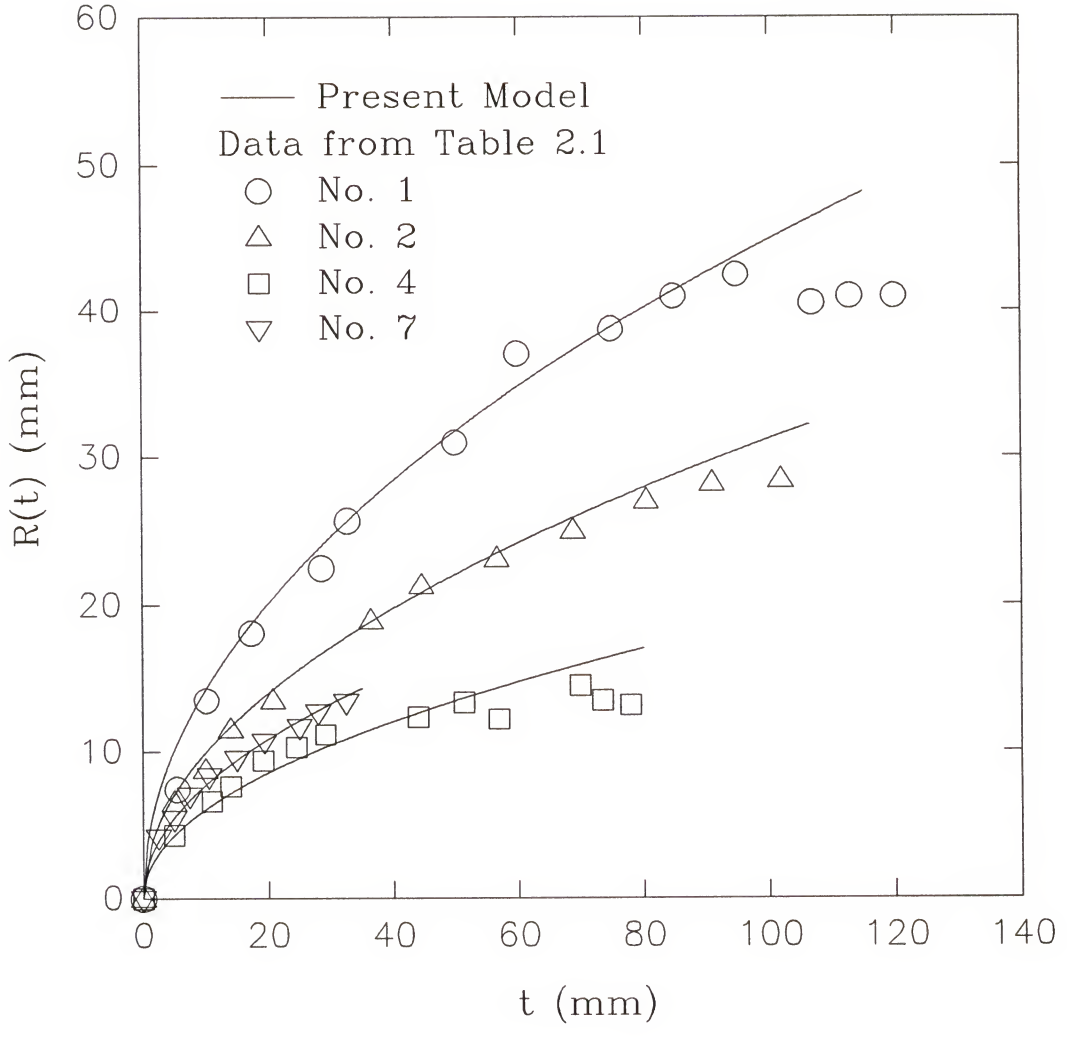

Figure 2.4a Comparison of the bubble growth rate R(t) between the present numerical prediction and the data of Van Stralen et al. (1975) using water as boiling liquid.

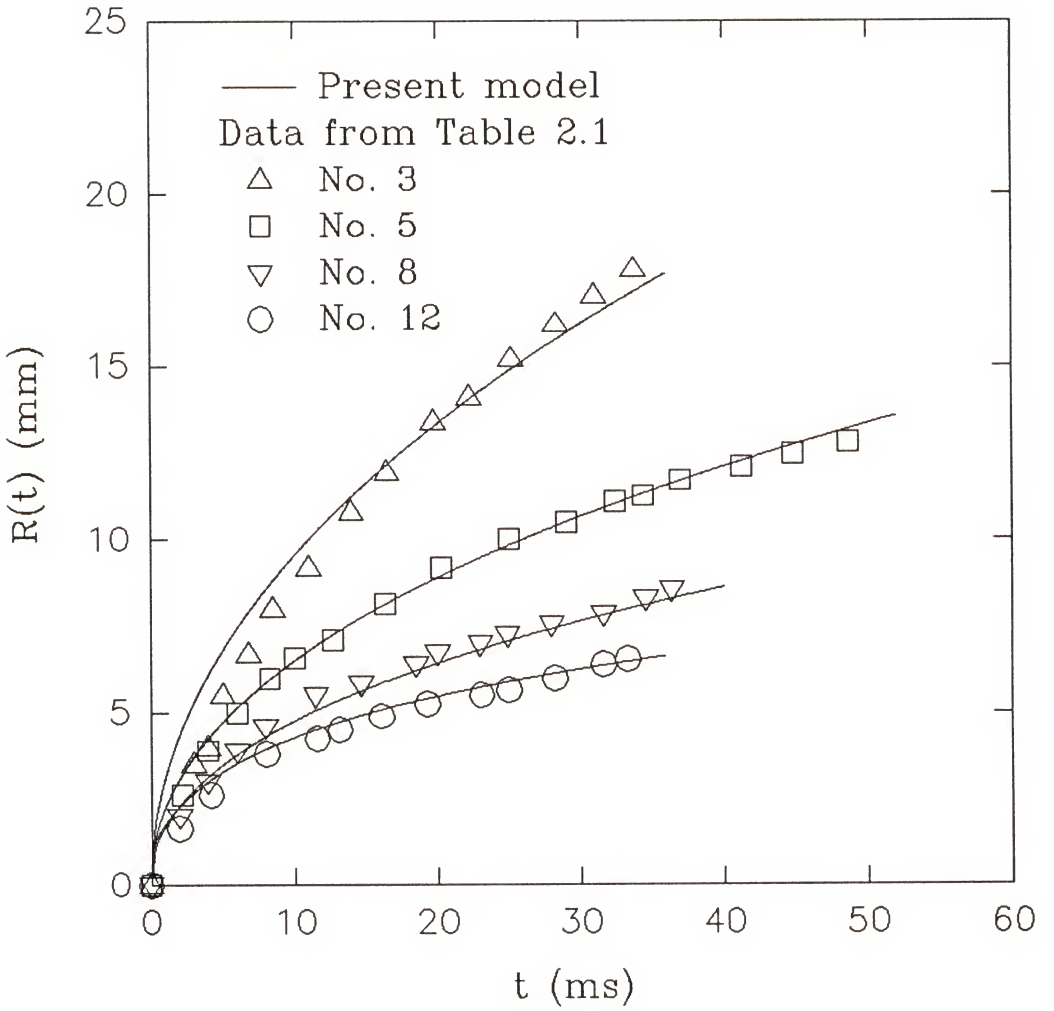

Figure 2.4b Comparison of the bubble growth rate R(t) between the present numerical prediction and the data of Cole and Shulman (1966) using water as boiling liquid.

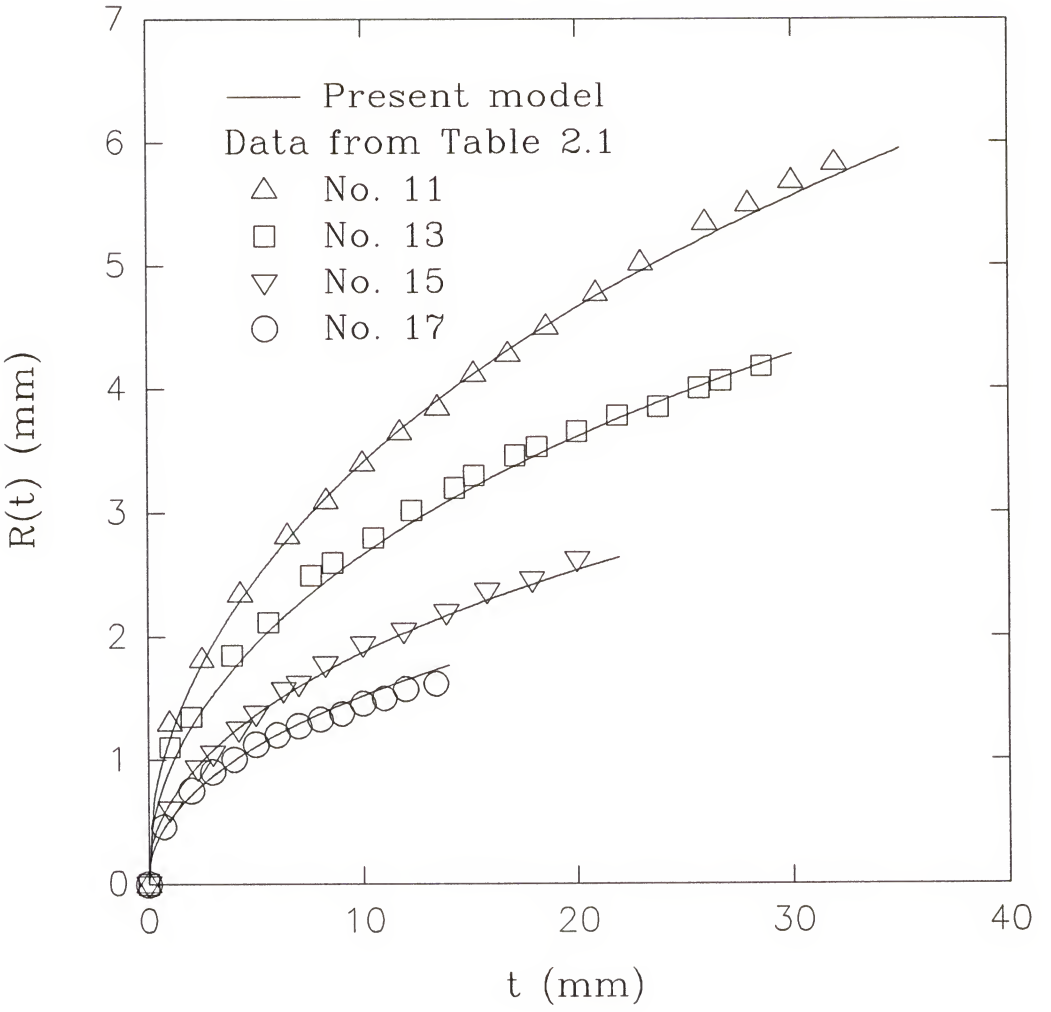

Figure 2.4c Compariison of the bubble growth rate R(t) between the present numerical prediction and the data of Cole and Shulman (1966) using methanol as boiling liquid.

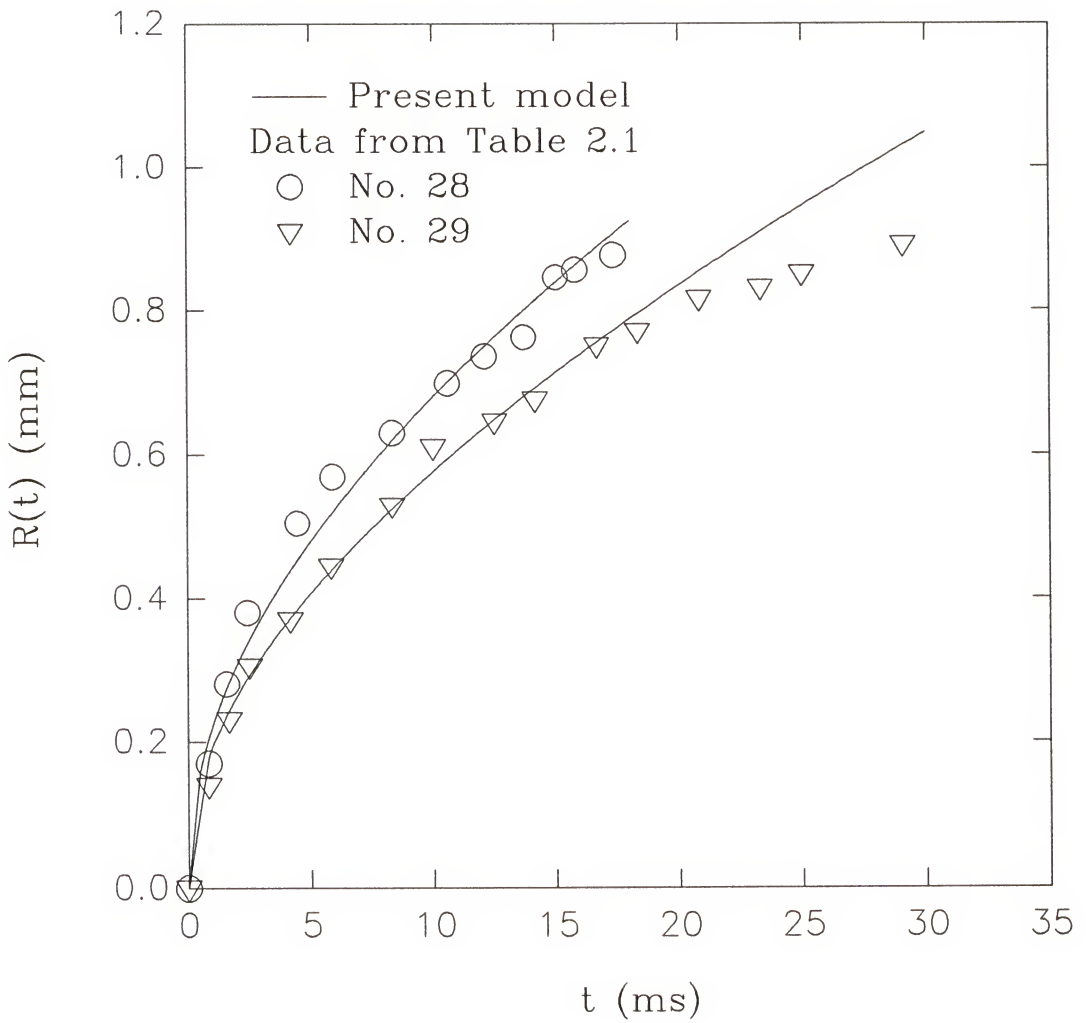

Figure 2.4d Comparison of the bubble growth rate R(t) between the numerical prediction and the data of Staniszewski (1959) using water as boiling liquid at elevated pressure.

and 40 psi), with Ja=11.24 and 9.16. Even at this elevated pressure with relatively low Jacob number, good agreement can still be observed for most of the time. From Figs. 2.4a-d, it is very obvious that R(t) strongly depends on Ja; an increasing Ja results in an increasing growth rate--a well established fact.

It is also noted that at 276 kpa pressure, the present model over-predicts R(t) at the later stage of growth. The data (No. 31 and No. 32 in Table 2.1) by Akiyama et al. (1969) were obtained at even higher pressure. For those two cases the Reynolds number is of O(1), especially at the later stage of growth. Hence, detailed hydrodynamics may need to be properly accounted for in order to improve the prediction. Another source of error for R(t) at low Jacob number may be associated with equation (2.4) in which the energy transfer at the vapor dome between the bubble and the bulk liquid is neglected based on the assumption that bulk liquid is at saturated conditions. This would only cause a small error if R(t) is much larger than the thermal layer thickness, δ_{th}, of the bulk liquid for most of the growth period. At low Ja, the bubble is typically small and, hence, the bubble growth may occur largely within the thermal layer. Under such conditions, the unsteady heat transfer between the vapor dome and the bulk liquid is no longer negligible. From this view point, the present analysis may not be directly applied to very low Jacob

number boiling systems without further study.

2.4 Summary

A numerical analysis is formulated to study the growth of vapor bubbles in saturated heterogeneous boiling. The thermal interaction of the temperature fields in the thin liquid microlayer and in the solid heater must be properly accounted for in order to accurately predict the growth rate of vapor bubbles attached to a heating surface. The vapor bubble shape parameter, C, and the microlayer wedge angle parameter, C_1, are two empirically determined constants which are used in the numerical computation. In particular, the wedge angle parameter, C_1, is obtained by matching the measured and predicted bubble growth rate. It is important to note that once C_1 is correctly specified in the computation, the predicted bubble growth rate compares very well with the reported experimental data over a wide range of conditions during the entire growth period. The empirically determined correlation for C_1 suggests that the liquid Prandtl number, hence the viscosity of the liquid, plays little role in the bubble growth process. A subsequent estimate indicates that the Reynolds number of the bulk liquid motion induced by the bubble is of inviscid nature; thus the viscosity is not important in determining the parameters C and C_1.

The dimensional analysis for the governing equations

and boundary conditions shows that there exists four relevant dimensionless parameters for bubble growth: Jacob number Ja, Fourier number Fo of the solid based on the thickness of the heater and the bubble departure time scale, the liquid-to-solid conductivity ratio κ, and the liquid-to-solid thermal diffusivity ratio α. The Jacob number is the most important one affecting C, C_1, and dimensionless growth rate $\bar{R}(\tau)$. The effects of the four parameters on $\bar{R}(\tau)$ and the thermal fields of the liquid and the slid heater will be discussed in chapter 3.

CHAPTER 3
VAPOR BUBBLE GROWTH IN SATURATED POOL BOILING --PART II. GROWTH RATE AND THERMAL FIELDS

3.1 Background

In Chapter 2 of the present study, the governing equations, the boundary conditions, and the initial conditions for the unsteady energy transfer from the solid heater through the liquid microlayer to the vapor bubble have been systematically formulated. A time varying coordinate system is used to resolve the large temperature variations over a small area beneath the vapor bubble. The bubble shape parameter, C, was correlated with Jacob number based on experimental bubble shape profiles, and the microlayer wedge angle parameter, C_1, was determined by matching the finite difference solution for the growth rate, R(t), with the existing experimental data over a large range of conditions. The numerical results for the bubble growth rate have compared very well with the existing data for the growth rate over a wide range of conditions. From the basic formulation, qualitative analysis, and the result for C_1, it is observed that the Prandtl number has little effect on the growth process.

The problem of vapor bubble growth in saturated

heterogeneous boiling involves many physical properties and boiling conditions: h_{fg}, ΔT_{sat0}, T_{sat}, ρ_v, ρ_ℓ, k_ℓ, k_s, α_ℓ, α_s, ν_ℓ, q'' (or q'''), and H (see nomenclature) which appear in the governing equations for the three phases, boundary conditions, and initial conditions. The dependent variables are R(t), T_ℓ, and T_s. The liquid kinematic viscosity ν_ℓ is listed above formally because in general the bubble shape depends on the hydrodynamics; it appeared in a previous investigation (Cooper and Lloyd, 1969). For intermediate and high Jacob numbers, it has been shown in Chapter 2, based on a qualitative estimate for the Reynolds number and an examination of existing bubble growth rate data, that ν_ℓ is not important. No particular attention was paid to the explicit effects of q'' (or q''') on R(t) because the contributions are usually small during the majority of the growth period. However, the implicit effects of q'' (or q''') through ΔT_{sat0} on R(t) are important and were incorporated.

Further examination of the dimensionless forms of the governing equations, boundary and initial conditions indicated that the dimensionless growth rate

$$\bar{R}(\tau) = \frac{R(t)}{R_c(t_d)} = \frac{R(\tau = t/t_d)}{R_c(\tau = 1)} \tag{3.1}$$

only depends on four dimensionless parameters: Jacob number Ja, Fourier number Fo, liquid-to-solid conductivity ratio κ, and liquid-to-solid diffusivity ratio α. In the above, R_c

is the solution for the growth rate based on a constant wall temperature and t_d is the time scale for bubble departure estimated from the analysis of Zeng et al. (1993a). Hence the complexity in understanding and describing the bubble growth rate is significantly reduced.

In order to further understand the dynamics governing vapor bubble growth in heterogeneous boiling, a systematic investigation is presented which considers the effects of (Ja, Fo, κ, α) on the growth rate $\bar{R}(\tau)$ and the thermal fields of the liquid and solid. The numerical results show that the liquid temperature in the microlayer is practically linear for a wide rage of conditions. The analysis and numerical solution have elucidated, for the first time, the development of the unsteady thermal field in the heater during a very short period of time through a very small volume which resides beneath a growing vapor bubble. Experimental techniques described in the existing literature are not capable of resolving the fine temporal and spatial scales considered investigation.

3.2 Effect of Ja, Fo, κ, and α on $\bar{R}(\tau)$

Since experimental measurements which reveal the effect of κ (or α, Fo) while holding Ja and other parameters constant are not available, the parametric study is especially useful for further understanding of the bubble growth process. In what follows, the effects of varying Ja,

Fo, κ, and α will be examined separately.

Fig. 3.1a shows the effect of varying Ja (from 1 to 1000) on $\bar{R}(\tau)$ at Fo=1, κ=0.005 and α=0.005. Because $R_c(t_d)$ strongly depends on Ja as indicated by equations (2.18) and (2.38), the most significant part of the Jacob-number-effect on R(t) has been accounted for by $R_c(t_d)$. Therefore the difference in $\bar{R}(\tau)$ among different values of Ja in Fig. 3.1a mainly reflects the effect of the coupling of the thermal fields between the solid heater and liquid microlayer. It will be shown in section 3.3 that the liquid temperature profile in the microlayer is practically linearly. Hence $\frac{\partial \theta_\ell}{\partial \bar{z}_\ell}$ practically does not vary with $\bar{z}_\ell$ during bubble growth. On the liquid-solid interface, since $C_1 Pr_\ell^{1/2} \propto Ja^{0.752}$, a small Ja implies a small $\frac{\partial \theta_\ell}{\partial \bar{z}_\ell}$ for a given $\frac{\partial \theta_s}{\partial \bar{z}_s}$, which results in a smaller $\bar{R}(\tau)$, as seen from equations (2.23) and (2.31). Because $\bar{R}(\tau)$ also appears in equation (2.31), a smaller $\bar{R}(\tau)$ is consistent with a smaller $\frac{\partial \theta_\ell}{\partial \bar{z}_\ell}$.

Fig. 3.1b shows the effect of changing Fo (from 0.01 to 10000) for Ja=10, κ=0.005, and α=0.005 for $\tau=t/t_d \leq 1$. Little difference in $\bar{R}(\tau)$ between Fo=0.01 (a thicker heater) and Fo=1 is observed for this set of parameters. As Fo increases, say due to decreasing thickness of the heater, H, or longer departure time, t_d, $\bar{R}(\tau)$ decreases. The decrease in H implies a reduction of the heater thermal capacity which will reduce the growth rate. Under otherwise identical conditions, a larger value of t_d implies more

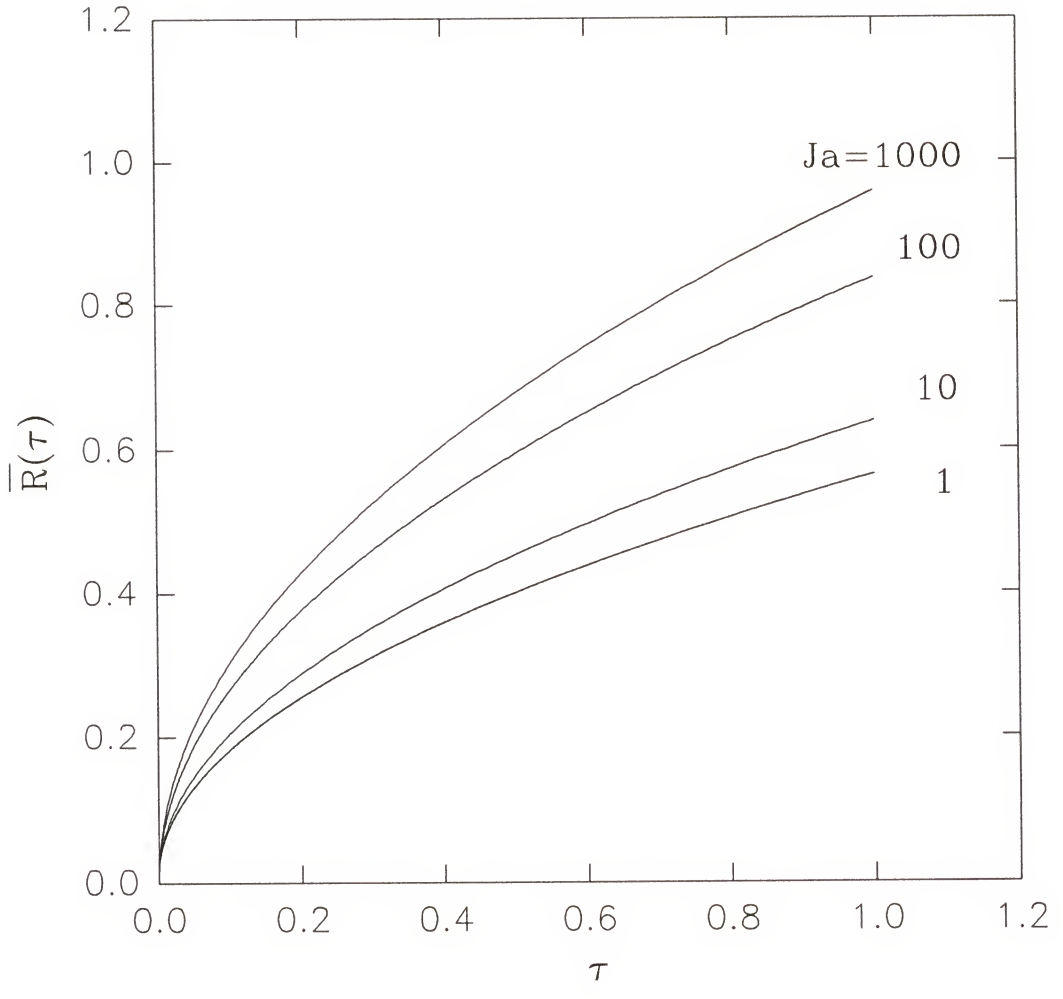

Figure 3.1a Parametric dependence of the normalized growth rate, Ja=1, 10, 100 and 1000 at (Fo,κ,α)=(1,0.005,0.005).

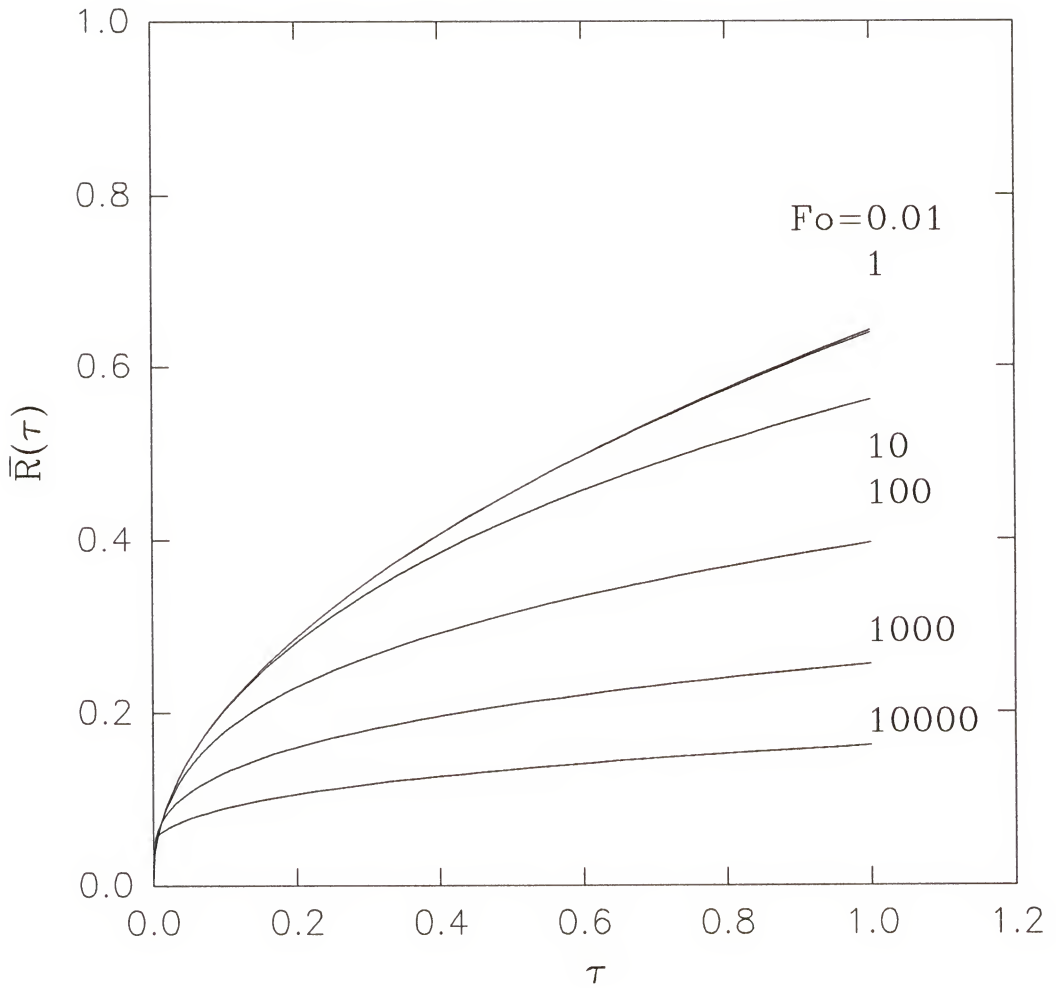

Figure 3.1b Parametric dependence of the normalized growth rate, Fo=0.01, 1, 10, 100, 1000 and 10000 at (Ja,κ,α)=(10, 0.005, 0.005).

energy is taken from the heater between t=0 (τ=0) and t=t_d (τ=1). Hence the growth rate at later stages, when τ is close to 1, is slower for larger t_d in comparison with that for smaller t_d. To better understand the effect of Fo on the growth rate, consider two cases: 1) Fo_1=1 and 2) Fo_2=10 while all other parameters are held the same. If the computation for R_1 stops at τ_1=10 while that for R_2 stops at τ_2 =1, the results for the two dimensional growth rates are identical if the same dimensional time is used, i.e., $R_1(Fo_1\tau_1)=R_2(Fo_2\tau_2)$ if $\tau_1 = \frac{Fo_2}{Fo_1}\tau_2$. This simply means that if one is interested in R(t) for $0 \le t < \infty$ the use of Fo is unnecessary and the relevant time scale should be H^2/α_s. Instead, an instantaneous Fourier number $Fo' = \frac{\alpha_s t}{H^2}$ should be used to characterize the thermal interaction. In one-g boiling, the bubble departs at some finite time t_d; thus no experimental information is available for R(t) beyond t_d. Since it is always desirable to sufficiently resolve the growth rate between t=0 and t=t_d, the use of τ=t/t_d and Fo makes the computation and the interpretation of R(t) considerably easier. It is also noted that as $t \to \infty$, $\frac{dR}{dt} \to 0$ because there is insufficient energy in the heater underneath the microlayer to sustain the growth. This scenario is equivalent to the case when $Fo \to \infty$, as was observed in the computations.

Fig. 3.1c shows the effect on $\bar{R}(\tau)$ of varying conductivity ratio κ (from 0.0005 to 0.05) at Ja=10, Fo=1,

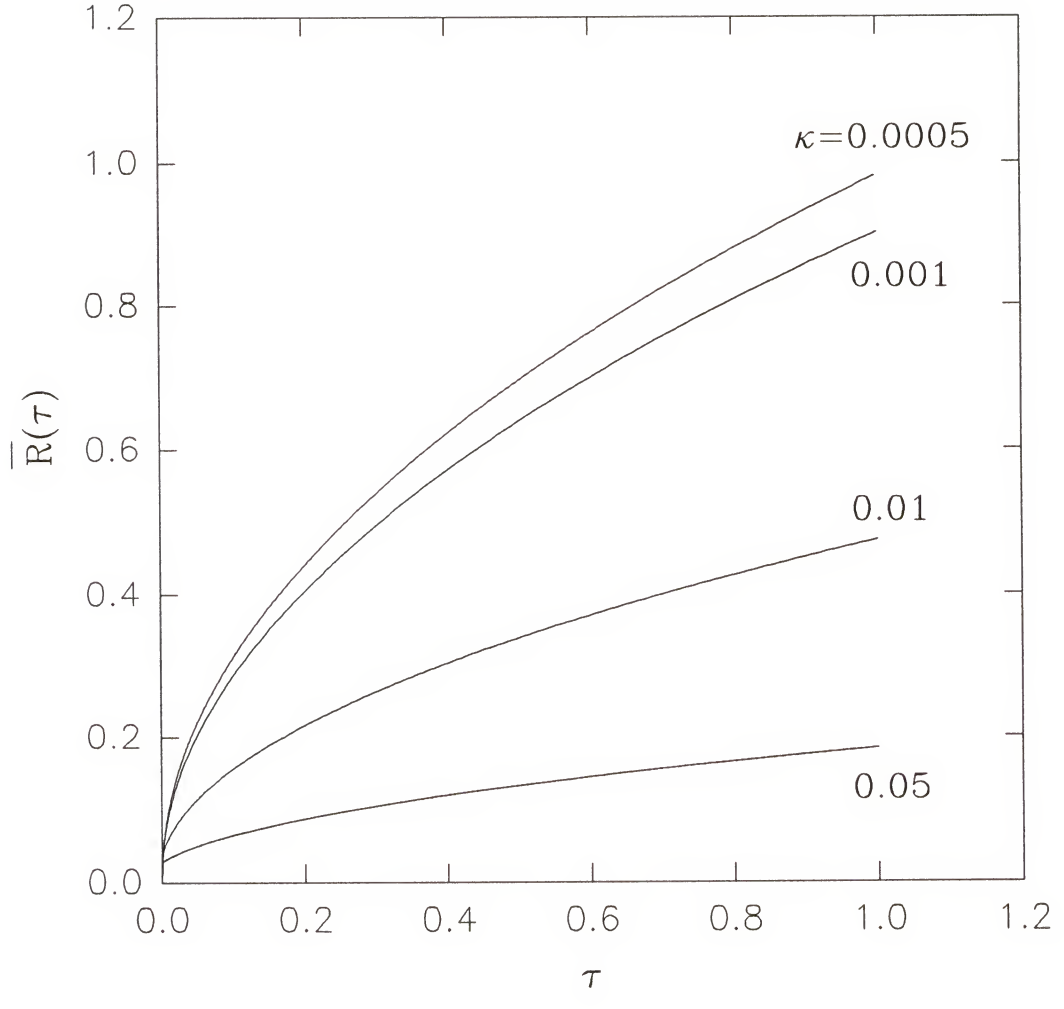

Figure 3.1c Parametric dependence of the normalized growth rate, κ=0.0005, 0.001, 0.01 and 0.05 at (Ja, Fo, α)=(10, 1, 0.005).

and α=0.005. Since κ appears only in the boundary condition (2.31), it is easy to see that a larger κ (which may result from using a low-conductivity solid heater) implies a smaller $\frac{\partial\theta_\ell}{\partial\bar{z}_\ell}$ for a given $\frac{\partial\theta_s}{\partial\bar{z}_s}$. Of course, $\frac{\partial\theta_s}{\partial\bar{z}_s}$ is not fixed; it increases with increasing κ as will be shown in Fig. 3.7. Nevertheless the net effect of increasing κ such that $\frac{1}{\kappa}\frac{\partial\theta_s}{\partial\bar{z}_s}$ decreases. A smaller $\frac{\partial\theta_\ell}{\partial\bar{z}_\ell}$ naturally implies a smaller amount of energy is conducted to the bubble which results in a smaller growth rate. Hence $\bar{R}(\tau)$ decreases as κ increases and vice versa, as shown in Fig. 3.1c.

Fig. 3.1d shows the effect on $\bar{R}(\tau)$ of changing α (0.0005 to 0.05) at Ja=10, Fo=1, and κ=0.005. Contrary to the effect of κ, an increasing α results in an increasing $\bar{R}(\tau)$. However, equation (2.31) indicates that $\frac{\partial\theta_\ell}{\partial\bar{z}_\ell}$, hence $\bar{R}(\tau)$, increases with increasing $\alpha^{1/2}$. From Figs. 3.1c-d, it is seen that when κ or α changes, say, by a factor of 10, the resulting change in $\bar{R}(\tau)$ is larger in Fig. 3.1c than in Fig. 3.1d. This simply results from the factor $\alpha^{1/2}/\kappa$ in equation (2.30).

To recapitulate, the effects of Ja, Fo, κ and α on the normalized growth rate $\bar{R}(\tau)$ are: 1) increasing Ja and α will result in an increasing $\bar{R}(\tau)$; 2) increasing Fo and κ will result in a decreasing $\bar{R}(\tau)$.

3.3 Thermal Field of the Liquid Microlayer

It is not clear from equation (2.25) what the shape of

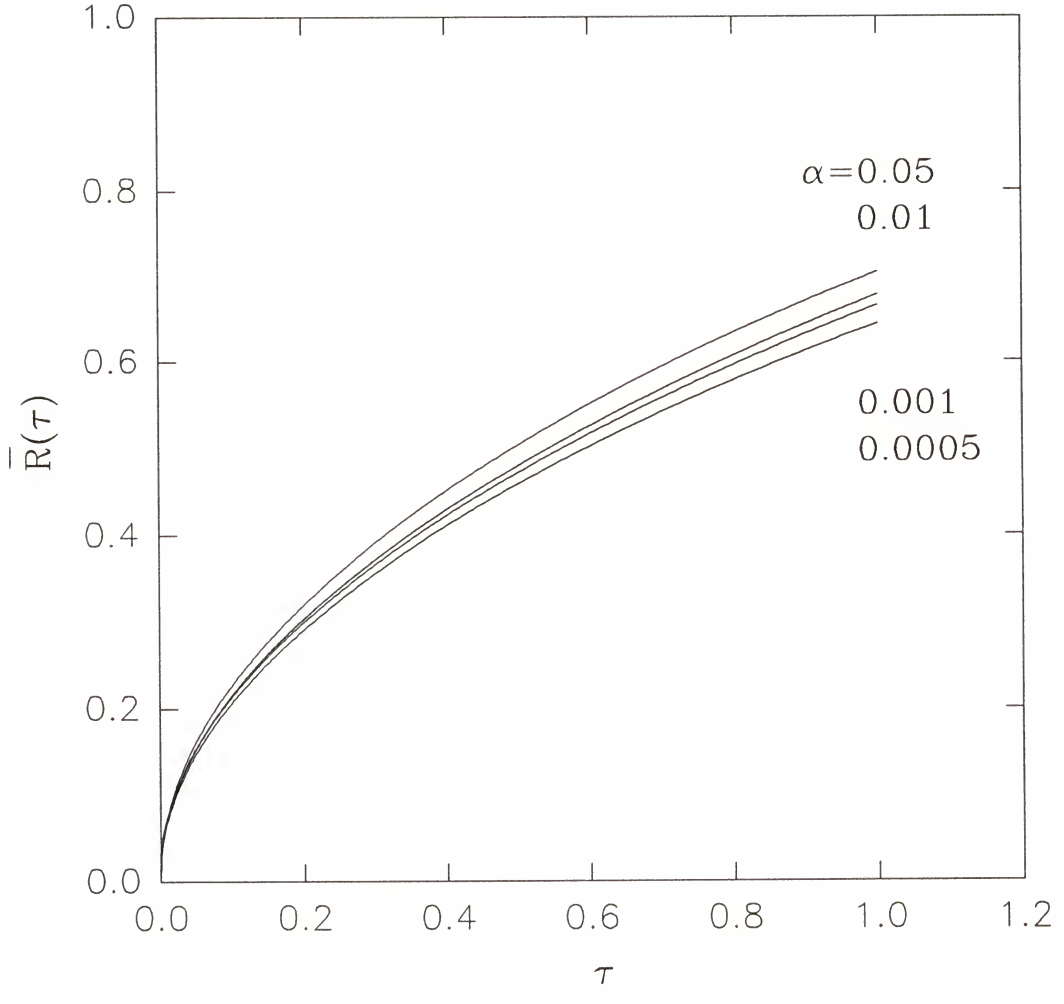

Figure 3.1d Parametric dependence of the normalized growth rate, α=0.0005, 0.001, 0.001 and 0.05 at (Ja, Fo, κ)=(10, 1, 0.005).

the liquid microlayer temperature θ_ℓ will be in the z-direction under general conditions. Only when C_1Pr_ℓ is small, it is clear that the temperature θ_ℓ will be almost linear in $\bar{z}_\ell$ because diffusion the term in (2.25) is clearly dominant. In order to qualitatively assess the linearity of θ_ℓ from a linear profile, we calculate the change in the slope, $\frac{\partial\theta_\ell}{\partial\bar{z}_\ell}$, relative to the slop. Since the change in the slope can be conveniently characterized by the second order derivative, $\frac{\partial^2\theta_\ell}{\partial\bar{z}_\ell^2}$, we use the following parameter

$$\Gamma(\tau) = \frac{1}{N}\sum_{n=1}^{N}\left|\frac{\partial^2\theta_\ell}{\partial\bar{z}_\ell^2}\Big/\frac{\partial\theta_\ell}{\partial\bar{z}_\ell}\right| \tag{3.2}$$

to represent the deviation from the linear profile. For $\Gamma<<1$ the deviation of θ_ℓ from a linear profile is quite small and as $\Gamma\to0$, the profile is exactly linear. In the above, the summation Σ is carried over N interior grid points of the computational domain within the microlayer.

Fig. 3.2a shows the variation of Γ during the bubble growth period, $0<\tau\leq1$, for: i) (Fo,κ, α)=(1, 0.005, 0.005) with Ja=10 and 1000; and ii) (Ja, κ, α)=(10, 0.005, 0.005) with Fo=10 and 1000. Fig. 3.2b shows the dependence of Γ on κ and α: i) (Ja, Fo, α)=(10, 1,0.005) with κ=0.05 and 0.0005; ii) (Ja, Fo, κ =(10, 1, 0.005) with α=0.05 and 0.0005. The largest value of Γ always occurs at the initial time step. Under otherwise identical conditions, a larger Ja results in a larger Γ. This is due to the fact that

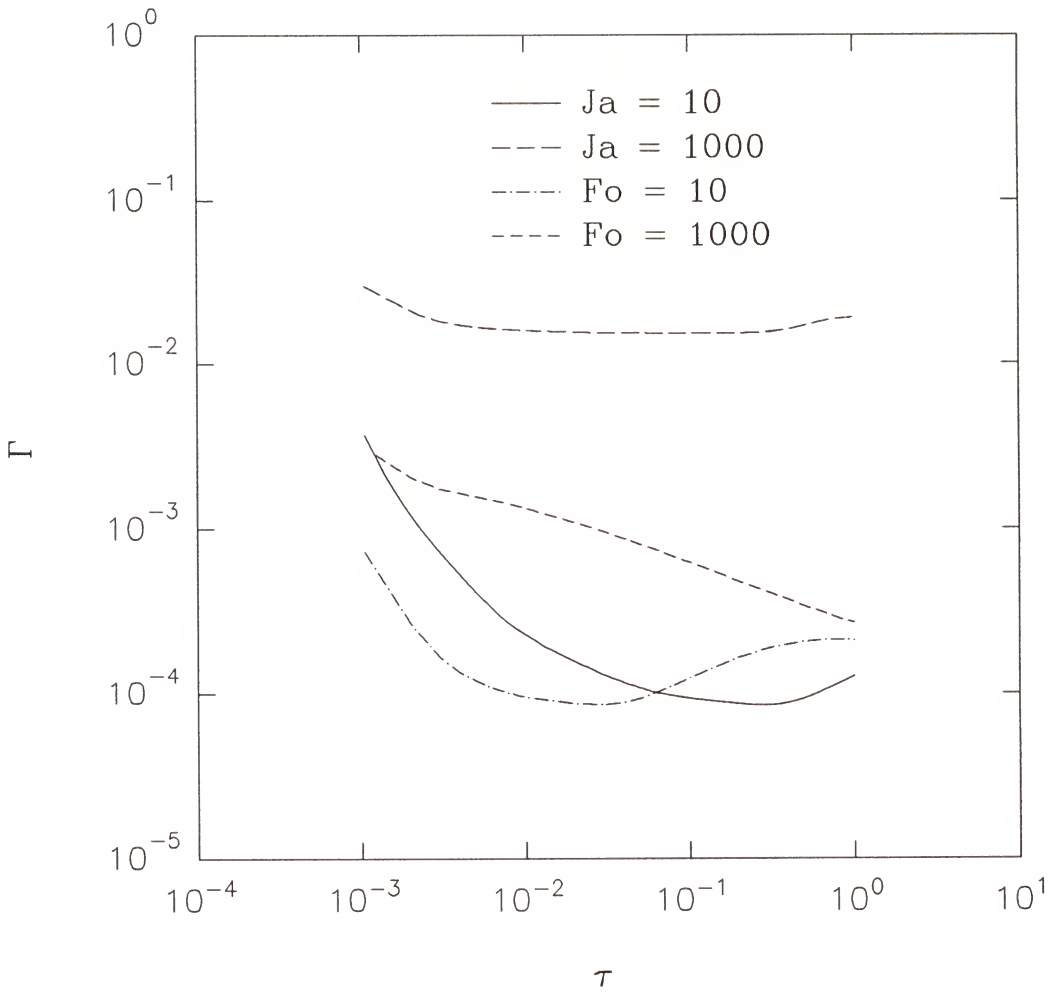

Figure 3.2a Deviation from the linearity of the liquid temperature profile in the microlayer, (Fo,κ,α)=(1, 0.005, 0.005) with Ja=10 and 1000 and (Ja,κ,α)=(10, 0.005, 0.005) with Fo=10 and 1000.

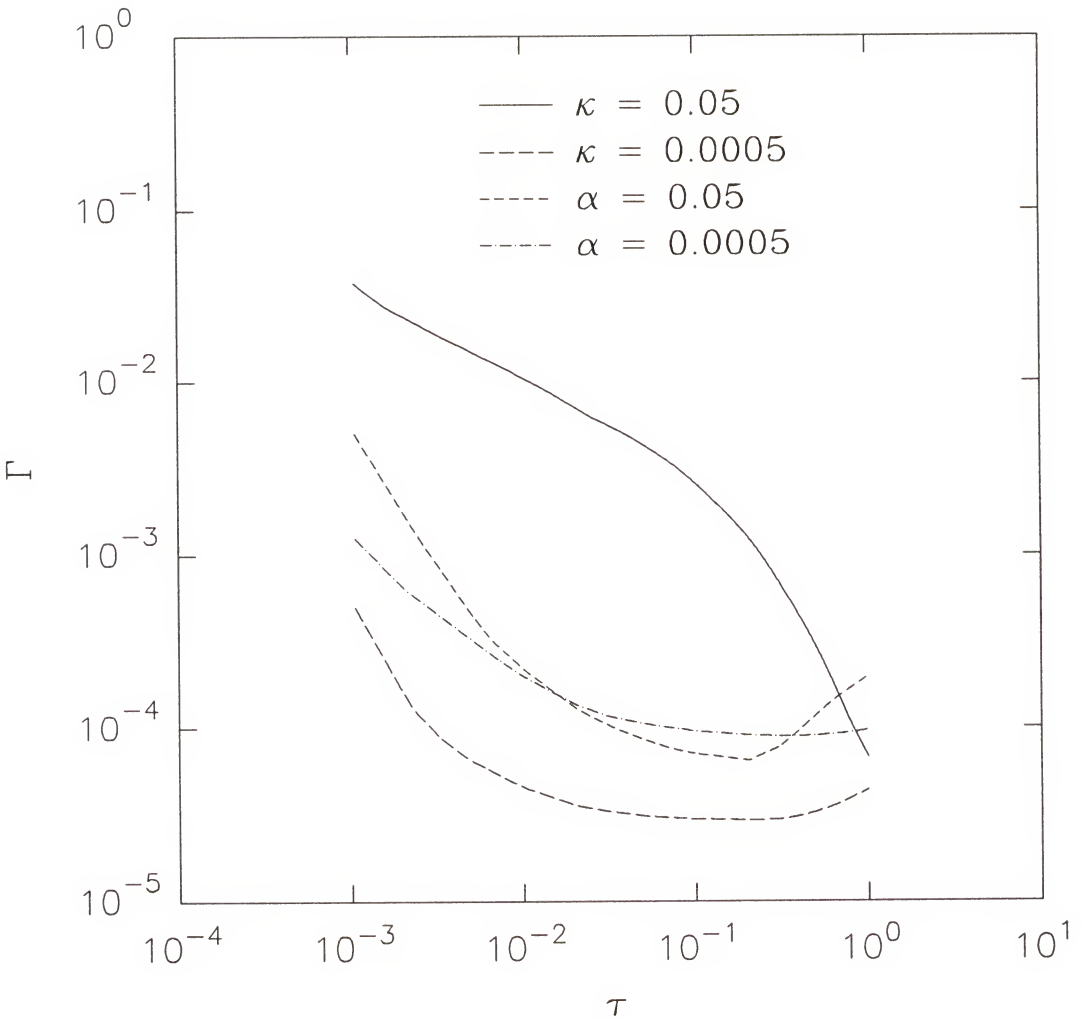

Figure 3.2b Deviation from the linearity of the liquid temperature profile in the microlayer, (Ja,Fo,α)=(10, 1, 0.005) with κ=0.0005 and 0.05 and (Ja,Fo,κ)=(10, 1, 0.005) with α=0.0005 and 0.05.

larger Ja results in a larger wedge angle, or thermal capacity, of the microlayer, as shown by equations (2.5) and (2.38). For Ja=10, $\Gamma<0.01$ for $\tau>0.001$. Even for Ja=1000, Γ is less than 2% for $\tau>0.01$ (or for 99% of the growth period). No substantial difference in Γ is observed as Fo is changed from 10 to 1000; the values of Γ are all less than 1%. A larger Γ occurs at $\kappa=0.05$ (a large value) because a large κ is associated with a rapid drop of the solid temperature on the liquid-solid interface underneath the microlayer, as will be demonstrated in Fig. 3.7. This larger transient variation of the temperature on the boundary causes the microlayer temperature to deviate more from a linear profile because the thermal diffusion term in equation (2.25) is not as dominant as it is with a smaller transient variation. Little variation of Γ is observed when α is changed from 0.0005 to 0.05. Even for $\kappa=0.05$, the largest Γ is only about 3-4% at $\tau=0.001$ as shown in Fig. 3.2b. It also needs to be commented that Γ is sensitive to the initial time, τ_0, when the computation is initiated. In Fig. 3.2, $\tau_0=0.0005$ was used and the results are presented for $\tau>0.001$. When the initial time τ_0 is reduced to 0.00001, Γ at $\tau=0.001$ is further reduced by a factor of 2 or more. The reason is that the initial conditions for the liquid and solid temperatures given by (2.16-17) are inconsistent with the actual thermal fields, although the inconsistency does not affect the accuracy of the bubble

growth rate. Hence, the actual values of Γ may be less than what were shown. The result of this parametric investigation is that the liquid temperature profile within the microlayer can be taken as linear for practical purposes. This result will be used as a starting point in chapter 4 to develop a simplified bubble growth rate model.

3.4 Thermal Field of the Solid Heater

To understand the energy transfer process in the solid heater, a qualitative description of the solid temperature field for a thick heater, Fo<<1, is first given based on the governing equations without resorting to extensive computations. For a thick heater, the temperature on the bottom of the solid layer is unaffected by the heat transfer from the solid to liquid for $t<t_d$. When energy is taken away from the solid, an unsteady thermal boundary layer develops in the z-direction, there is no convection term in (2.27). Hence, the relevant length scale for Fo<<1 in the z-direction is $\delta_z=\sqrt{\alpha_s t}$, which is a measure of the temperature penetration depth in the z-direction. In the r-direction, θ_s is affected strongly by the movement of the bubble (through the microlayer) and the relevant "convective" length scale is thus $\delta_{rc}=R_b(t)$. Over a distance of $r\sim\delta_{rc}$, θ_s changes appreciably. It is noted that $r=R_b(t)$ is also the location of the discontinuity in the boundary condition at $z_s=0$ given by equations (2.14b) and (2.15b. As

a rough estimate, the constant wall temperature solution for the bubble radius given by equation (2.18) can be used to characterize δ_{rc}. If dimensionless isothermal lines, θ_s, are sketched, the contours would resemble ellipses with δ_{rc} and δ_z being the major and minor axes, as shown in Fig. 2.1. Since

$$\frac{\delta_{rc}}{\delta_z} = \frac{C^3}{f(C)} \frac{Ja}{C_1 Pr_\ell^{1/2}} \left(\frac{\alpha_\ell}{\alpha_s} \right)^{1/2} \tag{3.3}$$

is roughly independent of time, the θ_s-contours are expected to expand in a form of similar ellipses. For the case with large Ja, $\delta_{rc}/\delta_z >> 1$, the penetration of the temperature in z-direction can be quite shallow.

When H is not large or Fo~O(1), the foregoing description on the qualitative features of the temperature contours are still valid near the nucleation site for small t as long as the instantaneous solid Fourier number is small, i.e., $Fo' = \frac{\alpha_s t}{H^2} \ll 1$. At later times, however, the temperature contour will be drastically different from those sketched in Fig. 2.1. For Fo~O(1) or larger, we resort to the computational results in order to elucidate the thermal fields of the heater.

Fig. 3.3a shows the four computed temperature contours corresponding to case No.22 in Table 2.1 with Ja=23.4, Fo=0.057, κ=0.0073, and α=0.00577, at four different times: τ=0.05, 0.1, 0.5, and 1. The parameter C_1=0.12 is taken

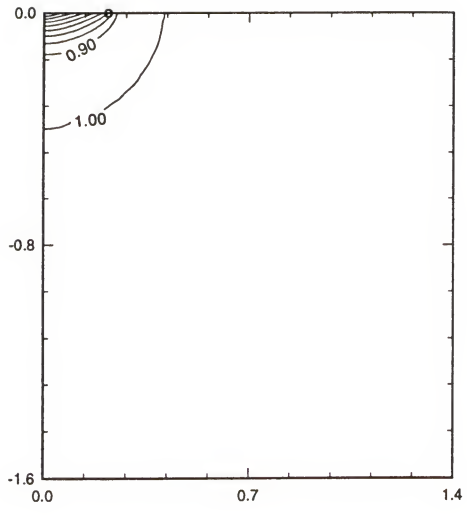

τ=0.05

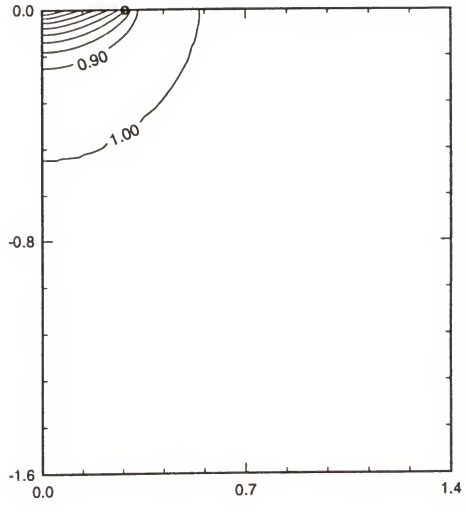

τ=0.1

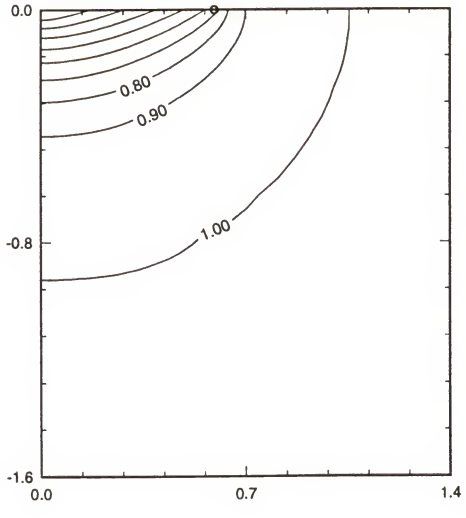

τ=0.5

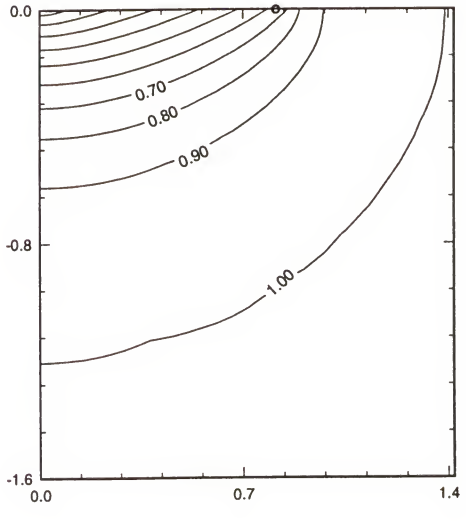

τ=1.0

Figure 3.3a Contours of temperature θ_s in a thick heater at (Ja,Fo,κ,α)=(23.4, 0.057,0.0073,0.00577) for τ=0.05, 0.1, 0.5 and 1. This condition corresponds to the experiment of Hospeti and Mesler (1969). All dimensions are in mm.

from Table 2.1. These four times roughly cover the early stages, later stage, and "departure" stage of the growth process. Since Fo<<1, the heater is quite thick and foregoing asymptotic description is valid for all time. The circle marker at z=0 is the location of the microlayer edge, $r=R_b(t)$. It is clearly seen that the temperature contours in the solid penetrate down and move to the right at a similar rate as the bubble grows. Fig. 3.3b shows the θ_s-contours corresponding to case No.19 in Table 2.1, with Ja=25.3, Fo=63.3, κ=0.00173, and α=0.00144, at four different times: τ=0.05, 0.1, 0.5, and 1. Since Fo>>1, the heater is very thin and the asymptotic description is not valid for all times. Nevertheless, for τ=0.05, the θ_s-contours in a small region near the bubble center, $r<<R_b(t)$, still agree with the asymptotic description. On a larger scale, $r\sim R_b(t)$ or $\bar{r}\sim 1$, the θ_s-contours between the case of Fo>>1 and Fo<<1 display a drastic difference. For a very thick heater, the heat flux in the z-direction from below is always maintained. For a thin heater the thermal capacity is small. As t increases, θ_s-contours penetrate down and reach the bottom of the heater; hence the thermal field near the liquid-solid interface, which determines the energy transfer to the bubble via the microlayer, is also influenced by the bottom of the heater. The growth of the bubble quickly depletes the energy stored in the region $0\le r\le R_b(t)$ and $-H\le z_s\le 0$. To maintain bubble growth, albeit

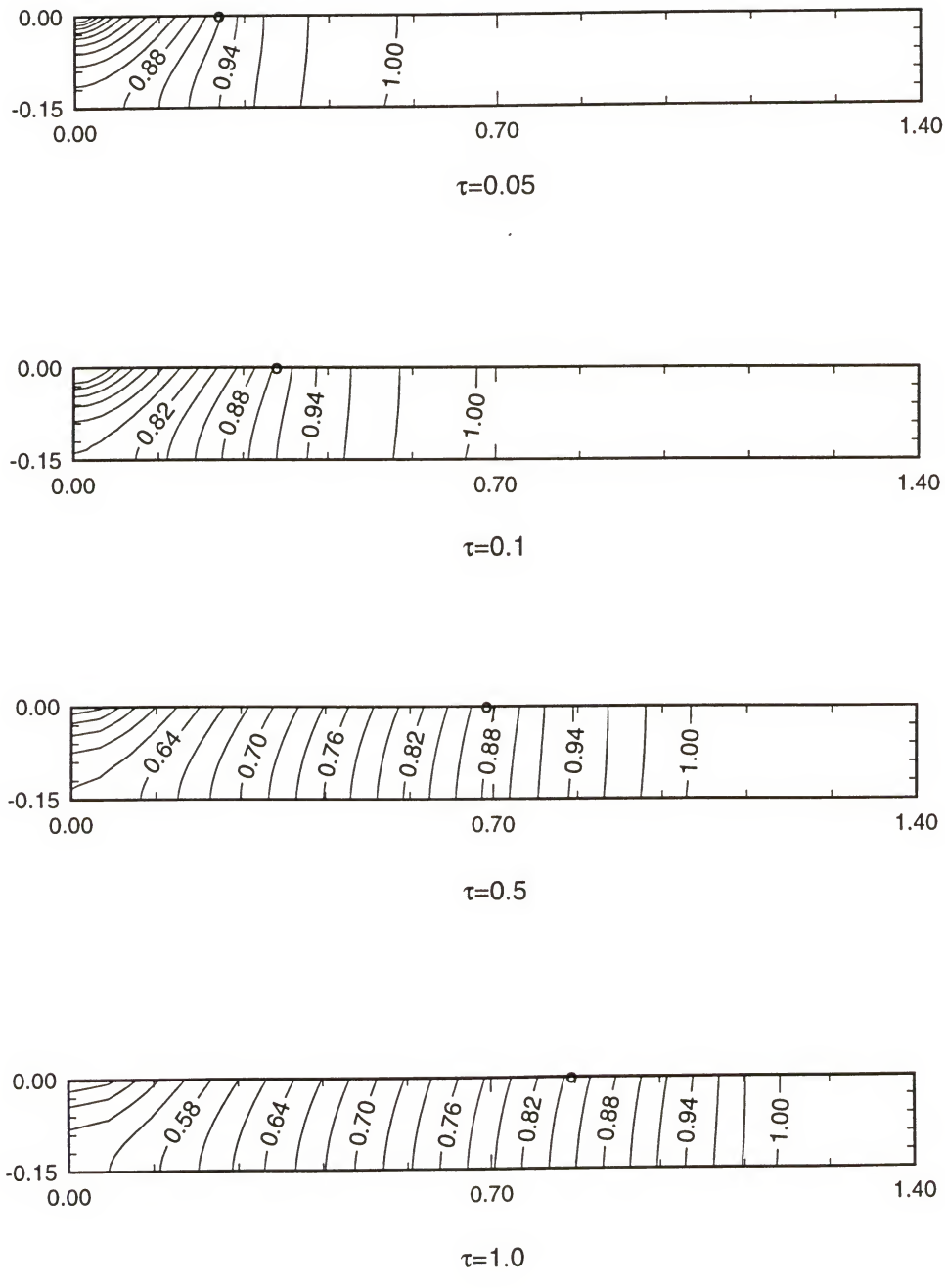

Figure 3.3b Contours of temperature θ_s in a thin heater at (Ja,Fo,κ,α)=(25.3,63.3,0.00173,0.00144) for τ=0.05, 0.1, 0.5 and 1. This condition corresponds to the experiment of Staniszewski (1959). All dimensions are in mm.

slow, energy must be drawn from the region outside $r=R_b(t)$. This creates an energy flow in the negative r-direction outside $r=R_b(t)$ within the thin heater. The relatively long distance the energy must flow, due to conduction, certainly results in a slower rate of energy transfer to the bubble and hence a slower vapor bubble growth rate. This qualitatively explains the discerned decreasing growth rate with increasing Fo shown in Fig. 3.1b. Another interesting and useful revelation from Fig. 3.3b is that even for a very thin heater, the temperatures at the bottom and at the interface in $r \leq R_b(t)$ are not the same. Hence, the temperature measurement on the bottom of heater fails to present the actual thermal field near the liquid-solid interface underneath the rapidly growing vapor bubble.

To parametrically examine the effects of Ja, Fo, κ and α on the solid temperature field during the growth period, two particular locations are selected: the centerline $\bar{r}=0$ and the liquid-solid interface $\bar{z}_s=0$. Temperatures at four times are examined: $\tau=0.05$, 0.1, 0.5 and 1 which represent the early stages, later stage and "departure" stage of bubble growth.

3.4.1 Effect of Ja

Figs. 3.4a-d show $\theta_s(\bar{z}_s)$ at $\bar{r}=0$, Fo=1, $\kappa=0.005$, and $\alpha=0.005$ with Ja=1,10, 100 and 1000. The growth rate for Ja=1 is smaller compared with that for Ja=1000; hence, the energy removed from the solid is less for Ja=1 than for

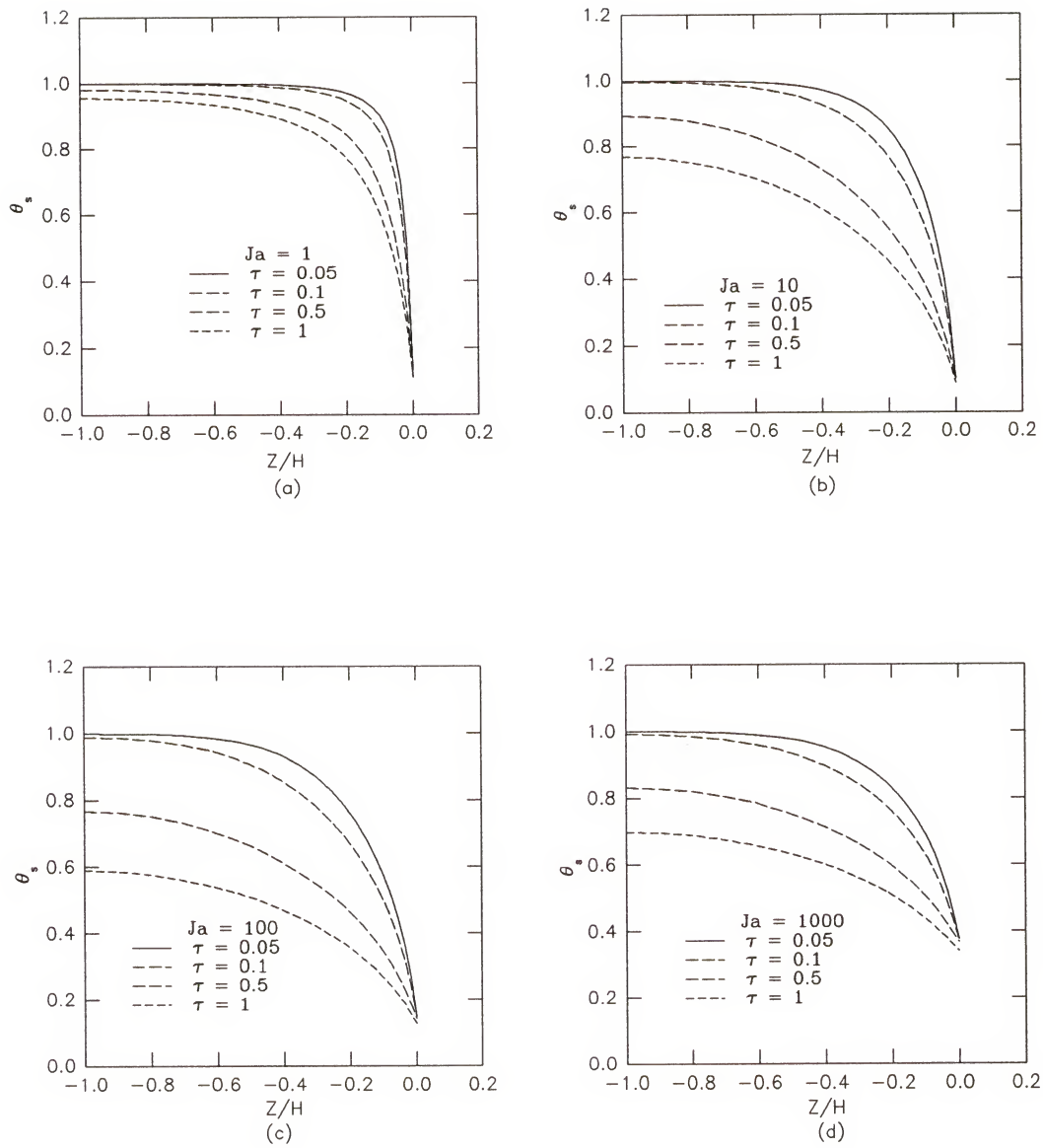

Figure 3.4 Effect of Jacob number Ja on the solid heater temperature θ_s along the centerline at various times (τ=0.05, 0.1, 0.5 and 1) for (Fo,κ,α)=(1, 0.005, 0.005). (a) Ja=1; (b) Ja=10; (c) Ja=100 and (d) Ja=1000.

Ja=1000. While the temperature θ_s near the bottom is nearly equal to one for Ja=1, θ_s through the whole heater (at $\bar{r}=0$) is reduced for Ja=100 and 1000 due to a large amount of energy removed from the heater. It also appears that the thermal diffusion in the z-direction is enhanced with increasing Ja; although it is clear from (2.27) that the diffusion in the z-direction is independent of Ja. To understand this phenomena the radial variations of $\theta_s(\xi=r/R_c(t_d))$ are examined next. Figs. 3.5a-d show the development of the thermal layer in the radial direction at (Fo, κ, α)=(1, 0.005, 0.005) for Ja=1, 10, 100 and 1000. Also marked on each curve are the locations of the microlayer edge, $r=R_b(t)$ or $\bar{r}=1$. For Ja=1000, there is hardly any thermal diffusion in the r-direction beyond $r=R_b(t)$ during the entire growth process. For Ja=1, very significant thermal diffusion in the r-direction can be identified for $r>R_b(t)$, in contrast to the very small diffusion of θ_s in the z-direction at the same Ja shown in Fig. 3.4a.

To elucidate the effect of Ja on the development of the thermal field within the solid, especially in the z-direction, equation (2.27) is revisited. The second term on the left-hand side is the convective energy transport due to the bubble growth. The first term on the RHS is the energy transport due to thermal diffusion in the

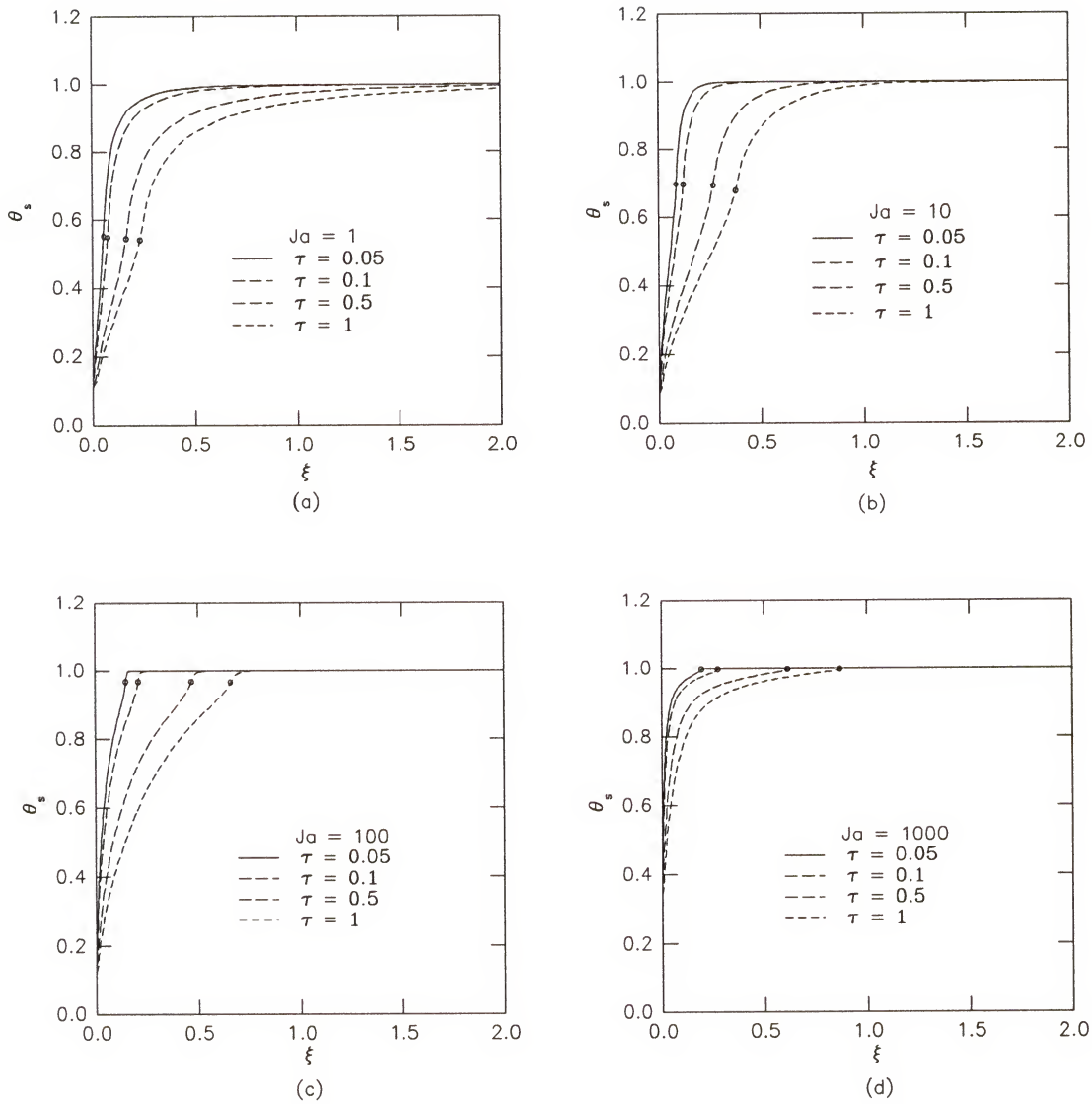

Figure 3.5 Effect of Jacob number Ja on θ_s on the liquid-solid interface at various times for (Fo,κ,α)=(1, 0.005, 0.005). (a) Ja=1; (b) Ja=10; (c) Ja=100 and (d) Ja=1000. Symbols indicate the edge of the microlayer, r=R_b(t).

r-direction. For a fixed (Fo, κ, α), the factor $\frac{f^2(C)C_1^2 Pr_l}{\alpha C^6 Ja^2}$, hence the extent of r-diffusion is large at small Ja and it decreases with increasing Ja. As Ja increases, the growth rate increases so that more energy from the heater is transferred to the bubble via the microlayer, as discussed previously. Since the r-diffusion is decreasing with increasing Ja, the z-diffusion must increase in order to provide the thermal energy to the growing bubble. This explains the trend in $\theta_s(\bar{z}_s)$ shown in Figs. 3.4a-c for Ja=1, 10, 100. However, as Ja becomes quite large, the extent of r-diffusion is limited. Since the bubble grows so fast, the convective heat transfer due to the bubble growth becomes important in that the edge of the expanding microlayer always experiences a solid surface temperature that is close to 1. Hence, at high Ja, the energy transfer to the microlayer is accomplished within a relatively thin thermal boundary layer near the liquid-solid interface; within this boundary layer, the r-convection and the z-diffusion are the dominant terms in equation (2.27). Thus, the diffusion in the z-direction at Ja=1000 does not penetrate as far toward the bottom of the heater as in the case when Ja=100.

3.4.2 Effect of Fo

Figs. 3.6a-d show $\theta_s(\bar{z}_s)$ at $\bar{r}=0$ for (Ja, κ, a) = (10, 0.005, 0.005) with Fo = 0.01, 1, 10, and 1000. For Fo=0.01, the bottom portion of the heater is unaffected by the growth

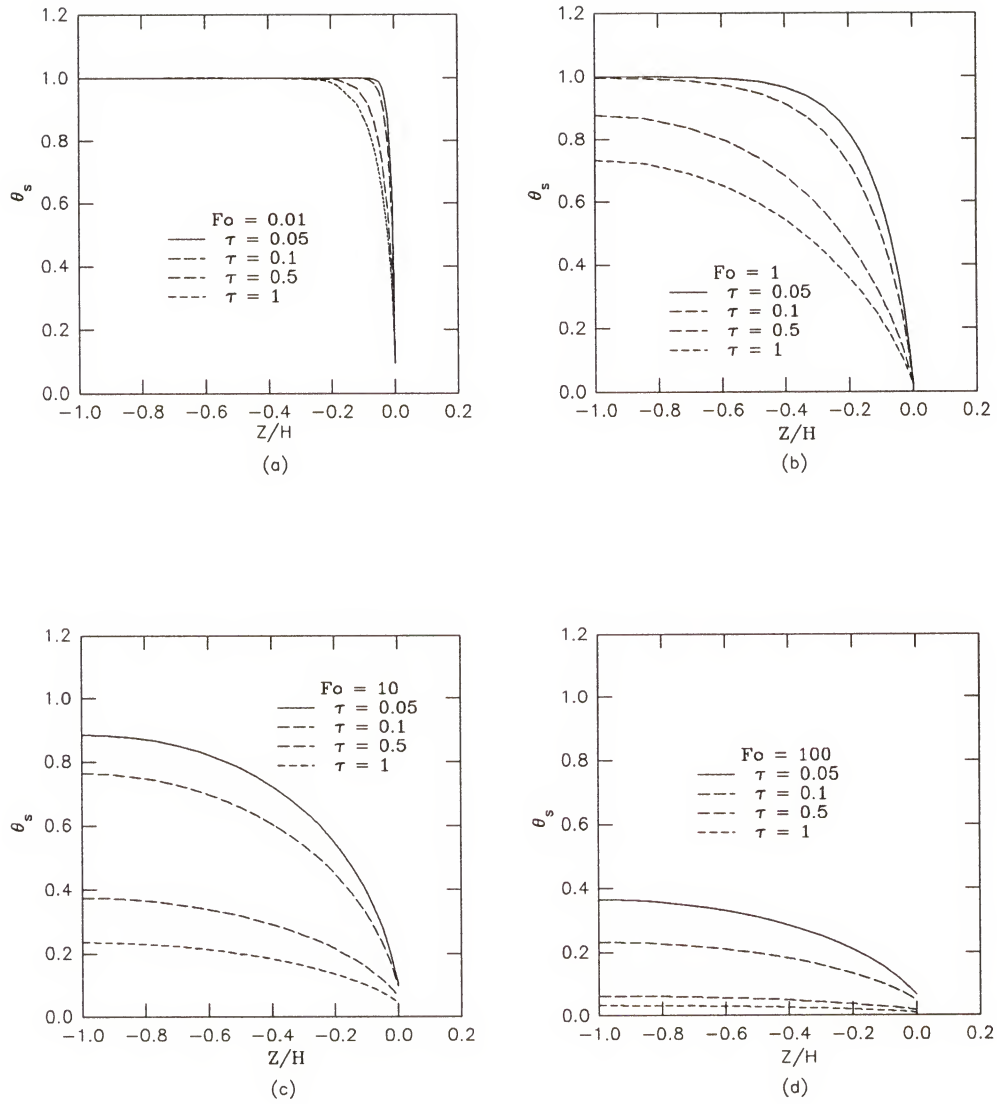

Figure 3.6 Effect of Fourier number Fo on θ_s along the centerline at various times for (Ja,κ,α)=(10, 0.005, 0.005). (a) Fo=0.01; (b) Fo=1; (c) Fo=10 and (d) Fo=100.

of the bubble during the entire growth process while for higher values of Fo the bottom temperature at $\bar{r}=0$ reaches 0.77, 0.24, and 0.033 near departure. The temperature gradient on the liquid-solid interface $\bar{z}_s=0$ is largest for Fo=0.01; the gradient decreases with increasing Fo, and thus the growth rate does as well. This is entirely consistent with the results shown in Fig. 3.1b for the effect of Fo on the growth rate. For Fo changing from 0.01 to 1, 10, 100, 1000 and 10000, the radial distribution of $\theta_s(\xi=r/R_c(t_d))$ is very similar to that in Fig. 3.5b; hence they are not presented. The insensitivity of $\theta_s(\xi)$ is primarily due to the explicit independence of the radial diffusion on Fo and the proper scaling of r using $R_c(t_d)$.

3.4.3 Effect of κ

Figs. 3.7a-d illustrate the effect of the conductivity ratio κ on $\theta_s(\bar{z}_s)$ at r=0. At (Ja, Fo, α) =(10, 10, 0.005), κ ranges from 0.0005, 0.001, 0.01 to 0.05. For a very small κ (say κ=0.0005 resulting from using a high-conductivity heater), only a small gradient in θ_s is needed to supply energy to the bubble through the microlayer. For larger κ (say κ=0.01) the required temperature change is much larger in order to maintain the energy flow to the microlayer. Such a description is consistent with the results presented in Fig. 3.1c. Figs. 3.8a-b show the radial variation of θ_s at (Ja, Fo, α)=(10, 1, 0.005) for κ=0.001 and 0.01. Together with Fig. 3.5b in which κ=0.005, it is seen that an

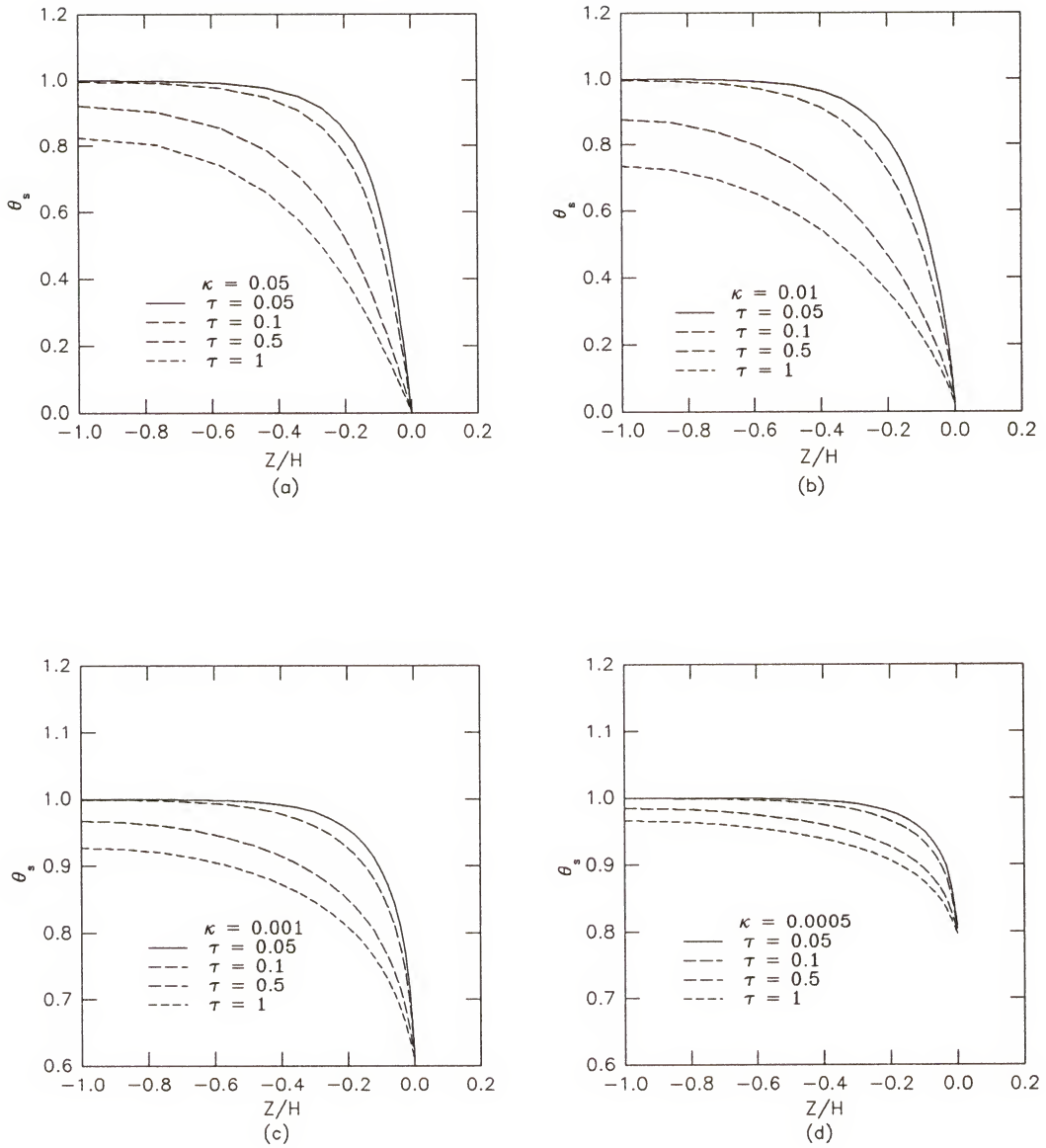

Figure 3.7 Effect of the conductivity ratio κ on θ_s along the centerline at various times for (Ja,Fo,α)=(10, 1, 0.005). (a) κ=0.05; (b) κ=0.01; (c) κ=0.001 and (d) κ=0.0005.

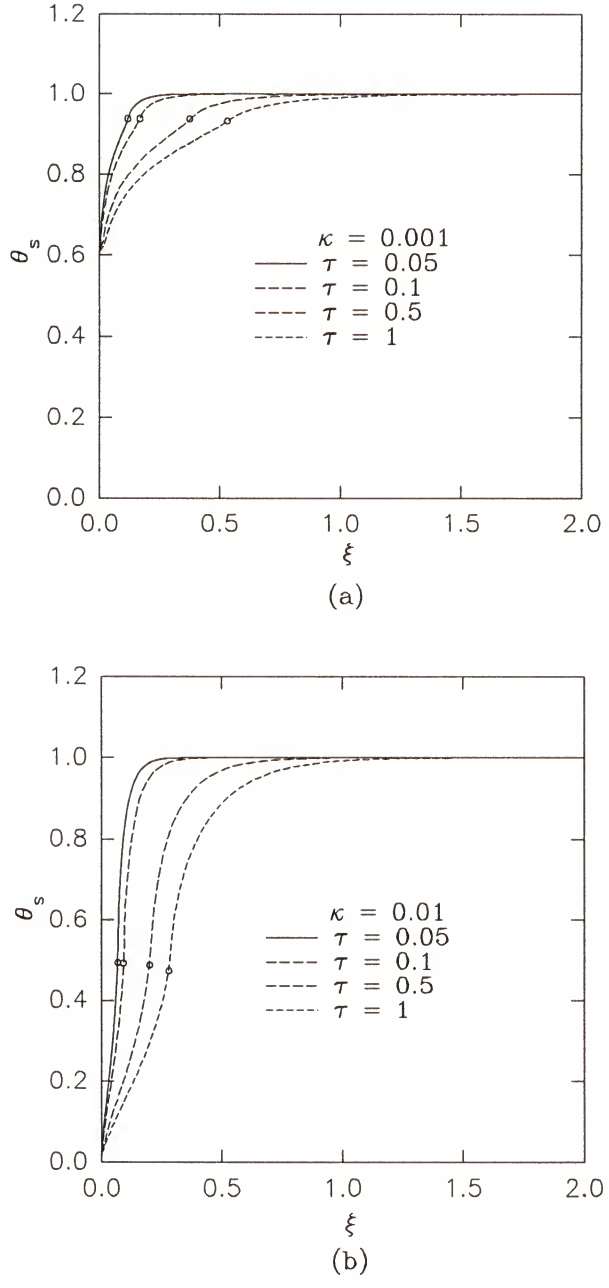

Figure 3.8 Effect of the conductivity ratio κ on θ_s on the liquid-solid interface at various times for (Ja,Fo,α)=(10, 1, 0.005). (a) κ=0.001 and (b) κ=0.01. Symbols indicate the edge of the microlayer, r=R_b(t).

increase in the temperature underneath the bubble is associated with decreasing κ, which is similar to the trend in the z-direction. The result at κ=0.0001 (not presented here) simply reveals that $\theta_s(\xi=0)$ is very close to 0.95 for $0<\tau<1$.

3.4.4 Effect of α

Figs. 3.9a-b show the effect of α on the $\theta_s(\bar{z}_s)$. It is seen, by comparing these two cases, that a small α results in a steeper gradient of θ_s at $\bar{z}_s = 0$ but a lesser penetration of the thermal layer through the thickness. The large gradient of θ_s on the interface at small α is needed to maintain the energy flow to the microlayer during the growth of the bubble, as seen from equation (2.31). However, a larger temperature variation for large α (which may result from a small solid thermal diffusivity) is observed in the z-direction along the centerline. This is quite similar to the effect of Ja on $\theta_s(\bar{z}_s)$. Figs. 3.10a-d show $\theta_s(\xi=r/R_c(t_d))$ at (Ja, Fo, κ)=(10, 1, 0.005) for α=0.0005, 0.001, 0.01, and 0.05. An increasing (decreasing) α results in reduced (enhanced) thermal diffusion in the r-direction. Since the z-direction conduction is controlled by Fo, not by α, the energy flow is more likely to be in the radial direction with smaller α (see Fig. 3.10a for α=0.0005) than with larger α (see Fig. 3.10d for α=0.05). Correspondingly, the z-direction diffusion is larger for α=0.05 than for α=0.0005 as shown in Fig. 3.9.

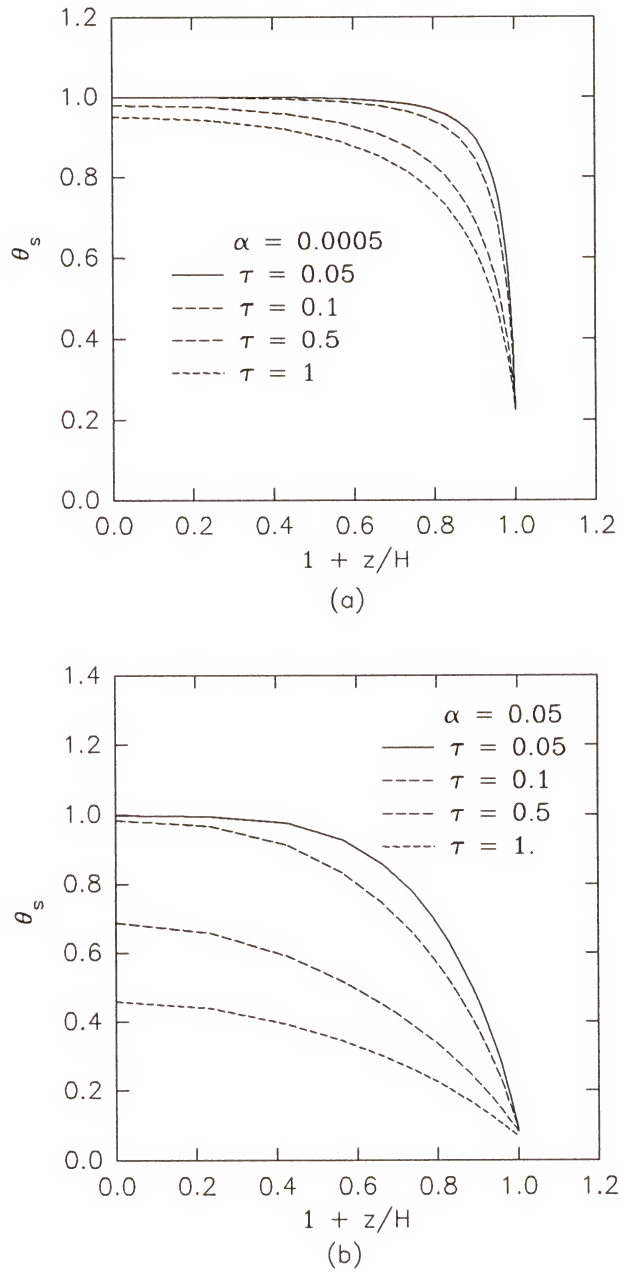

Figure 3.9 Effect of the diffusivity ratio α on θ_s along the centerline at various times for (Ja,Fo,κ)=(10, 1, 0.005). (a) α=0.0005 and (b) α=0.05.

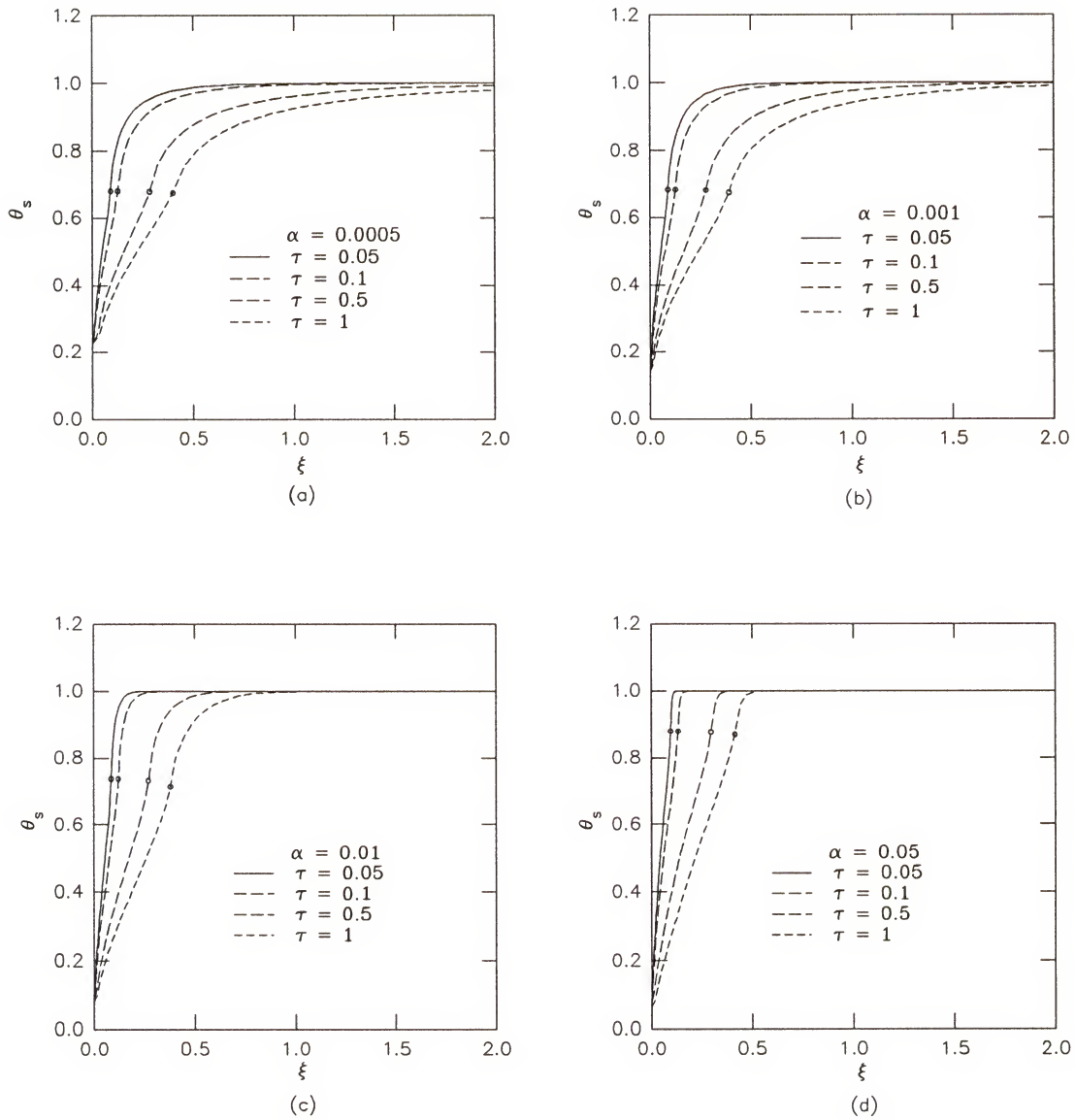

Figure 3.10 Effect of the diffusivity ratio α on θ_s on the liquid-solid interface at various times for (Ja,Fo,κ)=(10, 1, 0.005). (a) α=0.0005; (b) α=0.001; (c) α=0.01 and (d) α=0.05. Symbols indicate the edge of the microlayer, $r=R_b(t)$.

From the variation of $\theta_s(\bar{z}_s)$, it is also seen that: a) there is a large difference between θ_s on the liquid-solid interface and θ_s at the bottom of the heater; b) the temperature variation on $\bar{z}_s$ is typically large; c) the variation of θ_s depends on the four parameters (Ja, Fo, κ, α) in a complex manner. Hence, measurements of the solid temperature at the bottom of the heater does not clearly reveal the thermal field at the solid-liquid interface just beneath the bubble.

3.5 Summary

The numerical results show that the liquid temperature within the microlayer is practically linear during the entire growth period over a large range of conditions. The normalized growth rate $\bar{R}(\tau) = R(\tau)/R_c(\tau=1)$ clearly shows the effects of (Ja, Fo, κ, α): increasing Ja or α results in an increased $\bar{R}(\tau)$ while increasing Fo or κ results in a decreasing $\bar{R}(\tau)$. The asymptotic description and numerical solution have elucidated the detailed energy transfer process during a very short period of time over a very small volume residing beneath a growing vapor bubble. Those are the first solutions of the kind according to the literature survey. The dependence of the temperature field, θ_s, in the solid heater on the parameters (Ja, Fo, κ, α) are quite complicated. A large Ja has a large effect on θ_s due to a large amount of energy transferred from the solid to the

bubble. A large Fo (or a thin heater) implies a strong thermal interaction between the growing bubble and the heater through the microlayer because of the smaller thermal capacity of the heater. Therefore, there is a stronger energy flow within the solid heater in the radial direction to sustain the bubble growth. A larger κ also dictates a stronger thermal interaction because a larger gradient of θ_s must be maintained in order to supply an adequate amount of energy from the heater to the bubble through the liquid microlayer. For a relatively large α, the heat conduction in the radial direction is small while in the z-direction conduction is controlled by Fo, not by α. Hence, for an increasing α, the thermal diffusion in the z-direction becomes relatively stronger when that in the r-direction gets weaker. This results in a deeper penetration of the solid temperature towards the bottom of the heater with increasing α.

It is important to keep in perspective that the present computational analysis for vapor bubble growth is limited to saturated pool boiling in the isolated bubble regime. Because the hydrodynamics are not solved as an integral part of the analysis, it is expected that the present analysis is applicable only when the Reynolds number of the bulk liquid motion induced by the growing bubble is large. At low Jacob number boiling, the growth rate is small; hence the Reynolds number, $Re = 2R(t)\dot{R}(t)/\nu$, may approach order unity which

implies that both Reynolds number and Prandtl number are important in determining C and C_1. In fact it is possible that C and/or C_1 may be a function of time. Under these extreme circumstances, it is desirable to incorporate the hydrodynamics with the thermal analyses. Nevertheless, the present study is quite useful because it already covers a wide range of parameters encountered in pool boiling.

CHAPTER 4
A SIMPLIFIED MODEL FOR PREDICTING VAPOR BUBBLE GROWTH RATE IN HETEROGENEOUS BOILING

4.1 Background

In Chapters 2 and 3, a detailed numerical investigation of the vapor bubble growth rate and associated thermal fields in heterogeneous pool boiling has been considered. Four dimensionless parameters were identified to characterize the vapor bubble growth rate and associated temperature fields of the solid and liquid. In the formulation, a parameter, C_1, that characterizes the microlayer wedge angle was determined by matching the finite difference solution for the vapor bubble growth rate, R(t), with the experimental data over a wide range of boiling conditions. A parametric investigation has elucidated the detailed energy transfer process among the three phases. It was shown that the growth rate depends on the Jacob number, Ja, Fourier number, Fo, liquid-to-solid thermal conductivity ratim, κ, and liquid-to-solid thermal diffusivity ratio, α, in a complex manner. No simple correlation could be identified which reliably relates R(t) to these four parameters. The vapor bubble growth rate computation described in Chapters 2 and 3 is based on two-dimensional

axisymmetric unsteady heat conduction through a solid heater and liquid microlayer. Although the bubble growth computation is accurate and correctly accounts for the influence of Ja, Fo, κ, and α, it is tedious and is thus impractical to use as a design tool. The need for a simple bubble growth rate model which is accurate over a wide range of boiling conditions is the motivation for this work.

An energy balance on the liquid-vapor interface in conjunction with a lumped thermal analysis for the solid heater results in a first order ordinary differential equation which is used to calculate the vapor bubble growth rate. An empirical constant, C_2, is introduced to characterize the region of the solid heater influenced by microlayer evaporation. It is determined by matching the predicted and measured vapor bubble growth rate data. It is found that a modified Fourier number must be introduced to account for the finite thermal penetration depth when the Fourier number is less than one. Considering the complexity of bubble growth phenomena, as demonstrated by Chapters 2 and 3, excellent agreement is observed between the predicted and experimental bubble growth data for intermediate and moderately wetting fluids in which Jacob number ranges from 0.54 to 1974. Hence, for practical boiling problems of interest, such as the prediction of vapor bubble departure diameters in saturated pool boiling Zeng et al. (1993), the simple model developed here should be quite useful. As was

the case for the numerical model shown in Chapters 2 and 3, the present correlation is limited to saturated pool boiling in the isolated bubble regime.

4.2 Analytical Formulation

4.2.1 Vapor Bubble and Liquid Microlayer

Consideration is given to a vapor bubble growing from a solid heating surface into a saturated pool of liquid. The bubble shape is assumed to consist of a truncated sphere on a wedge-shaped microlayer as was assumed in Chapter 2, and shown in Fig. 2.1. The apex of the microlayer wedge is assumed to be at r=0 as shown in Fig. 2.1. This assumption alleviates the requirement to specify the movement of the three-phase contact point and thus greatly simplifies the analysis. As long as the vapor-solid contact area is small comparing with the liquid-solid areas in the wedge, this assumption will not cause significant error in predicting the heat transfer. In the parametric investigation conducted in Chapter 3, it was established that the temperature profile in the liquid microlayer is practically linear. Hence, the liquid temperature in the microlayer is approximately

$$T_\ell(r,z,t) = T_{sat} + \Delta T_{sat}(r,t)\left(1-\frac{z}{L(r)}\right), \tag{4.1}$$

where $\Delta T_{sat}(r,t)=T_s(r,z=0,t)-T_{sat}$, T_{sat} is the saturation temperature, $T_s(r,z,t)$ is the solid heater temperature, L(r)

is the local microlayer thickness, and t denotes time. Thus, the heat flux at the microlayer liquid-vapor interface is,

$$q_i'' = -k_\ell \left.\frac{\partial T_\ell}{\partial n}\right|_{z=L(r)} \approx \frac{k_\ell \Delta T_{sat}(r,t)}{L(r)}, \qquad for\ \phi \ll 1\ , \tag{4.2}$$

where it has been assumed that the microlayer wedge angle, ϕ, is very small as shown in Fig. 2.1. It is also assumed that the evaporation of the microlayer dominates the heat transfer to the vapor bubble during the bubble growth period. Thus, the change in the bubble volume V_b can be obtained through an energy balance on the liquid-vapor interface,

$$\rho_v h_{fg} \frac{dV_b}{dt} = \int_A -k_\ell \left.\frac{\partial T_\ell}{\partial n}\right|_{z=L(r)} dA \tag{4.3}$$

where h_{fg} is the latent heat, ρ_v is the vapor density, and A is the microlayer surface area. Denoting $R_b(t)$ as the microlayer base radius, R(t) as the bubble radius, as shown in Fig. 2.1, the bubble volume can be expressed as

$$V_b = \frac{4}{3}\pi R^3 f(C) = \frac{4}{3}\pi R^3 \left(1 - \frac{3}{4}(1-\sqrt{1-C^2})^2 + \frac{1}{4}(1-\sqrt{1-C^2})^3\right) \tag{4.4}$$

where $C=R_b(t)/R(t)\leq 1$ is the bubble shape factor, as was shown in Chapter 2. Since $dA \approx 2\pi r dr$ and $L(r) \approx r\phi$, (4.3) may be expressed as,

$$\frac{dR^2}{dt} \approx \frac{C}{f(C)} \frac{1}{\phi} \frac{k_\ell \Delta \bar{T}_{sat}(t)}{\rho_v h_{fg}}, \qquad for\ \phi \ll 1. \tag{4.5}$$

In the above, $\Delta\bar{T}_{sa}$(t) is the superheat on the boiling surface averaged over the area beneath the microlayer and is obtained from an energy balance within the solid heater. If the wall superheat was constant during the bubble growth period, $\Delta\bar{T}_{sat}=\Delta T_{sat}$, and equation (4.5) may be used to solve for the growth rate,

$$R_c(t) = \left(\frac{C}{\phi f(C)} Ja\, \alpha_\ell\, t \right)^{\frac{1}{2}} \tag{4.6}$$

where the subscript c denotes the solution for a constant wall superheat, α_ℓ is the liquid thermal diffusivity, and Ja is the Jacob number based on the initial wall superheat, ΔT_{sat0}. Typically, this superheat is either specified or determined by considering the total heat transfer from the solid heater. The microlayer wedge angle ϕ was generalized in chapter 2 based on the analysis of Cooper & Lloyd (1969) as

$$\phi = \frac{f(C) C_1^2 Pr_\ell}{C^3 Ja} \tag{4.7}$$

where Pr_ℓ is the liquid Prandtl number, and C_1 is an empirical parameter (see Eq. (4.17)) determined (Chapter 2) by matching the predicted and measured growth rate. The

case for time varying wall superheat is considered next.

4.2.2 Lumped Analysis for the Solid Heater

Most of the vapor bubble growth data available in the literature were obtained using thin heaters in which the temperature on the back side is almost equal to that on the boiling side. Consideration is given to thin heaters first. Under such circumstances, a "lumped capacitance" approach may be used to formulate the energy balance for the solid heater with thickness H as

$$V_s \rho_s C_{ps} \frac{d\Delta \bar{T}_{sat}}{dt} = q''' V_s - \dot{q}_{evap} \tag{4.8}$$

where V_s is the effective volume in the solid influenced by the microlayer evaporation, $\Delta \bar{T}_{sat}(t)$ is understood to be the volume averaged superheat in V_s, q''' is the internal heat generation per unit volume (or $q''' = q''/H$ in which q'' is the heat flux supplied from the bottom of the heater), $\dot{q}_{evap}$ is the rate of heat removal from the heating surface due to microlayer evaporation. The subscript s denotes that the quantities are for the solid heater. It is necessary to specify an effective heater volume, V_s, from which energy is extracted in order to satisfy the energy demand from bubble growth. Here it is assumed that $V_s = \pi (C_2 R)^2 H$ in which C_2 is a constant to be determined. Combining equations (4.3) and (4.5), and noting that $\dot{q}_{evap}$ is the right-hand-side of equations (4.3), (4.8) becomes

$$\frac{d\Delta \bar{T}_{sat}}{dt} = \frac{q'''}{\rho_s C_{p,s}} - \frac{4f(C)\rho_v h_{fg}}{C_2^2 \rho_s C_{p,s} H}\frac{dR}{dt}. \tag{4.9}$$

4.2.3 Non-dimensionalization

Following Chapter 2, the dimensionless variables (see nomenclature) are introduced to recast equations (4.5) and (4.9) as

$$\frac{d\bar{R}^2}{d\tau} = \theta \tag{4.10}$$

and

$$\frac{d\theta}{d\tau} = Q - B\frac{\theta}{\bar{R}} \tag{4.11}$$

where $$Q = \frac{q''' t_d}{\Delta T_{sat0}\rho_s C_{p,s}} \quad , \quad B = \frac{2\kappa}{C_2^2}\left(\frac{f(C)\,CFo}{\alpha\, Ja\phi}\right)^{1/2}. \tag{4.12}$$

In equation (4.12), Fo is the Fourier number which is defined previously. Eliminating θ from (4.10) and (4.11), a first order ordinary differential equation for $\bar{R}(\tau)$ results,

$$\frac{d\bar{R}^2}{d\tau} + 2B\bar{R} = Q\tau + 1 + 2B\bar{R}(0) \tag{4.13}$$

where $\bar{R}(0)$ is the initial bubble radius which is physically very small and is mathematically set to zero in this study. Equation (4.13) is easily solved using a Runge-Kutta method. When Q is negligibly small or q''' is negligible compared to the heat removed through microlayer evaporation, an exact solution to equation (4.13) is obtained,

$$\tau = -\frac{1}{2B^2}\ln(1-2B\bar{R}) - \frac{1}{B}\bar{R}. \tag{4.14}$$

For small B or small $\bar{R}$, a Taylor series expansion for the logarithmic term results in

$$\bar{R}(\tau) \sim \tau^{1/2} + H.O.T. \tag{4.15}$$

which is the dimensionless form of $R_c(t)$ given by equation (4.6). Since we are interested in $\bar{R}(\tau) \sim O(1)$ and in general B is not small unless Ja is very large, equation (4.6) or (4.15) is not a satisfactory solution for $\tau \sim O(1)$. This is the reason the solution based on the constant wall superheat is unsatisfactory when compared with experimental data over a wide range of Jacob number. It is also noted that for a thick heater, B→0 as Fo→0, and equation (4.14) again degenerates to the constant wall-superheat solution. Hence it fails to predict the actual bubble growth rate. From the previous two-dimensional computation (Chapters 2 and 3), it is known that for a small Fo, the penetration depth of the thermal field in the solid heater is actually somewhat limited prior to departure. Hence it is anticipated that when Fo is less than one, a modified, effective Fourier number should be used.

4.3 Results and Discussion

4.3.1 Results for Fo>1; Determination of the Empirical Constant C_2

The empirical constant C_2 mainly characterizes the region of the heating surface influenced by microlayer evaporation; it also partially accounts for the non-uniformity in the heater thermal field beneath the microlayer. It is determined by matching the predicted growth rates, computed from equation (4.13), with the experimental growth rate data. The two empirical constants, C and C_1, have been determined previously (see chapter 2) as

$$C = \left((0.4134\, Ja^{0.1655})^{-6} + (1 - 0.1\, e^{-0.0005\, Ja})^{-6} \right)^{-1/6} \tag{4.16}$$

and

$$C_1\, Pr_l^{0.5} = 0.00525\; Ja^{0.752}\, \kappa^{-0.113}\, \alpha^{-0.117}.$$

There are 32 data listed in Chapter 2. Nine of them have Fo<1. Based on the remaining 23 data for Fo>1, C_2 is determined by best fitting the predicted growth rate with the measured ones. The results for C_2 are given in Table 4.1. Based on the results for C_2, a correlation is developed as

$$C_2 = 1.26\, Fo^{0.072} (0.73 + e^{-0.18\, Ja}). \tag{4.18}$$

This gives a relative deviation

Table 4.1 The empirical constant C_2 determined from various sources

No.	Ja	Fo	C_1	C_2	P (atm)	Source
1	1973.6	5.2E-5	3.10		0.040	Van Stralen et al. (1975)
2	887.3	5.0E-5	1.75		0.079	Van Stralen et al. (1975)
3	766.2	6.92	1.30	1.06	0.066	Cole and Shulman (1966)
4	389.5	3.5E-5	1.20		0.132	Van Stralen et al. (1975)
5	289.3	10.0	0.65	1.17	0.129	Cole and Shulman (1966)
6	210.0	11.15	0.33	1.18	0.063	Cole and Shulman (1966)
7	201.0	1.5E-5	0.47		0.203	Van Stralen et al. (1975)
8	178.7	7.69	0.55	1.18	0.257	Cole and Shulman (1966)
9	156.0	7.11	0.30	1.04	0.182	Cole and Shulman (1966)
10	150.5	1.3E-5	0.45		0.267	Van Stralen et al. (1975)
11	130.0	7.69	0.25	1.03	0.268	Cole and Shulman (1966)
12	90.6	6.92	0.20	1.27	0.474	Cole and Shulman (1966)
13	67.1	5.77	0.17	1.02	0.40	Cole and Shulman (1966)
14	50.6	1.92	0.30	0.84	0.689	Cole and Shulman (1966)
15	50.0	4.23	0.16	0.95	0.522	Cole and Shulman (1966)
16	42.3	67.86	0.52	1.05	1.0	Staniszewski (1959)
17	37.6	2.69	0.15	0.92	0.711	Cole and Shulman (1966)
18	35.8	84.57	0.38	1.0	1.0	Staniszewski (1959)

Table 4.1 (continued)

No.	Ja	Fo	C_1	C_2	P (atm)	Source
19	25.3	60.77	0.25	1.30	1.0	Staniszewski (1959)
20	25.0	53.18	0.30	1.40	1.0	Staniszewski (1959)
21	24.5	2.11	0.10	0.85	1.0	Cole and Shulman (1966)
22	23.4	5.6E-2	0.12		1.0	Hospeti and Mesler (1969)
23	23.0	46.59	0.18	1.60	1.0	Staniszewski (1959)
24	18.9	3.4E-2	0.10		1.0	Hospeti and Mesler (1969)
25	18.4	4.7E-5	0.28		1.0	Keshock and Siegel (1964)
26	14.9	4.5E-2	0.07		1.0	Hospeti and Mesler (1969)
27	11.5	1.12	0.06	1.0	2.0	Akiyama et al. (1969)
28	11.2	91.15	0.20	1.55	1.90	Staniszewski (1959)
29	9.16	151.92	0.16	1.40	2.72	Staniszewski (1959)
30	7.73	54.89	0.05	1.60	1.90	Staniszewski (1959)
31	1.17	1.05	0.015	1.30	8.0	Akiyama et al. (1969)
32	0.52	3.36	0.007	2.15	15.0	Akiyama et al. (1969)

$$r.d. = \frac{1}{23}\sum_{n=1}^{23} \frac{|C_{2,n} - C_{2,n}^*|}{C_{2,n}^*} \sim 0.085 \qquad (4.19)$$

where $C_{2,n}^*$ is the value given in Table 4.1 which is determined by matching the measured and predicted growth rates. As was mentioned before, C_2 is a constant which characterizes the effective volume in the solid influenced by the microlayer evaporation. It is observed from the data that C_2 is mainly correlated with Fo and Ja: C_2 increases with increasing Fo and decreasing Ja. As the heater gets thinner (which increases Fo), the energy transfer has to rely more on the radial conduction than the vertical conduction in order to sustain the vapor bubble growth. This leads to a larger spreading of the region of influence by the microlayer. The effect of increasing (or decreasing) Ja on the radial thermal diffusion has been discussed in detail in Chapter 3; it was observed that as Ja decreases the radial conduction is enhanced. This is consistent with the trend observed for the C_2 dependence on Ja.

To validate the present simplified model based on the lumped analysis, comparisons are first made between the predicted R(t), which includes the present prediction (equation 4.13) and the computational prediction from Chapter 2, and the measured R(t) for Fo>1. The results are shown in Figures 4.1a-c. It is noted that for the predicted growth rate, R(t), shown in Figure 4.1, C_2 was calculated

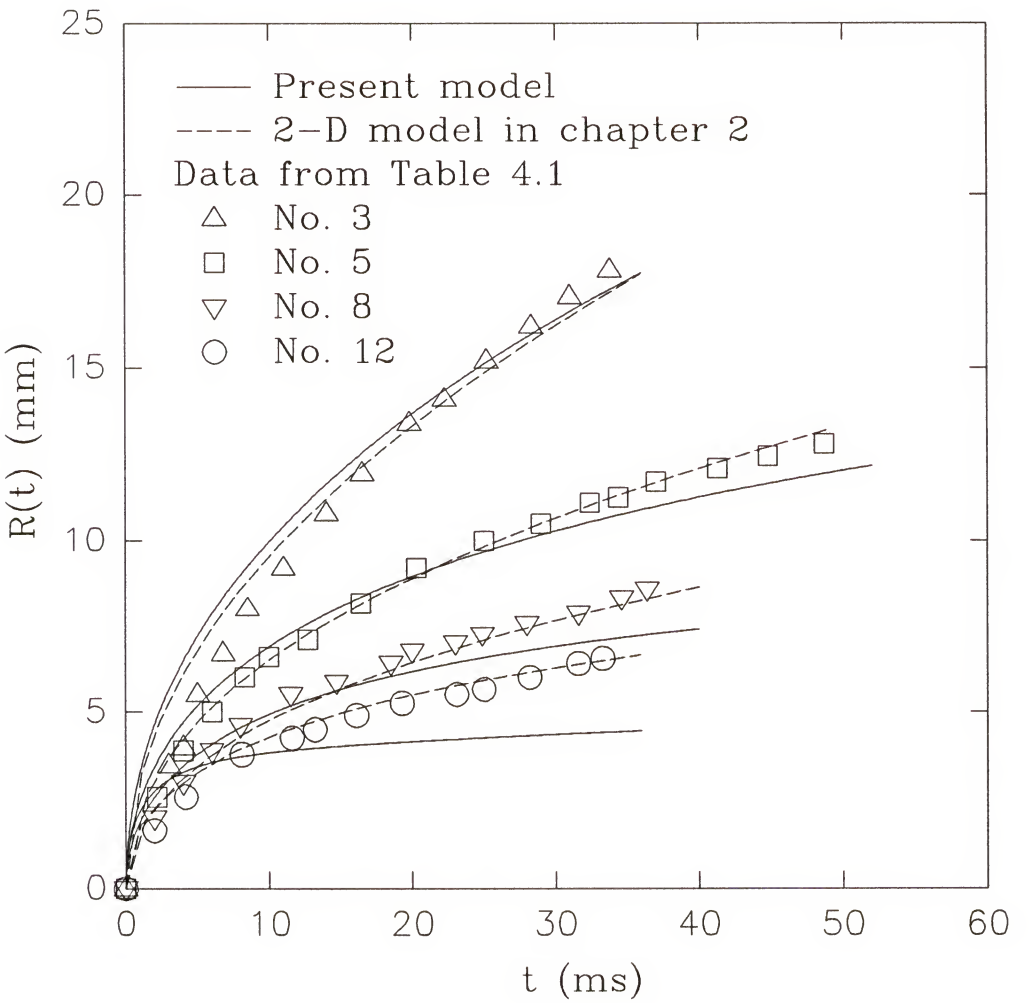

Figure 4.1a Comparision of the bubble growth rate R(t) between the present model, two-dimensional model, and the experimental data of Cole and Shulman (1966) using water as boiling liquid.

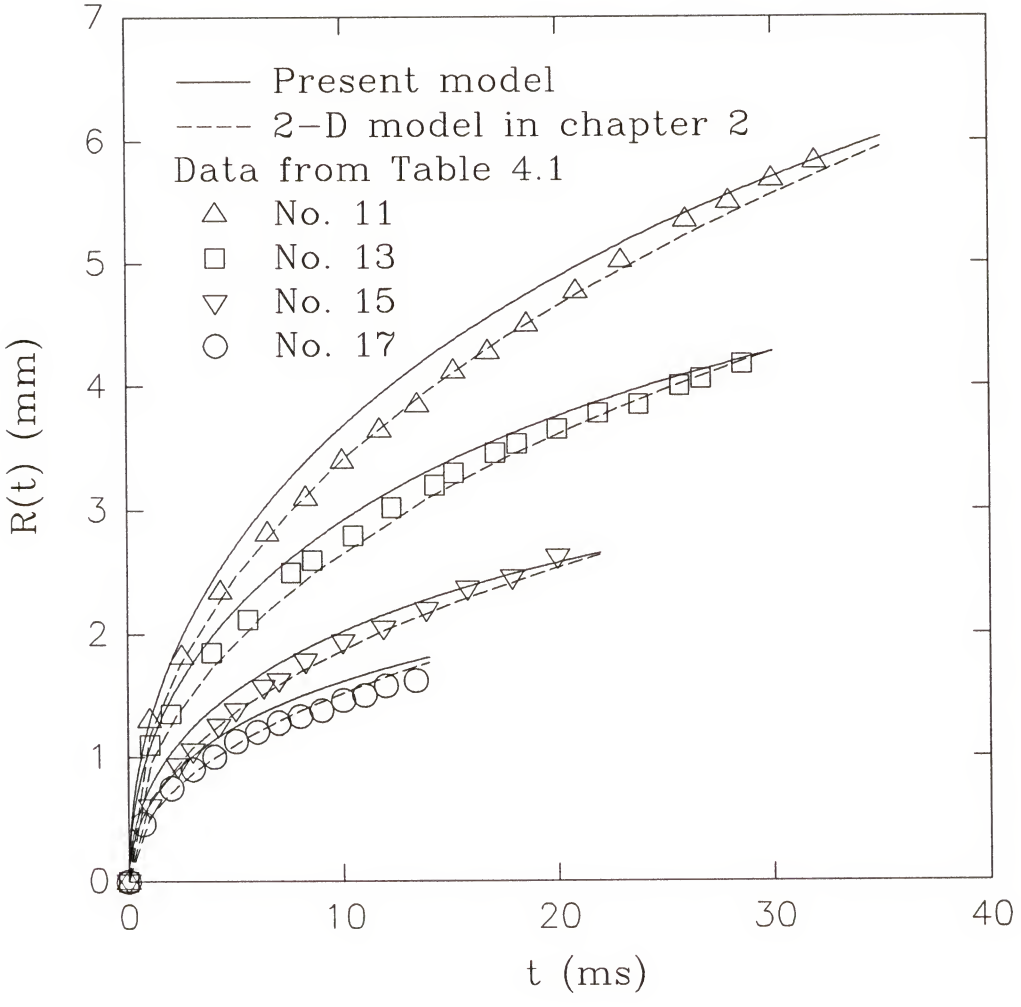

Figure 4.1b Comparison of the bubble growth rate R(t) between the present model, two-dimensional model, and the experimental data of Cole and Shulman (1966) using methanol as boiling liquid.

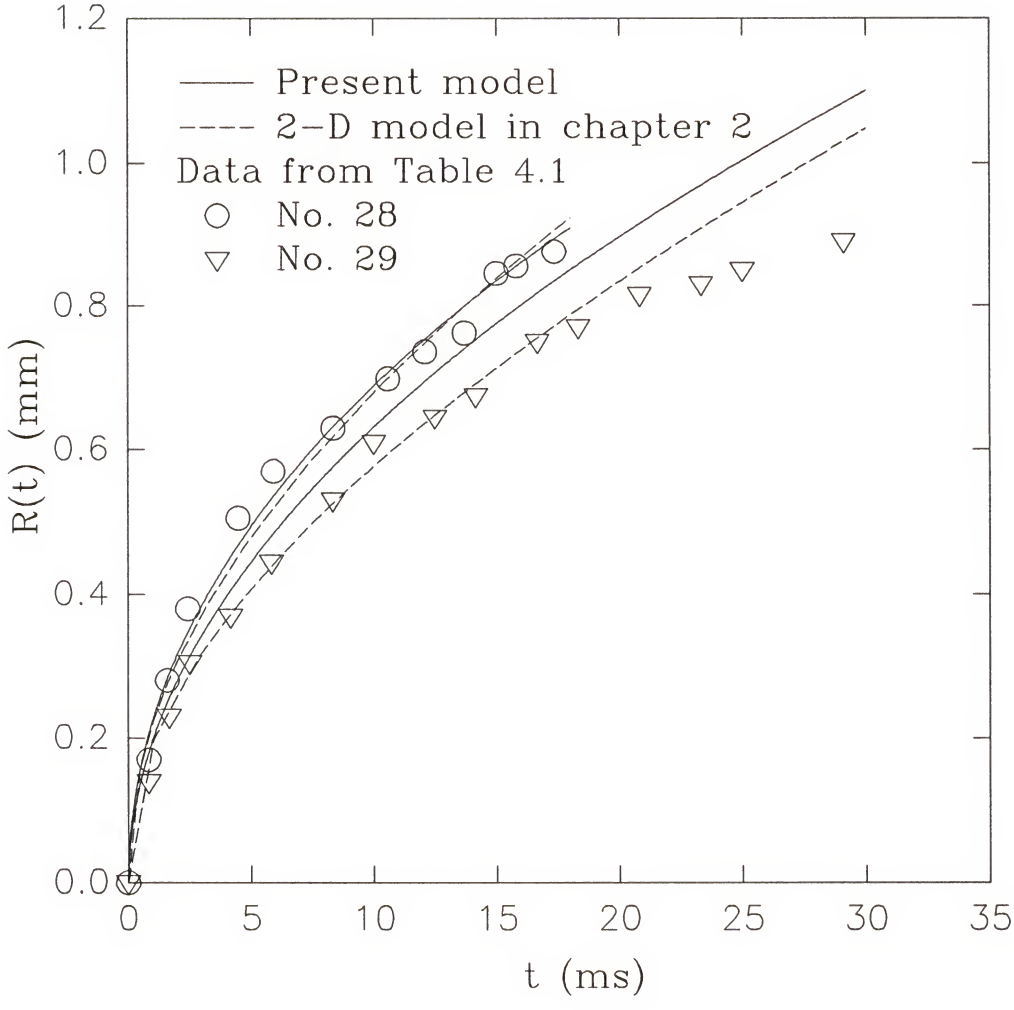

Figure 4.1c Comparison of the bubble growth rate R(t) between the present model, two-dimensional model, and the data of Staniszewski (1959) using water as boiling liquid.

using equqtion (4.18) (values for C_2 given in Table 1 were not used). However, C_1 is taken from the values listed in Table 4.1. In this way, the difference between the predictions based on the present model and that based on the two-dimensional model is only due to the modeling of the lumped system and the correlation for C_2, not C_1. In Figure 4.1a, the data are from Cole & Shulman (1966) in which Ja ranges from intermediate to high values, water is the boiling liquid, and the heater material is a polished zirconium ribbon. Excellent agreement for R(t) is observed except for data No. 12. In the case of data No. 12, the relative deviation between C_2 based on the correlation equation (4.18) and the best fit value listed in Table 4.1 is about 17%, which is the reason for the poor agreement. The comparison with data No. 12 is included here because the agreement is the worst among the 32 sets of data. Figure 4.1b compares the present prediction with the data of Cole and Shulman (1966) in which Ja is considered in the intermediate range and methanol is the boiling liquid. Very good agreement is again observed. Fig. 4.1c compares the present prediction with the data of Staniszewski (1959) in which water is the boiling liquid, the heater material is copper and Ja is considered low. Good agreement is observed for most of the growth period.

4.3.2 Results for Fo<1; Modified Fourier Number (Fo_m)

The bubble growth computation of chapter 3 indicates

that the bubble growth rates $\bar{R}(\tau)$ for Fo=0.01 and for Fo=1 are almost the same; but $\bar{R}(\tau)$ for Fo=1 are larger than for Fo=10 when other parameters are held the same. The reason is as follows: once the thickness of the heater exceeds some value, the thermal field in the bottom portion of the heater is unaffected by the growth of the vapor bubble during the entire growth period, $\tau \leq 1$. For such cases, H in the present lumped analysis must be modified to reflect the effective thermal penetration depth which is, unfortunately, time dependent. To alleviate this difficulty, we use a modified Fourier number, Fo_m. When using equation (4.18) to evaluate C_2, Fo is replaced by Fo_m in which

$$Fo_m = \begin{cases} Fo & , \quad Fo > 1 \\ 1.29 - 0.29\exp(1 - Fo^{3.5}) & , \quad Fo \leq 1 \end{cases} \tag{4.20}$$

and Fo_m also replaces Fo in equations (4.12) and (4.13). It is noted that in the limit $Fo \to 1$, $Fo_m \to 1$; as $Fo \to 0$, $Fo_m \to 0.5$. For the remaining nine data with Fo<1, which can be identified in Table 4.1, the present predictions for R(t) agree well with the measured ones. Figure 4.1d compares the predicted R(t) and the measured R(t) for Fo<1 in the high Jacob number range. The data are from Van Stralen et al. (1975) with water as the boiling liquid on a copper heater. As seen, the predicted bubble growth rates shown in Figure 4.1d compare well with the measured data.

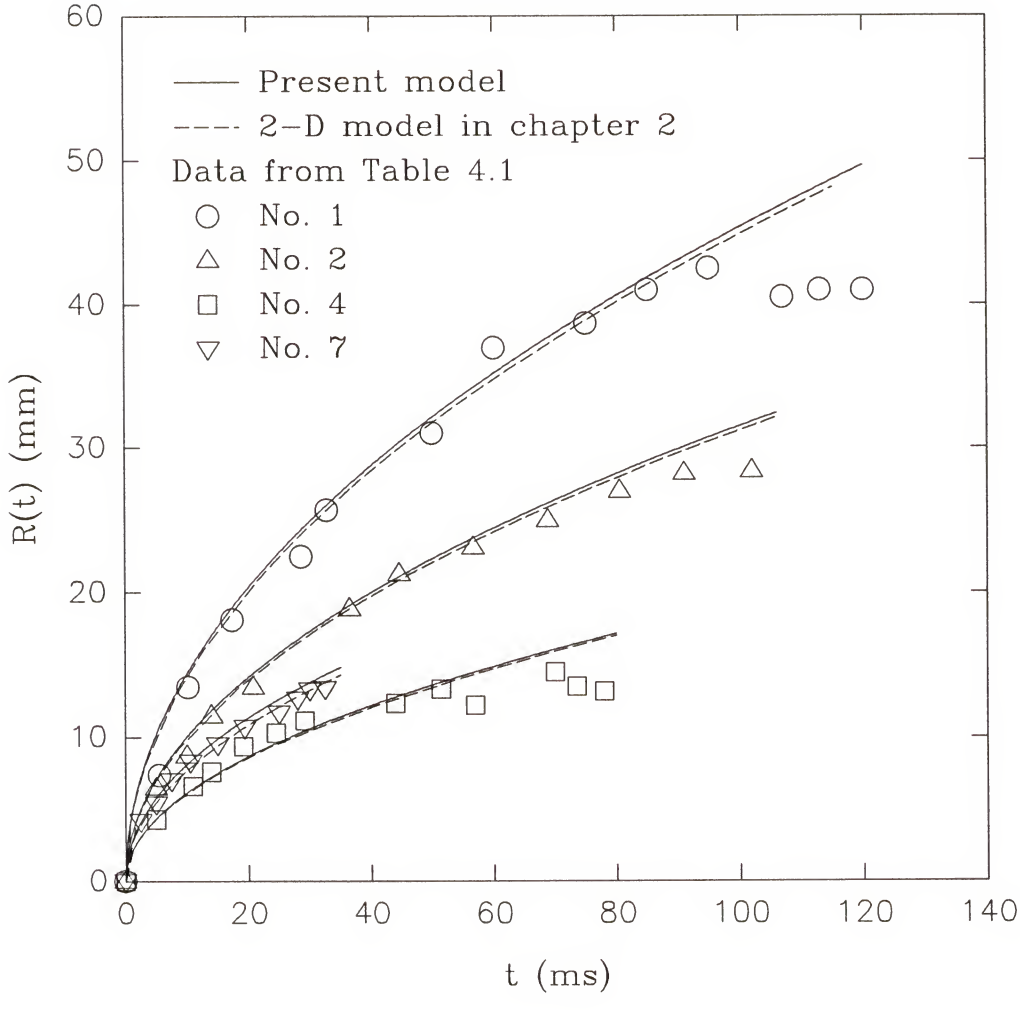

Figure 4.1d Comparison of the bubble growth rate R(t) between the present model, two-dimensiional model, and the data of Van Stralen et al. (1975) using water as boiling liquid for Fo<1.

4.4 Summary

In this study, a simplified model is formulated to predict the growth rate of vapor bubbles in saturated heterogeneous pool boiling for the isolated bubble regime based on the same physical mechanisms identified in Chapters 2 and 3. A first order ordinary differential equation is obtained, which when numerically solved, yields the vapor bubble growth rate. The predicted bubble growth rates compare well with the reported experimental data in which the working fluids are intermediate and moderately wetting and the Jacob number ranges from 0.52 to 1974. A correlation for C_2, which characterizes the region of the heating surface influenced by the microlayer evaporation, is presented. For thick heaters with $Fo<1$, a modified Fourier number is introduced to account for the finite thermal penetration depth which allows the vapor bubble growth rate to be accurately predicted. The present bubble growth model provides a simple and apparently reliable alternative to the intensive two dimensional finite difference computation presented in Chapters 2 and 3. Due to the empiricism involved in the model development, it must, nevertheless, be used with caution.

CHAPTER 5
VAPOR BUBBLE GROWTH IN SUBCOOLED HETEROGENEOUS BOILING

5.1 Background

In previous investigations discussed in Chapters 2 and 3, detailed theoretical and numerical analyses of vapor bubble growth in saturated heterogeneous pool boiling have been studied over a wide range of boiling conditions. In the formulation, the simultaneous coupling of the thermal fields in a thin liquid microlayer and in the solid heater takes into account the continuously decreasing heating surface temperature beneath the growing bubble. In the parametric investigation, four dimensionless parameters were identified to characterize the vapor bubble growth rate and associated temperature fields in the solid and liquid microlayer. The numerical analysis has elucidated the detailed energy transfer process for the solid thermal field. In saturated pool boiling, the bulk liquid surrounding the bubble cap is nearly saturated, and thus the heat and mass transfer in this region is small. In subcooled boiling, the unsteady heat transfer between the vapor bubble dome and the bulk liquid is no longer negligible due to the effect of subcooling. During the early stages of growth, the vapor bubble dome obtains energy

from the surroundings because a large portion of the bubble surface area is within the thermal boundary layer. Thus, the overall energy for the bubble growth comes from the liquid microlayer and the vapor bubble dome. As the bubble continues to grow, a large portion of the bubble dome protrudes the thermal boundary layer. At the same instant, the energy into the bubble from the microlayer is smaller than that lost from the dome to the surrounding subcooled liquid, and the bubble starts to collapse. In this study, the vapor bubble growth process is considered to be controlled by the unsteady energy transfer among four regions: a wedge shaped liquid microlayer, a vapor bubble whose shape is assumed to be a truncated sphere, a subcooled bulk liquid, and a solid heater. A linear temperature profile across the liquid microlayer is assumed based on the investigation in Chapter 3. The unsteady energy equation in the subcooled liquid which is assumed to be axisymmetric with respect to the axis normal to the heating surface, is strongly coupled with the momentum equation. The momentum equation is approximated by the Laplace equation by assuming an inviscid flow. Good agreement between the predicted and measured bubble radius is achieved. The present study contributes to the basic understanding of the bubble growth mechanisms during subcooled nucleate boiling.

5.2 Theoretical Formulation

5.2.1 Vapor Bubble and Liquid Microlayer

Consideration is given to an isolated vapor bubble growing from a solid heating surface into a subcooled liquid pool as shown in Figure 5.1. The bubble shape is assumed to be a truncated sphere on a wedge-shaped microlayer. This assumption alleviates the requirement to specify the movement of the three-phase contact point and thus greatly simplifies the analysis. In the parametric investigation for saturated boiling (Chapter 2), it was established that the temperature profile in the liquid microlayer is practically linear and the liquid temperature in the microlayer is given by

$$T_\ell(r,z,t) = T_{sat} + \Delta T_{sat}(r,t)\left(1 - \frac{z}{L(r)}\right), \tag{5.1}$$

where $\Delta T_{sat}(r,t)=T_s(r,z=0,t)-T_{sat}$, $L(r)=r\phi$ is the local microlayer thickness, and ϕ is the microlayer wedge angle which is generally very small. During the bubble growth and collapse, the change in the bubble volume V_b can be obtained through an energy balance on the microlayer liquid-vapor interface and the subcooled bulk liquid-vapor interface,

$$\rho_v h_{fg}\frac{dV_b}{dt} = \int_{A_m} -k_\ell \left.\frac{\partial T_\ell}{\partial n}\right|_{z=L(r)} dA_m + \int_{A_b} -k_\ell \left.\frac{\partial T_{b\ell}}{\partial n}\right|_{R'=R(t)} dA_b\,, \quad for\ \phi \ll 1\,, \tag{5.2}$$

where $T_{b\ell}$ is the temperature of the subcooled liquid, A_m is the surface area of wedge on the microlayer liquid-vapor

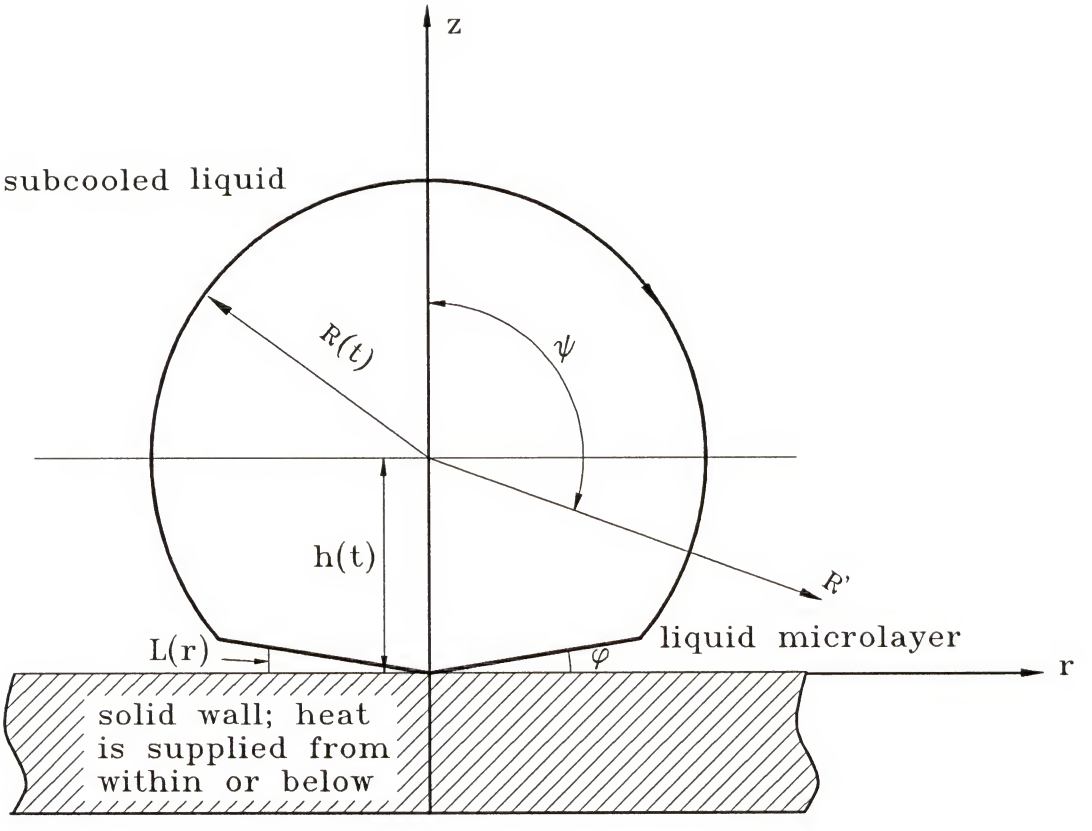

Figure 5.1 Sketch for the growing bubble, liquid microlayer, subcooled bulk liquid, and heating solid.

interface, A_b is the surface area of the vapor bubble dome on the subcooled bulk liquid-vapor interface, $\partial/\partial n$ is differentiation along the outward-drawn normal at the boundary surface, and R' is the spherical coordinate in the radial direction attached to the moving bubble. Equation (5.2) simply states that the energy conducted from the solid to the bubble through the microlayer and the energy transfer between the vapor bubble and subcooled bulk liquid cause the vapor bubble to grow or condense. Denoting $R_b(t)$ as the microlayer base radius and R(t) as the bubble radius, the bubble volume can be expressed as

$$V_b = \frac{4}{3}\pi R^3 f(C(t)) = \frac{4}{3}\pi R^3 \left(1 - \frac{3}{4}\left(1 - \sqrt{1-C^2(t)}\right)^2 + \frac{1}{4}\left(1 - \sqrt{1-C^2(t)}\right)^3\right) \qquad (5.3)$$

where $C(t)=R_b(t)/R(t)\leq 1$ is the bubble shape factor, as was mentioned in chapters 2 and 4. In the limit as the bubble shape approaches a hemisphere, $C(t)\rightarrow 1$, and as the bubble shape approaches a sphere, $C(t)\rightarrow 0$. Based on experimental evidence by Cochran and Aydelott (1966) and Ellion (1954), the bubble shape in subcooled pool boiling changes with time from a hemispherical dome in the early stage towards a spherical dome. Thus, C varies with time.

5.2.2 Subcooled Bulk Liquid

By assuming axisymmetry for the temperature and velocity fields, the unsteady energy equation for the subcooled bulk liquid in cylindrical coordinates (r,z) is

$$\frac{\partial T_{b\ell}}{\partial t} + u_r \frac{\partial T_{b\ell}}{\partial r} + u_z \frac{\partial T_{b\ell}}{\partial z} = \alpha_\ell \left(\frac{1}{r} \frac{\partial}{\partial r} \left(r \frac{\partial T_{b\ell}}{\partial r} \right) + \frac{\partial^2 T_{b\ell}}{\partial z^2} \right), \tag{5.4}$$

where α_ℓ is the thermal diffusivity, (u_r, u_z) are the liquid velocity components in the (r,z) directions. The initial condition specified for the liquid thermal field is based on Marcus and Dropkin's (1965) investigation of the thermal boundary layer above a copper surface in saturated nucleate pool boiling of water:

$$\frac{T_{b\ell} - T_{sub0}}{T_w - T_{sub0}} = \begin{cases} 1 - w\dfrac{Z}{\delta}, & \dfrac{Z}{\delta} \le 0.57 \\ D\left(\dfrac{Z}{\delta}\right)^{-\lambda}, & \dfrac{Z}{\delta} \ge 0.57 \end{cases} \tag{5.5}$$

where T_w is the average temperature of the boiling surface, w and λ are experimentally determined constants based on the measurements of the subcooled liquid temperature, $D=(1-0.57w)0.57^{\lambda}$, and δ is the extrapolated superheat-layer thickness. It is noted that w=1 in saturated nucleate pool boiling. In subcooled pool boiling, equation (5.5) is adopted by noting that the value of w, which can be obtained from the data of Wiebe and Judd (1971) may be a function of heat flux and degree of subcooling and varies from 1 to 1.75 for the data considered here. λ is set to be 1.2 in the numerical computation. The extrapolated superheat-layer thickness, δ, is estimated by Hsu (1962) using the expression given which was obtained assuming the thermal

layer is governed by one-dimensional unsteady heat conduction,

$$T_w - T_{sub0} = T_{sat} - T_{sub0} + \frac{2AC_3}{\delta} + \sqrt{\left(2(T_{sat} - T_{sub0}) + \frac{2AC_3}{\delta}\right)\left(\frac{2AC_3}{\delta}\right)}, \qquad (5.6)$$

where C_3 is equal to 1.6, A is equal to $2\sigma T_{sat}/\rho_v h_{fg}$, and σ is the surface tension. Hsu has demonstrated the usefulness of equation (5.6) for the prediction of the incipience point over a range of subcooling and pressure. As suggested by Wiebe and Judd (1971) equation (5.6) is used in this study to estimate the extrapolated superheat-layer thickness δ.

Since there is no strong mean flow over the bubble, the flow induced by the growth of the bubble is mainly of inviscid nature. Thus the liquid velocity field may be determined by solving the Laplace equation $\nabla^2\Phi = 0$ for the velocity potential Φ and the velocities are given by,

$$u_r(r,z) = \frac{\partial\Phi}{\partial r} \quad and \quad u_z(r,z) = \frac{\partial\Phi}{\partial z}. \qquad (5.7)$$

Since the bubble is a growing truncated sphere, the velocity field needs to be solved at each time step. If the vapor bubble is exactly hemispherical, which is the case during the early growth stage, the liquid velocities are

$$u_r(r,\psi) = \dot{R}(t)\frac{R^2(t)}{r^2}\sin^2(\psi) \quad and \quad u_z(r,\psi) = \dot{R}(t)\frac{R^2(t)}{r^2}\cos^2(\psi), \qquad (5.8)$$

where $\dot{R}(t) = \frac{dR(t)}{dt}$ and ψ is measured from the axis of

symmetry, i.e., z-axis. The general boundary conditions for Φ will be given in the transformed coordinates when a non-hemispherical bubble is considered.

5.2.3 Solid Heater

The energy equation for the solid is

$$\frac{\partial T_s}{\partial t} = \alpha_s\left[\frac{1}{r}\frac{\partial}{\partial r}\left(r\frac{\partial T_s}{\partial r}\right) + \frac{\partial^2 T_s}{\partial z^2}\right] + \frac{\alpha_s}{k_s}q''', \quad for\ 0 \le r < \infty,\ -H \le z \le 0 \tag{5.9}$$

subject to the initial condition

$$T_s = T_{sat} + \Delta T_{sat0} \qquad at\ t=t_0 \ll t_c$$

and the boundary conditions

$$\frac{\partial T_s}{\partial r} = 0 \qquad at\ r=0 \quad and \quad r\to\infty, \tag{5.11}$$

$$\frac{\partial T_s}{\partial z} = -q''/k_s \qquad at\ z=-H, \tag{5.12}$$

$$k_\ell\frac{\partial T_\ell}{\partial z} = k_s\frac{\partial T_s}{\partial z} \qquad at\ z=0, \quad 0\le r\le R_b(t), \tag{5.13}$$

$$-k_s\frac{\partial T_s}{\partial z} = \bar{h}(T_s - T_{sub0}) \qquad at\ z=0, \quad r>R_b(t) \tag{5.14}$$

where α_s and k_s are the thermal diffusivity and conductivity of the solid, t_c is the bubble collapse time scale, T_{sub0} is the subcooled bulk liquid temperature at infinity, $\bar{h}$ is the average convective heat transfer coefficient in the subcooled bulk liquid, q'' is the heat flux (on the

average), and q''' is the volummetric heating (on the average).

5.2.4 Non-dimensionalization and Grid Generation

To obtain a better understanding of the physics of the problem, the following dimensionless variables are introduced,

$$\tau = \frac{t}{t_c}, \quad \bar{r}_s = \frac{r}{R_b(t)}, \quad \bar{r}_{b\ell} = \frac{r}{R(t)}, \quad \bar{z}_s = \frac{z}{H}, \quad \bar{z}_{b\ell} = \frac{z}{R(t)},$$

$$\bar{R}(\tau) = \frac{R(t)}{R_c(t_c)}, \quad \theta_s = \frac{T_s - T_{sat}}{\Delta T_{sat0}}, \quad \theta_{b\ell} = \frac{T_{b\ell} - T_{sub0}}{T_{sat} - T_{sub0}}, \tag{5.15}$$

where $R_c(t_c)$ is defined in Chapter 2. Following Chapter 2, by using equation (5.15) and applying coordinate transformations,

$$\bar{r}_s = \bar{r}_\infty \{1 - S_r \tan^{-1}[(1-\zeta)\tan(1/S_r)]\} \qquad for\ 0 \le \zeta \le 1, \tag{5.16}$$

$$\bar{z}_s = -1 + S_z \tan^{-1}[(1-\varepsilon)\tan(1/S_z)] \qquad for\ 0 \le \varepsilon \le 1, \tag{5.17}$$

and $\tau=\sigma^2$, equation (5.9) becomes

$$\frac{1}{2\sigma}\frac{\partial\theta_s}{\partial\sigma} - \frac{\dot{R}_b t_c}{R_b}\bar{r}_s\frac{\partial\theta_s}{\partial\zeta}\frac{\partial\zeta}{\partial\bar{r}_s} = \frac{\phi\, f(C(\tau))}{\alpha\, Ja\, C^2(\tau)}\frac{1}{\bar{R}^2(\tau)}\frac{1}{\bar{r}_s}\frac{\partial}{\partial\zeta}\left(\bar{r}_s\frac{\partial\theta_s}{\partial\zeta}\frac{\partial\zeta}{\partial\bar{r}_s}\right)\frac{\partial\zeta}{\partial\bar{r}_s}$$

$$+ Fo\frac{\partial}{\partial\varepsilon}\left(\frac{\partial\theta_s}{\partial\varepsilon}\frac{\partial\varepsilon}{\partial\bar{z}_s}\right)\frac{\partial\varepsilon}{\partial\bar{z}_s} + \frac{\alpha_s t_c q'''}{k_s \Delta T_{sat0}}, \tag{5.18}$$

where α and κ are defined in the nomenclature, $\bar{r}_\infty$ is the radial position at which equation (5.9) is applied, the

constant S_r determines the percentage of the grid number allocated to the region of $\bar{r}_s \leq 1$, and S_z is a constant characterizing the stretching in the z-direction.

For the subcooled bulk liquid, the energy equation in dimensionless form is

$$\frac{1}{2\sigma}\frac{\partial \theta_{b\ell}}{\partial \sigma} + \left(u_r - \dot{R}\bar{r}_{b\ell}\right)\frac{t_c}{R}\frac{\partial \theta_{b\ell}}{\partial \bar{r}_{b\ell}} + \left(u_z - \dot{R}\bar{z}_{b\ell}\right)\frac{t_c}{R}\frac{\partial \theta_{b\ell}}{\partial \bar{z}_{b\ell}}$$

$$= \frac{t_c \alpha_\ell}{R^2}\left(\frac{\partial^2 \theta_{b\ell}}{\partial \bar{r}_{b\ell}^2} + \frac{1}{\bar{r}_{b\ell}}\frac{\partial \theta_{b\ell}}{\partial \bar{r}_{b\ell}} + \frac{\partial^2 \theta_{b\ell}}{\partial \bar{z}_{b\ell}^2}\right). \tag{5.19}$$

To solve the Laplace equation for Φ and energy equation for $\theta_{b\ell}$, an algebraic grid generation technique is used for the bulk liquid outside the growing bubble. Figure 5.2 shows the computational grids for the numerical simulation. The clustering of grids near the bubble surface is necessary to resolve large temperature gradients. The $\bar{r}_{b\ell}$ and $\bar{z}_{b\ell}$ within the physical domain are calculated as

$$\bar{r}_{b\ell}(i,j) = D(j)\sin(\gamma(i,j)),$$

$$\bar{z}_{b\ell}(i,j) = D(j)\cos(\gamma(i,j)) + \bar{z}_h, \tag{5.20}$$

where

$$\omega(j) = \frac{\pi}{2} + \sin^{-1}\left(\frac{\bar{z}_h}{D(j)}\right),$$

$$\gamma(i,j) = \omega(j)\frac{i-1}{M}, \tag{5.21}$$

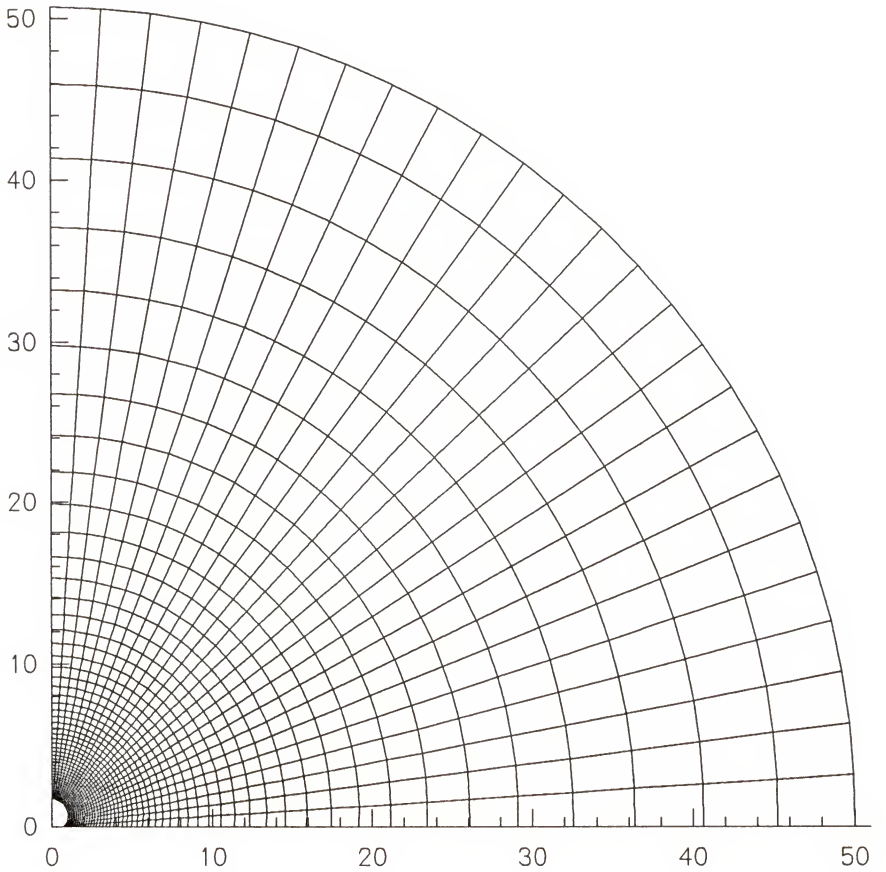

Figure 5.2 The computational grids for the numerical simulation.

$\bar{z}_h = \frac{h}{R} = \sqrt{1-C^2}$, and $D(j) = 1 + (\bar{R}_\infty - 1)\left\{1 - S_{R'} \tan^{-1}[(1-\eta)\tan(1/S_{R'})]\right\}$. $\bar{R}_\infty$ is the radial position at infinity and the constant $S_{R'}$ determines the percentage of the grid number near the bubble surface. Figure 5.3 illustrates the grid parameters.

The transformed energy and Laplace equations for the subcooled bulk liquid are

$$\begin{aligned}\frac{1}{2\sigma}\frac{\partial \theta_{b\ell}}{\partial \sigma} + A_r J\left(\bar{z}_{b\ell_\eta}\frac{\partial \theta_{b\ell}}{\partial \xi} - \bar{z}_{b\ell_\xi}\frac{\partial \theta_{b\ell}}{\partial \eta}\right) + A_z J\left(\bar{r}_{b\ell_\xi}\frac{\partial \theta_{b\ell}}{\partial \eta} - \bar{r}_{b\ell_\eta}\frac{\partial \theta_{b\ell}}{\partial \xi}\right) \\ = \frac{t_c \alpha_\ell}{R^2} J^2\left(a\frac{\partial^2 \theta_{b\ell}}{\partial \xi^2} + 2b\frac{\partial^2 \theta_{b\ell}}{\partial \eta \partial \xi} + c\frac{\partial \theta_{b\ell}}{\partial \eta^2} + d\frac{\partial \theta_{b\ell}}{\partial \eta} + e\frac{\partial \theta_{b\ell}}{\partial \xi}\right) \\ + \frac{t_c \alpha_\ell}{R^2}\frac{J}{r_{b\ell}}\left(\bar{z}_{b\ell_\eta}\frac{\partial \theta_{b\ell}}{\partial \xi} - \bar{z}_{b\ell_\xi}\frac{\partial \theta_{b\ell}}{\partial \eta}\right)\end{aligned} \tag{5.22}$$

and

$$J^2\left(a\frac{\partial^2 \Phi}{\partial \xi^2} + 2b\frac{\partial^2 \Phi}{\partial \eta \partial \xi} + c\frac{\partial \Phi}{\partial \eta^2} + d\frac{\partial \Phi}{\partial \eta} + e\frac{\partial \Phi}{\partial \xi}\right) + \frac{J}{r_{b\ell}}\left(\bar{z}_{b\ell_\eta}\frac{\partial \Phi}{\partial \xi} - \bar{z}_{b\ell_\xi}\frac{\partial \Phi}{\partial \eta}\right) = 0 \tag{5.23}$$

where $J = \frac{1}{\bar{r}_{b\ell_\xi}\bar{z}_{b\ell_\eta} - \bar{z}_{b\ell_\xi}\bar{r}_{b\ell_\eta}}$ which is the Jacobian,

$a = \bar{r}_{b\ell_\eta}{}^2 + \bar{z}_{b\ell_\eta}{}^2$, $b = \bar{r}_{b\ell_\eta}\bar{r}_{b\ell_\xi} + \bar{z}_{b\ell_\eta}\bar{z}_{b\ell_\xi}$, $c = \bar{r}_{b\ell_\xi}{}^2 + \bar{z}_{b\ell_\xi}$,

$d = J(\beta_1 \bar{z}_{b\ell_\xi} + \beta_2 \bar{r}_{b\ell_\xi})$, $e = J(\beta_2 \bar{r}_{b\ell_\eta} + \beta_1 \bar{z}_{b\ell_\eta})$, $\beta_1 = a\bar{r}_{b\ell_{\xi\xi}} - 2b\bar{r}_{b\ell_{\xi\eta}} + c\bar{r}_{b\ell_{\eta\eta}}$,

$\beta_2 = a\bar{z}_{b\ell_{\xi\xi}} - 2b\bar{z}_{b\ell_{\xi\eta}} + c\bar{z}_{b\ell_{\eta\eta}}$, $A_r = (u_r - \dot{r})t_c/R$, and $A_z = (u_z - \dot{z})t_c/R$.

The temperature boundary conditions are $\theta_{b\ell}$=1 along the

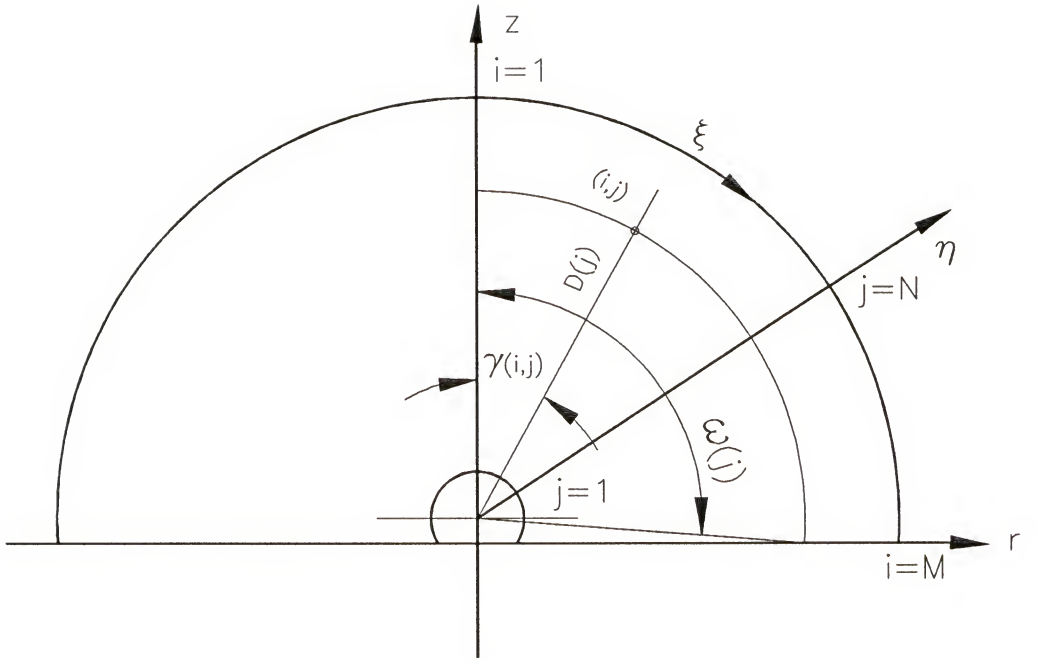

Figure 5.3 Grid parameters

vapor-liquid interface, and the temperature gradient is zero along the line of symmetry. The heat flux at the solid heater is equal to the heat flux to the subcooled bulk liquid along the wall. The far-field boundary condition for $\theta_{b\ell}$ is approximated by zero heat flux. The boundary conditions for velocity potential are zero velocity potential gradient along the wall and the line of symmetry. The far-field boundary condition is approximated by a zero flux condition. The boundary condition at the vapor-liquid interface is $\frac{\partial \Phi}{\partial n} = \dot{R} + \dot{h}\cos\psi$, where $\dot{h} = \frac{dh(t)}{dt}$ is the bubble vertical velocity due to its moving center, and h(t) is the distance from the wall to the bubble center. Equation (5.22) is solved using the ADI method (Anderson et al., 1984) and equation (5.23) is solved using SOR by line (Anderson et al., 1984).

5.3 The Asymptotic Analysis of $\theta_{b\ell}$

To gain a basic understanding of the behavior of $\theta_{b\ell}(t,r,z)$ associated with a rapidly growing vapor bubble, an asymptotic analysis for $\theta_{b\ell}$ is presented in this study. For simplicity, we consider the growth of a hemispherical bubble. As mentioned early, during the earlier stage of the bubble growth, the bubble shape is indeed hemispherical. Due to the rapid bubble growth and the limited extent of the heat diffusion effect, there exists a thin thermal boundary layer adjacent to the bubble surface. Thus an asymptotic

analysis can be used to describe the complex phenomena.

Using the dimensionless variables in equation (5.15) and defining a new dimensionless variable as $\bar{R}' = \frac{R'}{R(t)}$, the energy equation for the subcooled liquid in spherical coordinates is,

$$\frac{R}{t_c \dot{R}} \frac{\partial \theta_{b\ell}}{\partial \tau} + \left(\frac{1}{\bar{R}'^2} - \bar{R}' \right) \frac{\partial \theta_{b\ell}}{\partial \bar{R}'} = \frac{\alpha_\ell}{R\dot{R}} \left(\frac{\partial^2 \theta_{b\ell}}{\partial \bar{R}'^2} + \frac{2}{\bar{R}'} \frac{\partial \theta_{b\ell}}{\partial \bar{R}'} \right) + \frac{\alpha_\ell}{R\dot{R}} \frac{1}{\sin\psi} \frac{1}{\bar{R}'^2} \frac{\partial}{\partial \psi} \left(\sin\psi \frac{\partial \theta_{b\ell}}{\partial \psi} \right). \tag{5.24}$$

During the early stage of growth, the bubble growth rate is high and expands rapidly so that

$$A = \frac{R\dot{R}}{\alpha_\ell} \gg 1. \tag{5.25}$$

Thus, the solution for equation (5.24) includes the outer approximation and inner approximation (boundary layer solution). To obtain the outer solution for equation (5.24), the diffusion term in equation (5.24) is neglected. This results in, to the leading order,

$$\frac{R}{\dot{R}} \frac{\partial \theta_{b\ell}^{out}}{\partial t} + \left(\frac{1}{\bar{R}'^2} - \bar{R}' \right) \frac{\partial \theta_{b\ell}^{out}}{\partial \bar{R}'} = 0. \tag{5.26}$$

The general solution of equation (5.26) is

$$\theta_{b\ell}^{out} = F\left[R(t) \left(\bar{R}'^3 - 1 \right)^{1/3} \right] \tag{5.27}$$

where F is an arbitrary function and it is determined from the initial condition. It is noted that the solution for $\theta_{b\ell}$ is described by $R(t)(\bar{R}^{/3}-1)^{1/3}$ = constant along the characteristic curve . Due to the discontinuity in $\frac{\partial T_{b\ell}}{\partial z}$ of the initial condition, equation (5.5), we use the following continuous function instead of equation (5.5), in discussing the analytical solution for $\theta_{b\ell}$,

$$\frac{T_{b\ell}-T_{sub0}}{T_w-T_{sub0}}=e^{-w\frac{z}{\delta}}. \tag{5.28}$$

This function matches the linear part of equation (5.5) and the computational results indicate that there only exists about 3~4% difference in the computed bubble radius R(t) when equation (5.28) is used. To determine F, the initial condition given by equation (5.28) is employed,

$$\theta_{b\ell}^{out}=\theta_{sub0}\exp\left\{-W\frac{R_0\cos\psi}{\delta}\left[1+\frac{R^3}{R_0^3}\left(\bar{R}^{\beta}-1\right)\right]^{1/3}\right\} \tag{5.29}$$

where

$$\theta_{sub0}=\frac{T_w-T_{sub0}}{T_{sat}-T_{sub0}}\ ,$$

and R_0 is the initial bubble radius at $t=t_0 \ll t_c$ and R_0 can be easily obtained from equation (5.2). As long as the bubble growth rate is high, i.e. $A \gg 1$, equation (5.29) is not only an accurate outer solution for a hemispherical bubble, but also is a good approximation for the far field boundary

condition for $\theta_{b\ell}$ in equation (5.22) for non-hemispherical bubbles.

The outer solution automatically satisfies the condition for $\theta_{b\ell}$ as $\bar{R}'\to\infty$. However, on the bubble surface, $\bar{R}'=1$, $\theta_{b\ell}=1$ cannot be satisfied by $\theta_{b\ell}^{out}$. The smooth transition of $\theta_{b\ell}$ from $\theta_{b\ell}^{out}$ $(\bar{R}'=1)$ to $\theta_{b\ell}=1$ at $\bar{R}'=1$ calls for an inner (or boundary layer) solution. In this thin boundary layer, the effect of heat conduction is no longer negligible and must be properly accounted for. For large A, a boundary layer coordinate X is introduced

$$X=\frac{\bar{R}'-1}{\delta^*(A)} \tag{5.30}$$

where δ^*(A) is the scale of the boundary layer which is determined by balancing the convection term with the conduction term in the boundary layer. Substituting equation (5.30) into equation (5.24) results in

$$\frac{R}{t_c\dot{R}}\frac{\partial\theta_{b\ell}^{in}}{\partial\tau}+\frac{R}{t_c\dot{R}}\frac{\partial X}{\partial\tau}\frac{\partial\theta_{b\ell}^{in}}{\partial X}+\left(\frac{1}{(1+\delta^*X)^2}-1-\delta^*X\right)\frac{1}{\delta^*}\frac{\partial\theta_{b\ell}^{in}}{\partial X}$$

$$=\frac{1}{A\delta^{*2}}\left(\frac{\partial^2\theta_{b\ell}^{in}}{\partial X^2}+\frac{2\delta^*}{1+\delta^*X}\frac{\partial\theta_{b\ell}^{in}}{\partial X}\right)+\frac{1}{A}\frac{1}{(1+\delta^*X)^2}\frac{1}{\sin\psi}\frac{\partial}{\partial\psi}\left(\sin\psi\frac{\partial\theta_{b\ell}^{in}}{\partial\psi}\right). \tag{5.31}$$

Since

$$\frac{1}{(1+\delta^* X)^2} = 1 - 2\delta^* X + 3\delta^{*2} X^2 + O(\delta^{*3}),$$

$$\frac{1}{1+\delta^* X} = 1 - \delta^* X + \delta^{*2} X^2 + O(\delta^{*3}), \tag{5.32}$$

equation (5.31) becomes

$$\frac{R}{t_c \dot{R}} \frac{\partial \theta_{b\ell}^{in}}{\partial \tau} = \frac{1}{A\delta^{*2}} \left(\frac{\partial^2 \theta_{b\ell}^{in}}{\partial X^2} + 2\delta^* (1 - \delta^* X + \delta^{*2} X^2) \frac{\partial \theta_{b\ell}^{in}}{\partial X} \right)$$

$$+ 3X\left(1 - \frac{R}{3 t_c \dot{R} X} \frac{\partial X}{\partial \tau} - \delta^* X\right) \frac{\partial \theta_{b\ell}^{in}}{\partial X} + \frac{1 - 2\delta X + 3\delta^{*2} X^2}{A} \frac{1}{\sin\psi} \frac{\partial}{\partial \psi} \left(\sin\psi \frac{\partial \theta_{b\ell}^{in}}{\partial \psi} \right), \tag{5.33}$$

in the limit $\delta^*(A) \to 0$ as $A \to \infty$. The balance between the convection term and the diffusion term requires $\delta^* = A^{-1/2}$. Thus, equation (5.33) results in

$$\frac{R}{t_c \dot{R}} \frac{\partial \theta_{b\ell}^{in}}{\partial \tau} = \frac{\partial^2 \theta_{b\ell}^{in}}{\partial X^2} + \left(3 - \frac{R}{2 t_c \dot{R}} \frac{\dot{A}}{A}\right) X \frac{\partial \theta_{b\ell}^{in}}{\partial X} \tag{5.34}$$

subject to the boundary conditions

$$\theta_{b\ell}^{in} = 1 \qquad at \qquad X = 0 \tag{5.35}$$

$$\theta_{b\ell}^{in} = \theta_{sub0} \qquad at \quad X \to \infty . \tag{5.36}$$

For $\tau \ll 1$, $R(t) \propto t^{1/2}$ and $\frac{R}{t_c \dot{R}} \sim \tau$. Thus, the LHS of equation (5.34) is small and equation (5.34) reduces to

$$\frac{\partial^2 \theta_{b\ell}^{in}}{\partial X^2} + 3X\frac{\partial \theta_{b\ell}^{in}}{\partial X} = 0, \qquad for\ \tau \ll 1. \tag{5.37}$$

The solution for equation (5.37) is

$$\theta_{b\ell}^{in} = 1 + (\theta_{sub0} - 1)\ erf(\sqrt{3/2}\,X). \tag{5.38}$$

The uniformly valid solution for $\theta_{b\ell}$ for $\tau \ll 1$ is $\theta_{b\ell}^{uv} = \theta_{b\ell}^{in} + \theta_{b\ell}^{out} - \theta_{b\ell}^{cp}$. Since $\theta_{b\ell}^{cp} = \theta_{sub0}$, we have

$$\theta_{b\ell}^{u.v.} = 1 + (\theta_{sub0} - 1)\ erf(\sqrt{3/2}\,X)$$

$$+ \theta_{sub0} \exp\left\{ -W\frac{R_0 \cos\psi}{\delta}\left[1 + \frac{R^3}{R_0^3}\left(\bar{R}^{/3} - 1 \right) \right]^{1/3} \right\} - \theta_{sub0}. \tag{5.39}$$

Equation (5.39) is an approximate asymptotic solution for $\theta_{b\ell}$ for $\tau \ll 1$. As $R/\dot{R}$ increases, equation (5.39) becomes increasingly inaccurate due to the neglect of the LHS in equation (5.34).

5.4 Results and Discussion

The shape parameter C(t) mainly describes how the shape of the vapor bubble changes during the bubble growth and collapse. Due to a lack of experimental information, the bubble shape factor in this study is assumed to vary as

$$C(t) = \begin{cases} 1 & , \ 0 \le t \le t_s \\ \sin\left(\frac{\pi}{2}\left(2 - \frac{1}{1+(t/t_s - 1)^2}\right)\right) & , \ t_s < t \end{cases} \tag{5.40}$$

where t_s is the time when the bubble shape begins to change from a hemisphere to a sphere. The determination for t_s employs a dimensionless parameter $\mu = \frac{\dot{R}(t)\, t}{R(t)}$ which characterizes the relative growth rate. It is noted that μ_s (i.e. $t=t_s$) is determined by matching the computed growth rates with the experimental data in order to achieve the best fit. In this study μ_s ranges from 0.23 to 0.48.

Two empirical parameters, ϕ and μ_s, need to be specified for the present computation. Through the comparison of predicted growth rates with experimental results, ϕ and μ_s can be determined via the best fit. From the numerical results there exists only one combination of ϕ and μ_s for the best agreement with experimental data. Although the present computational model seems crude due to the uncertainty in the two empirical constants, the main contribution lies in the basic understanding of the bubble growth mechanisms during subcooled nucleate boiling.

5.4.1 Validation of the Model by the Comparison of Growth Rate

To validate the present numerical computation and to understand the effect of subcooling on the growth rate,

comparisons are made between the predicted and the measured R(t) by Ellion (1954) and Cochran and Aydelott (1966). Figure 5.4a shows comparisons in the high subcooling range, ΔT_{sub0}=55.6°C~83.3°C. The data are taken from Ellion (1954) who used distilled degassed water as the boiling liquid. The heating surface consists of a 304 stainless-steel strip with a thickness of 0.11 mm. For each subcooling there are 5 sets of data at the same boiling conditions. The data shown in Figure 5.4a consist of a set which falls within the average value of the experimental results. Close agreement between the predicted and the measured growth rates is observed for most of the time. Figure 5.4a also shows that the maximum R(t) and the bubble lifetime increase with an increase in bulk liquid temperature. In the later stage of collapse, the bubble radius is over-predicted. It may be due to an improper specification of the shape factor, C(t), at later time. In Figure 5.4b the computed bubble volume is compared with the measured data of Cochran and Aydelott (1966). The subcooling ΔT_{sub0} ranges from 7.4°C~21.4°C, and the boiling liquid is water. The heater material is a 0.13 mm thick chromel strip. Good agreement for the bubble volume is observed for most of the time. A little discrepancy is observed at the later stage of collapse. It is also evident that the vapor bubble has a larger volume when the bulk liquid temperature is higher. From Figures 5.4a-b we see that when the subcooling decreases, the bubble

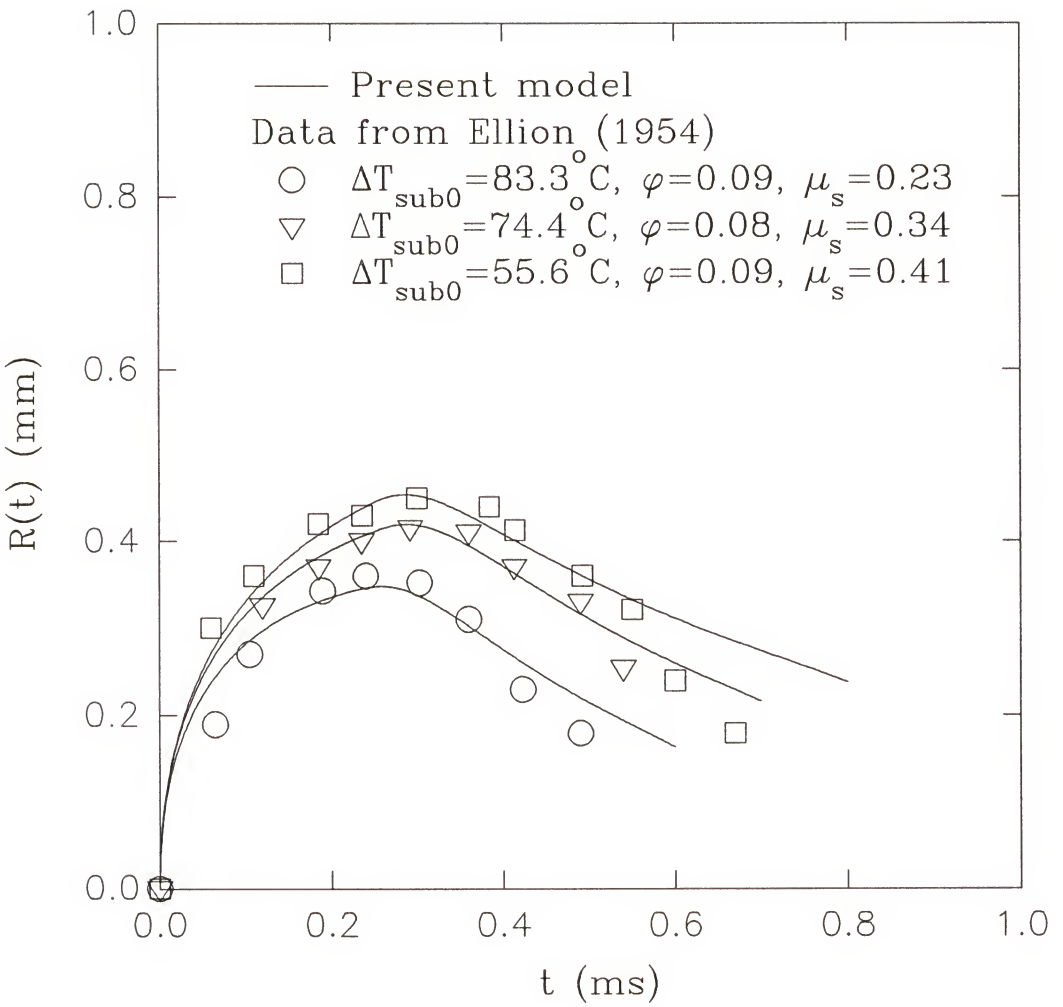

Figure 5.4a Comparison of the bubble growth rate between the present model and the experimental data of Ellion (1954).

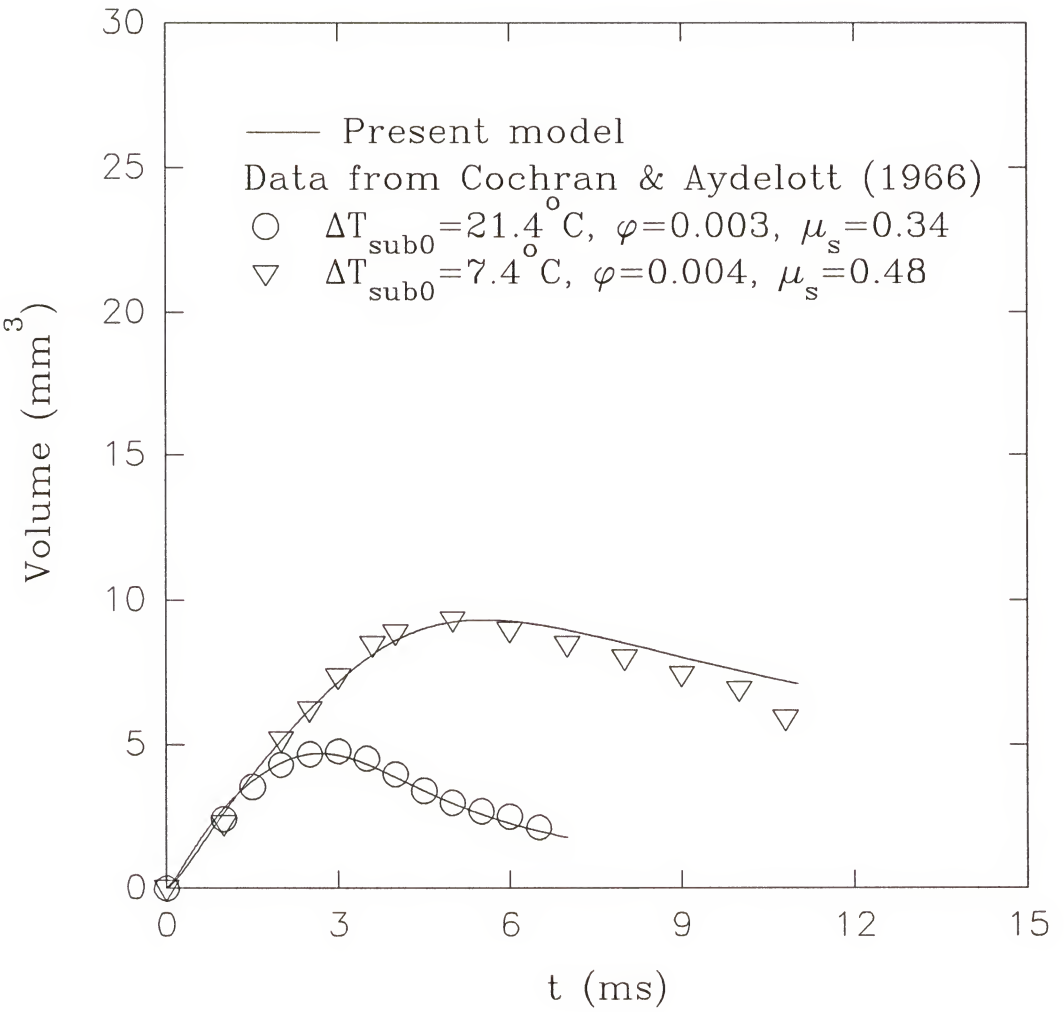

Figure 5.4b Comparison of the vapor bubble volume between the present model and the experimental data of Cochran and Aydelott (1966).

collapse rate is reduced at the later stage.

5.4.2 Behavior of the Heat Transfer Rate to the Bubble during Growth

In Figure 5.5 the numerical results for the total heat transfer rate between the liquid microlayer and the vapor bubble dome are shown. The boiling condition corresponds to that of Ellion (1954) with T_{sub0}=44.4°C. It is evident that the microlayer continuously supplies energy to the bubble. At the early stage, the bubble grows rapidly within the thermal boundary layer, in which only a small portion of the top of the dome is exposed to the subcooled bulk liquid. Because of the rapid increase in the bubble surface area, the total heat transfer rate increases during the early stage. In the middle stage of the bubble growth, more of the top portion of the bubble surface area is exposed to the subcooled liquid which results in decreasing the heat transfer rate to the bubble. As the total heat transfer rate becomes negative, the bubble starts to collapse. When the bubble is collapsing at the later stage, an increasing portion of the surface area is exposed to the thermal boundary layer again. This results in a decreasing rate of bubble collapse.

5.4.3 Thermal Field in the Solid Heater during the Growth

Figure 5.6 shows the four computed temperature contours at Ja=83 and Fo=0.1 for τ=0.1, 0.25, 0.5, 1. For Fo=0.1, the heater is considered to be thick and the asymptotic

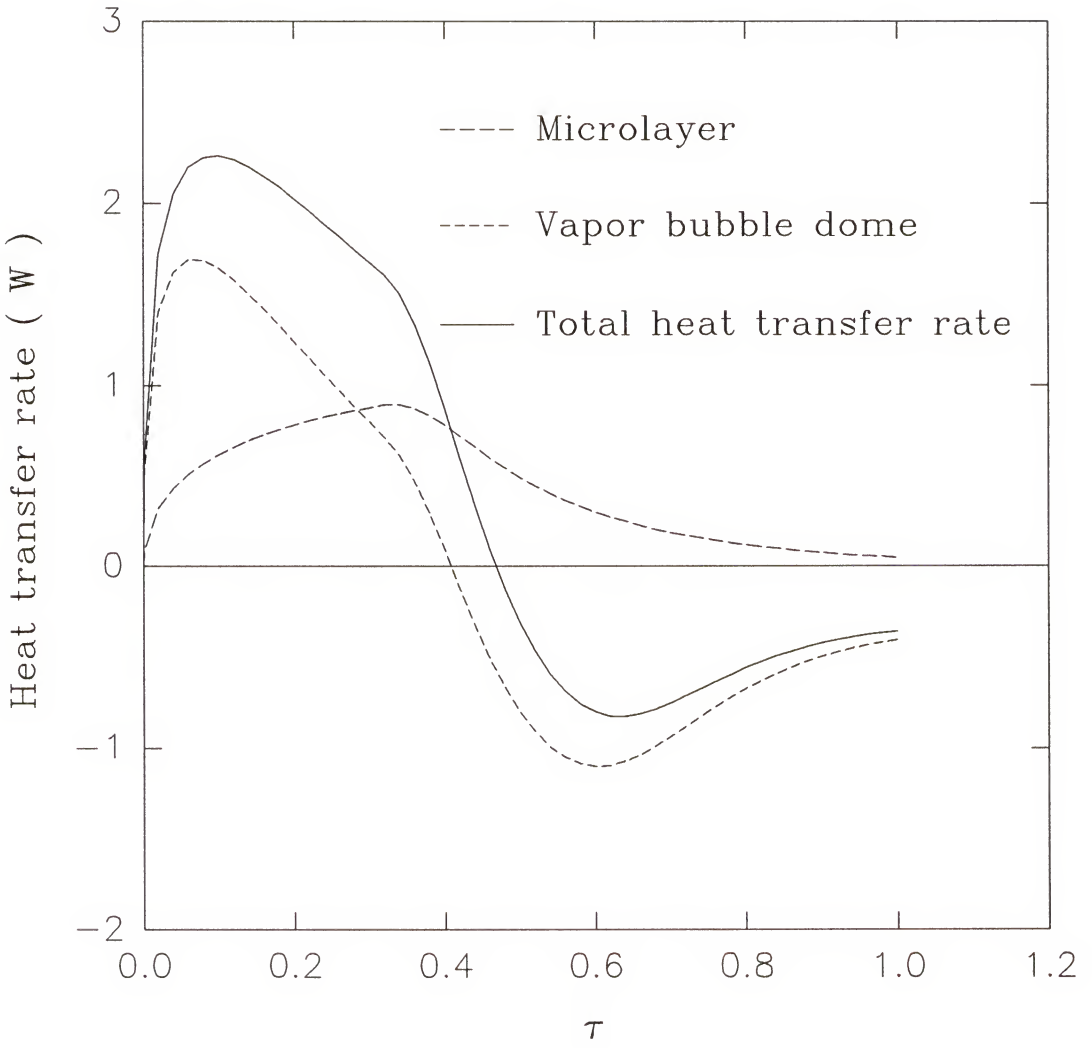

Figure 5.5 The total heat transfer rate between the liquid microlayer and the vapor bubble dome.

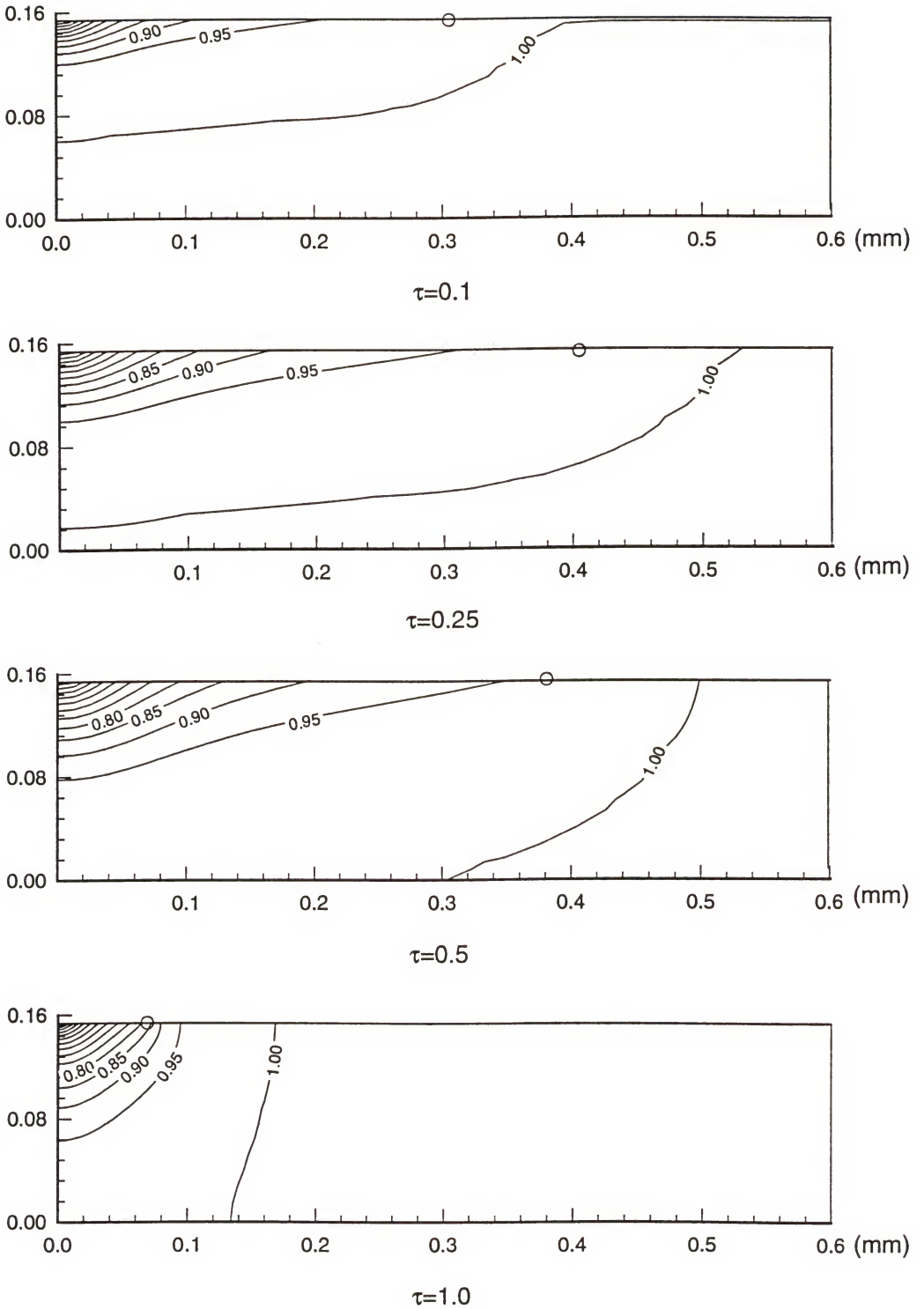

Figure 5.6 The four computed temperature contours at Ja=83 and Fo=0.1 for τ=0.1, 0.25, 0.5, and 1.

behavior (Chapter 3) is valid for most of the time. The circular markers are the locations of the microlayer edge. During the bubble growth period, it is easy to see that the temperature contours in the solid penetrate down and move to the right in a similar way as the bubble grows. When the bubble collapses, the temperature contours move to the left following the movement of the microlayer edge.

Figure 5.7 shows the development of the thermal field at the surface of the solid heater at Fo=0.1 and Ja=83 in which T_{sub0}=44.4°C. The circular markers are the locations of the microlayer edge. During bubble growth, the temperature behaves similarly to the saturated boiling case (Chapter 3). It is clearly seen that the thermal field moves to the right following the bubble growth. During the bubble collapse period, the surface temperature quickly recovers and the thermal field shifts back to the left.

5.4.4 Thermal Field of the Bulk Liquid

Figure 5.8 shows the computed isotherms in the subcooled liquid surrounding a growing and collapsing vapor bubble. It is seen that there exists an unsteady thermal boundary layer around the vapor bubble. The crease of the temperature contours is adjacent to the bubble surface in a very thin thermal layer. These results are very difficult to obtain experimentally. Ellion (1954) has stated that there exists an unsteady thermal boundary layer contiguous to the vapor bubble during the bubble growth and collapse.

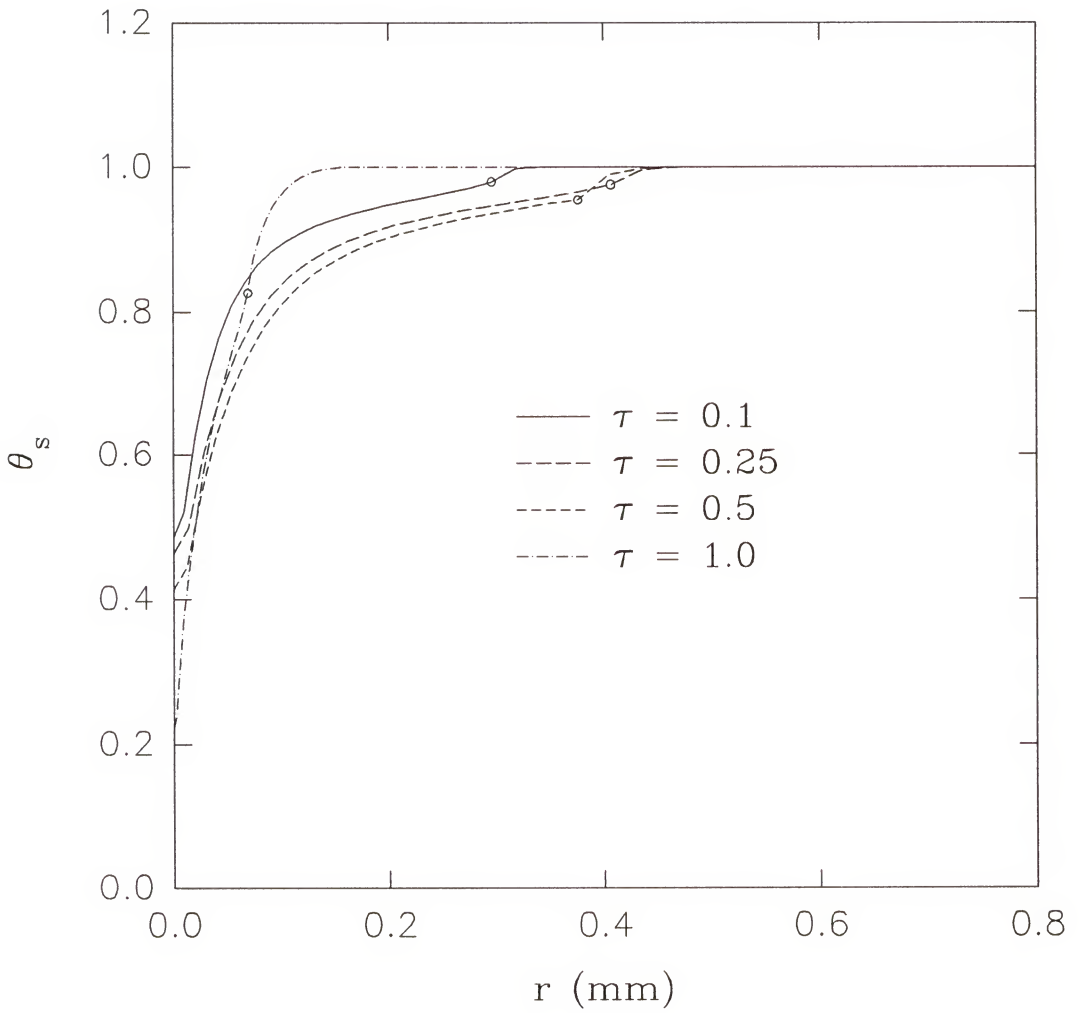

Figure 5.7 Development of the thermal layer at the surface of the solid heater.

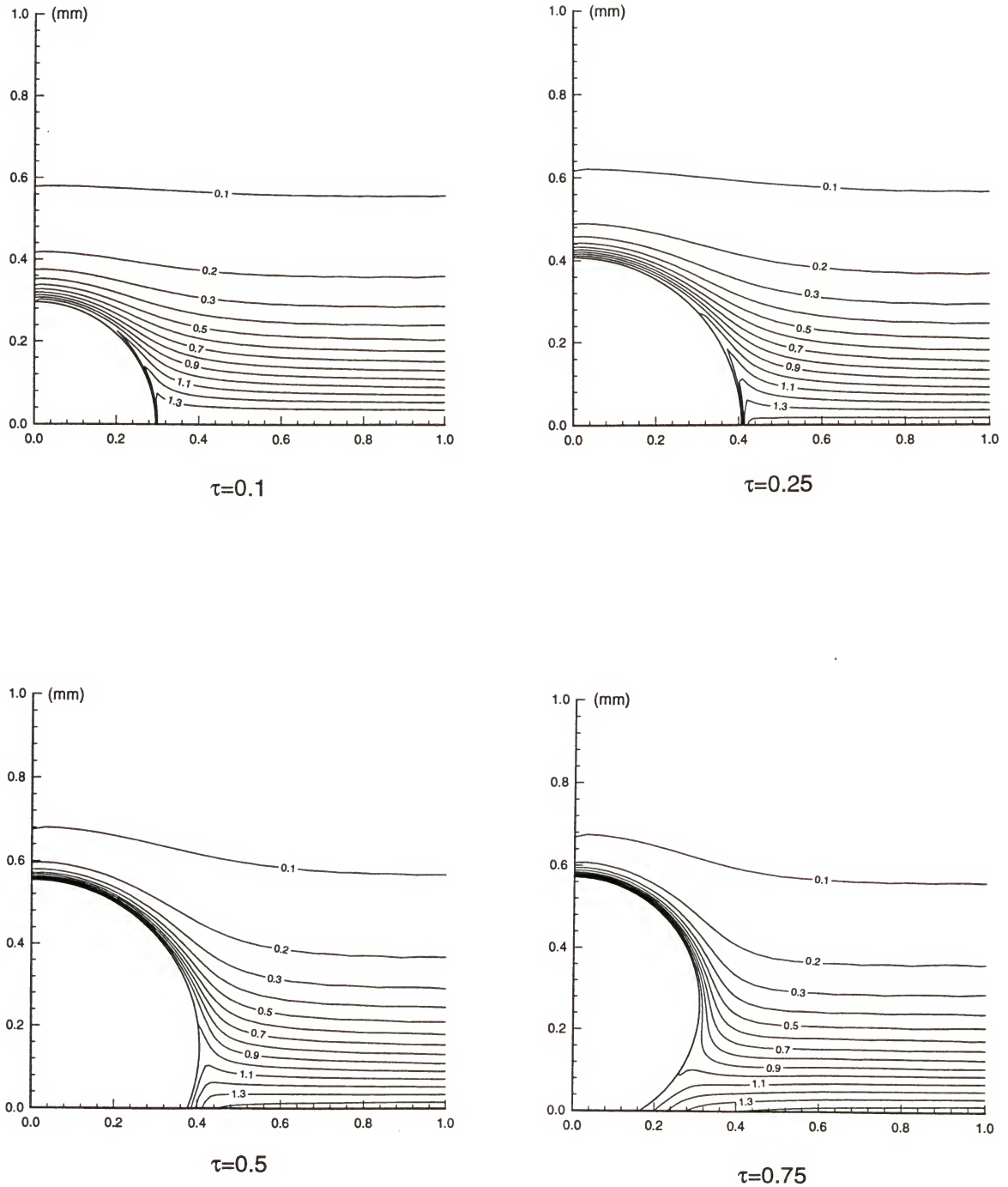

Figure 5.8 The computed isotherms in the subcooled liquid surrounding a growing and collapsing vapor bubble at four different times.

Lee and Nydahl (1989) investigated the effect of hydrodynamics surrounding the dome of the growing bubble by assuming a constant wall temperature in saturated boiling. Their numerical results also showed the folding of the temperature contours near the bubble surface. During the early stage of growth, we indeed see that most of the bubble surface is exposed to the thermal boundary layer, while a portion of the bubble surface is outside the thermal boundary layer when the bubble is collapsing. Figure 5.8 also showed that the folding of the temperature contours near the wall always exist during bubble growth and collapse. The folding is associated with the temperature distribution near the bubble surface and will be further elucidated by examining the asymptotic solution.

5.4.5 Asymptotic Behavior of $\theta_{b\ell}$ during Rapid Growth

To further understand the thermal boundary layer near the bubble surface, $\theta_{b\ell}$ based on the asymptotic solution and numerical solution are compared. Figure 5.9 shows the comparison for $\theta_{b\ell}$ between the asymptotic solutions and numerical solutions at τ=0.001, 0.01, 0.1, and 0.3 for ψ=0°, 30°, and 75°. It is clearly seen that the numerical solutions compare well with the asymptotic solutions at τ=0.001 and 0.01. As mentioned early, the inner solution is only valid when $\tau \ll 1$. At τ=0.1 and 0.3, $R/(t_c\dot{R})$ is equal to 0.3 and 1.2. Thus, the inner solution given by equation (5.36), is no longer accurate. However the outer solution

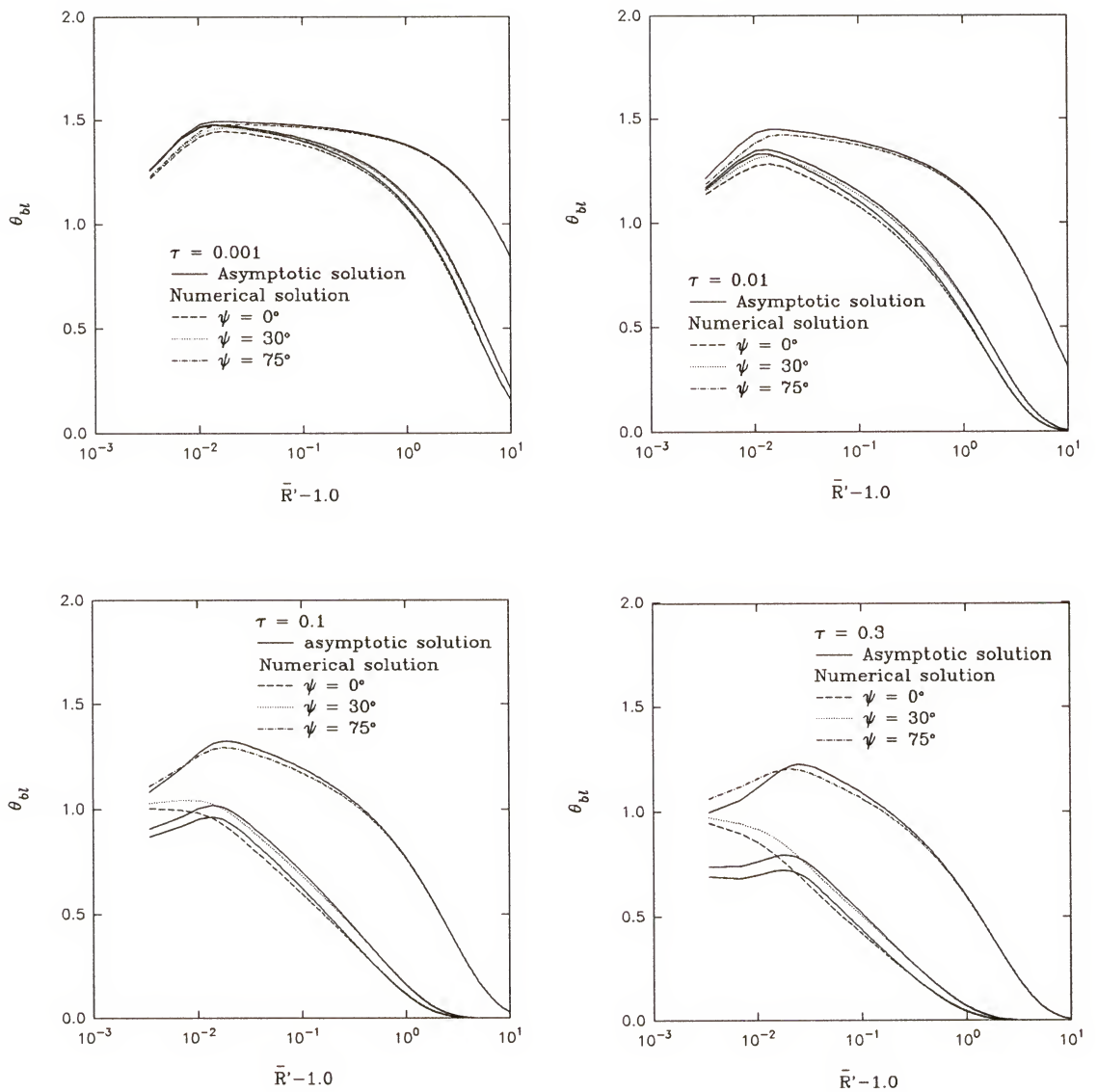

Figure 5.9 Comparison of the asymptotic solutions and the numerical solutions at τ=0.001, 0.01, 0.1, and 0.3 for ψ=0°, 30°, and 75°.

should remain valid because A$\gg$1 is the only requirement. Figure 5.9 also shows the detailed structure of the thin thermal boundary layer adjacent to the vapor bubble surface. For example, at τ=0.001 and 0.01, A=$R\dot{R}/\alpha_\ell$ = 14280 and 10950, and the thermal boundary layer scale is δ^*=$A^{-1/2}$=0.0084 and 0.0096. It is easily seen that the thermal boundary layer thickness in Figure 5.9 at τ=0.001 and 0.01 is the same order as δ^*. It increases with time because A decreases with time.

At τ=0.001 and 0.01, the entire bubble surface is within the thermal boundary layer and $\theta_{b\ell}$ exhibits non-monotonic behavior at ψ=0° and ψ=30°. This non-monotonic behavior is reflected by the folding of the thermal contours. At τ=0.1 and 0.3, the temperature profile is monotonic at ψ=0° and 30°. The temperature profile is always non-monotonic at ψ=75°. This explains why the folding of the temperature contours near the wall always exists during bubble growth and collapse.

5.4.6 Velocity Field of the Bulk Liquid

Figure 5.10 shows the computed velocity vectors and the streamlines. At τ=0.25, the flow field resembles that of a source flow. This source flow mainly results from the growth of the bubble. At τ<0.4, the flow field is due to the combination of a source and a moving doublet; the moving doublet is caused by the motion of the bubble center in the z-direction. At τ=0.4, the velocity vectors are almost

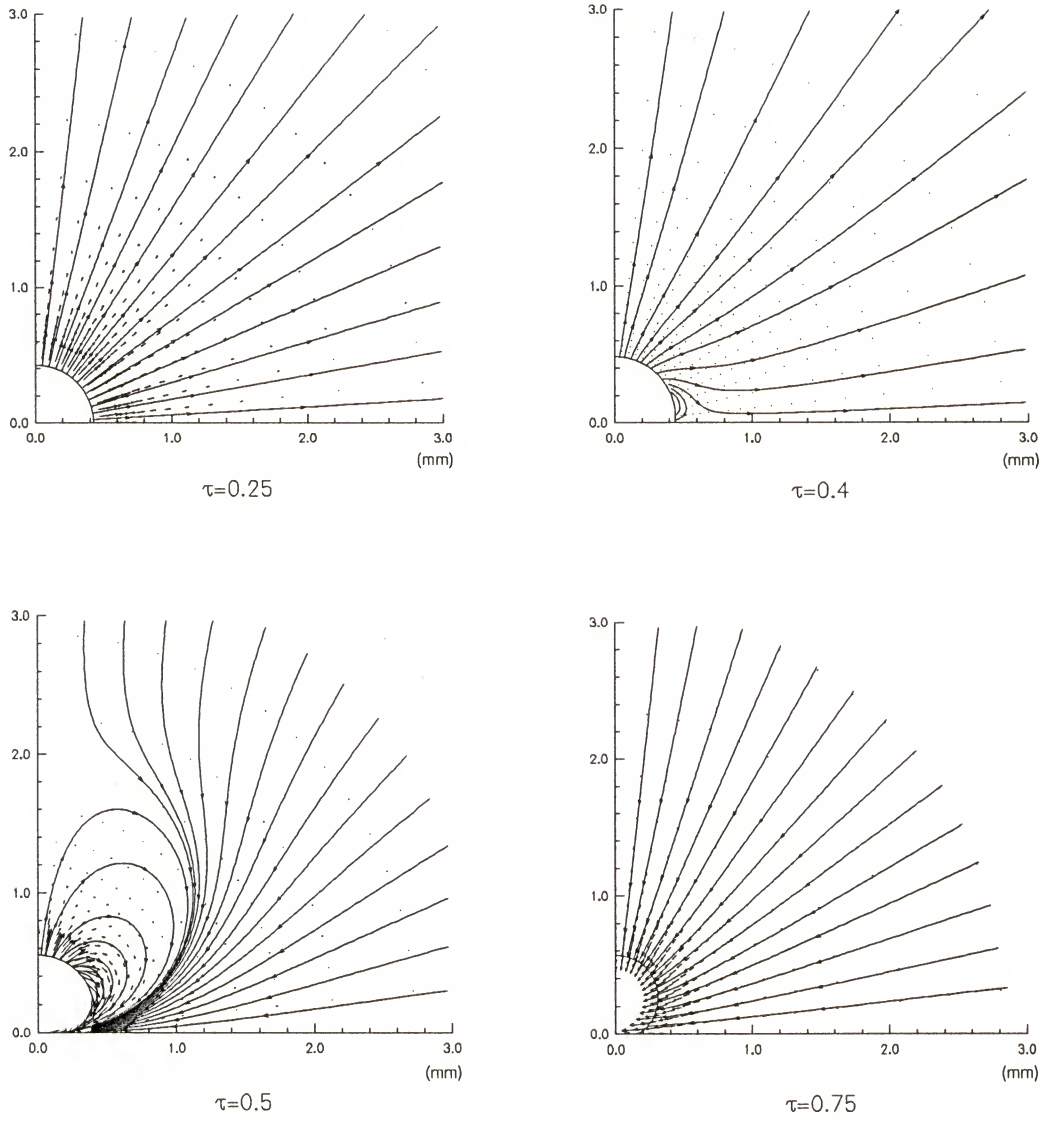

Figure 5.10 The computed velocity vectors and streamlines at four different times.

zero. At this point, the bubble growth rate is close to zero, and the bubble begins to collapse. At τ=0.5, the flow field can be interpreted as a combination of a sink and a doublet that is moving upwards. The doublet is moving upward because dh(t)/dt>0. At this instance the vapor bubble continues to collapse. Its shape is becoming more spherical. Between τ=0.5 and τ=0.75, the bubble collapse rate increases and dh(t)/dt becomes negative at some instance. At τ=0.75, the flow field is mainly due to the sink as the bubble continues to collapse.

5.5 Summary

Detailed theoretical and numerical analyses are presented to elucidate the effect of the energy transfer and hydrodynamics on the growth rate of a vapor bubble in highly subcooled pool boiling. The bubble growth or collapse rates are obtained by combining the energy transfered from the liquid microlayer and from the bulk liquid. The microlayer wedge angle, ϕ, and the relative growth rate (at $t=t_s$), μ_s, are two empirically determined constants which are used in the numerical simulation. There only exists one combination for ϕ and μ_s to obtain the best fit for the bubble radius. As long as ϕ and μ_s are correctly specified, the predicted bubble growth rate compares well with the reported experimental data. The numerical results also reveal elegance of the energy transfer process in the solid heater

and the subcooled bulk liquid during the bubble growth and collapse. The rapid variation of the thermal field of the bulk liquid during the rapid growth of the bubble is elucidated by short time asymptotic solution that is uniformly valid in the bulk liquid. The folding of the temperature contours is explained via the asymptotic and numerical solution of $\theta_{b\ell}$ near the bubble surface. It is shown that the velocity field in the subcooled bulk liquid has a significant effect on the vapor bubble growth and collapse. The present study for vapor bubble growth is limited to pool boiling in the isolated bubble regime.

CHAPTER 6

CONCLUSIONS AND RECOMMENDATIONS FOR FUTURE RESEARCH

This chapter summarizes the major research accomplishments from this study and provides suggestions for future work.

6.1 Achievements

This research has significantly progressed the understanding of the bubble growth process during nucleate pool boiling.

1. A numerical analysis has been carried out to study vapor bubble growth in saturated heterogeneous pool boiling. The predicted bubble growth rate in saturated pool boiling compares very well with the reported experimental data over a wide range of conditions. The empirically determined correlation for C_1 suggests that the liquid Prandtl number has little effect on the bubble growth rate. Thus, the viscosity of the liquid plays little role in the bubble growth process. A subsequent estimate for the Reynolds number indicates that the liquid motion induced by the expanding bubble is mainly of inviscid nature.

2. The dimensional analysis for the governing equation and boundary conditions shows that there exists four

relevant dimensionless parameters for bubble growth: Jacob number Ja, Fourier number Fo, the liquid-solid conductivity ratio κ, and the liquid-solid thermal diffusivity ratio α. The Jacob number is the most important one affecting C, C_1, and the dimensionless growth rate $\bar{R}(\tau)$. The numerical results in the systematic investigation assist in the basic understanding of bubble growth mechanisms in saturated heterogeneous boiling. It is also shown that the liquid temperature within the microlayer is practically linearly during the entire growth period.

3. A simplified bubble growth model is developed in saturated heterogeneous pool boiling. A first order ordinary differential equation is obtained for the bubble growth rate. Good agreement between the predicted and measured bubble radius is obtained over a wide range of boiling conditions. The present model is a simple and apparently reliable alternative to the previous finite difference computation, and provides modelers of boiling heat transfer with a very useful tool.

4. Detailed theoretical and numerical analyses have been considered for predicting vapor bubble growth in subcooled heterogeneous boiling. Two empirical constants, the microlayer wedge angle ϕ and the relative growth rate, μ_s, need to be input in order to start the computation. As long as the two empirical parameters are correctly specified, good agreement can be obtained between the

predicted and measured bubble radius. It is noted that there is only one combination for ϕ and μ_s that provides the best fit to the bubble growth rate data. An asymptotic solution for small time has been conducted for the subcooled bulk liquid. The numerical solutions compare well with the asymptotic solution. The computational study for the solid and the subcooled bulk liquid thermal fields elucidates the energy transfer process during the bubble growth and collapse. It is revealed that the subcooled bulk liquid flow has a significant effect on the vapor bubble growth and collapse process.

6.2 Suggestions for Future Work

The motivation for the present research is to gain a fundamental understanding of the vapor bubble growth process in saturated and subcooled nucleate pool boiling. Although significant progress has been made toward achieving goal, uncertainties remain. In order to build on the present research and continue further studies, the following future investigations are recommended:

1. Develop a reliable model for predicting vapor bubble incipience.

2. Extend the finite difference computation to include the simultaneous bubble growth of multiple bubbles in heterogeneous pool boiling.

3. Develop a reliable bubble departure model in

subcooled heterogeneous pool boiling.

4. Extend the bubble growth model to include flow boiling. In the case of flow boiling. the liquid inertia will distort the bubble shape. In addition the bubble slides along the heating surface prior to detachment.

REFERENCES

Abdelmessih, A.H., Hooper, F.C., and Nangia, S., 1972, "Flow effects on bubble growth and collapse in surface boiling," Int. J. Heat Mass Transfer, Vol. 15, pp. 115-125.

Akiyama, M., Tachibana, F., and Ogawa, N., 1969, "Effect of pressure on bubble growth in pool boiling," Bulletin of JSME, Vol. 12, No. 53, pp. 1121-1128.

Anderson, D.A., Tennehill, J.C., and Pletcher, R.H., 1984, Computational Fluid Mechanics and Heat Transfer, pp. 549, McGraw-Hill, New York.

Bankoff, S.G. and Mikesell, R.D., 1958, "Bubble growth rates in highly subcooled Nucleate boiling," A.I.Ch.E. Heat Transfer Conference, Chicago.

Chen, W.C., Klausner, J.F., and Mei, R., "A simplified model for predicting vapor bubble growth rates in heterogeneous boiling," to appear in Journal of Heat Transfer Trans. ASME, (1995).

Chen, W.C., Mei, R, and Klausner, J.F., "Vapor bubble growth rates in highly subcooled heterogeneous boiling," to be presented at Engineering Foundation Conferences, Banff, Alberta, Canada (1995).

Cochran, T.H. and Aydelott, J.C., 1966, "Effects of subcooling and gravity level on boiling in the discrete bubble region," NASA Tech. Note TN D-3449.

Cole, R., and Shulman, H.L., 1966, "Bubble growth rate of high Jacob numbers," Int. J. Heat Mass Transfer, Vol. 9, pp. 1377-1390.

Cooper, M.G., 1983, "The microlayer and bubble growth in nucleate pool boiling," Int. J. Heat Mass Transfer, Vol. 12, pp. 915-933.

Cooper, M.G. and Lloyd, A.J.P., 1969, "The microlayer in nucleate boiling," Int. J. Heat Mass Transfer, Vol. 12, pp. 895-913.

Cooper, M.G., Mori, K., and Stone, C.R., 1983, "Behavior

of vapor bubbles growing at a wall with forced flow," Int. J. Heat Mass Transfer, Vol 26, No. 10, pp. 1489-1507.

Cooper, M.G. and Vijuk, R.M., 1970, "Bubble growth in nucleate pool boiling," Proc. 4th Int. Heat Transfer Conf., Paris, Versailles, Vol. V, p. B2.1. Elsevier, Amsterdam.

Dergarabedian, P., 1953, "The rate of growth of vapour bubbles in superheated water," J. Appl. Mech., Vol. 20, pp. 537-545.

Dzakowic, G. S. and Frost, W., 1970, "Vapour bubble growth in saturated pool boiling by microlayer evaporation of liquid at the heated surface," Proceedings of the 4th Int. Heat Transfer Conf., Paris, paper, B 2.2.

Ellion, M.E., 1954, "A study of the Mechanism of boiling heat transfer," Ph.D. Diss. Calif. Inst. Tech, Pasadena.

Forster, H.K. and Zuber, N., 1954, "Growth of a vapour bubble in superheated liquid," J. Appl. Phys., Vol. 25, pp. 474-478.

Fyodorov, M.V. and Klimenko, V.V., 1989, "Vapour bubble growth in boiling under quasi-stationary heat transfer conditions in a heating wall," Int. J. Heat Mass Transfer, Vol. 32, pp. 227-242.

Griffith, P., 1958, "Bubble growth rates in boiling," ASME Trans., Vol. 80, pp. 721-727.

Gunther, F.C. and Kreith, F., 1950, "Photographic study of bubble formation in heat transfer to subcooled water," Prog. Rept. No. 4-120, Jet Prop. Lab., Calif. Inst. Tech..

Han, C.Y. and Griffith, P., 1965, "The mechanism of heat transfer in nucleate pool boiling, Part I: bubble initiation, growth and departure," Int. J. Heat Mass Transfer, Vol. 8, pp. 887-904.

Hospeti, N.B. and Mesler, R.B., 1969, "Vaporization at the base of bubbles of different shape during nucleate boiling of water," AIChe Journal, Vol. 15, No. 2, pp. 214-219.

Hsu, Y.Y., 1962, " On the size range of active nucleation cavities on a heating surface," J. Heat transfer, Vol. 84, No. 3, pp. 207-216.

Keshock, E.G., and Siegel, R., 1964, "Forces acting on bubbles in nucleate boiling under normal and reduced gravity conditions," NASA Tech. Note TN D-2299.

Klausner, J.F., Mei, R., Bernhard, D.M., and Zeng, L.Z., 1993, "Vapor bubble departure in forced convection boiling," Int. J. Heat Mass Transfer, Vol. 36, pp. 651-662.

Koffman, L.D. and Plesset, M.S., 1983, "Experimental observations of the microlayer in vapor bubble growth on a heated solid," Journal of Heat Transfer, Trans. ASME, Vol. 105, pp. 625-632.

Labuntsov D.A., 1963, "Mechanism of vapour bubble growth in boiling on the heating surface," J. Engng Phys., Vol. 6, pp. 33-39.

Lee, R.C., and Nydahl, J.E., 1989, "Numerical calculation of bubble growth in Nucleate boiling from inception through departure," Journal of Heat Transfer, Trans. of ASME, Vol. 111, pp. 474-479.

Marcus, B.D. and Dropkin, D., 1965, " Measured temperature profiles within the superheated boundary layer above a horizontal surface in saturated nucleate pool boiling of water," J. Heat Transfer, Vol. 87, No. 3, pp. 333-341.

Mei, R., Chen, W.C., and Klausner, J.F., 1995a, "Vapor bubble growth in heterogeneous boiling --Part I. Formulation," Int. J. Heat Mass Transfer, Vol. 38, No. 5, pp. 909-919.

Mei, R., Chen, W.C., and Klausner, J.F., 1995b, "Vapor bubble growth in heterogeneous boiling --Part II. Growth rate and thermal fields," Int. J. Heat Mass Transfer, Vol. 38, No. 5, pp. 921-934.

Mikic, B.B., Rohsenow, W.M., and Griffith, P., 1969, "On bubble growth rates," Int. J. Heat Mass Transfer, Vol. 13, pp. 657-666.

Moore, F.M., and Mesler, R.B., 1961, "The measurement of rapid surface temperature fluctuations during nucleate boiling of water," A.I.Ch.E. Journal, Vol. 7, No. 4, pp. 620-624.

Plesset, M.S. and Zwick, S.A., 1954, "The growth of vapour bubbles in superheated liquids," J. Appl. Phys., Vol. 25, pp. 493-500.

Scriven, L.E., 1959, "On the dynamics of phase growth," Chem. Engng. Sci., Vol. 10, pp. 1-13.

Skinner, L.A. and Bankoff S.G., 1964, "Dynamics of vapor bubbles in spherically symmetric temperature fields of general variation," Physics Fluids, Vol 7, pp. 1-6.

Srinivas, N.S. and Kumar, R., 1984, "Prediction of bubble growth rates and departure volumes in nucleate boiling at isolated sites," Int. J. Heat Mass Transfer, Vol. 27, pp. 1403-1409.

Staniszewski, B.E., 1959, "Bubble growth and departure in nucleate boiling," Tech. Rept. No. 16, MIT, Cambridge, Mass.

Van Stralen, S.J., 1966, "The mechanism of nucleate boiling in pure liquids and in binary mixtures, Parts I-II," Int. J. Heat Mass Transfer, Vol. 9, pp. 995-1020, 1021-1046.

Van Stralen, S.J., 1967, "The mechanism of nucleate boiling in pure liquids and in binary mixtures, Parts III-IV," Int. J. Heat Mass Transfer, Vol. 10, pp. 1469-1484, 1485-1498.

Van Stralen, S.J.D., Sohal, M.S., Cole, R., and Sluyter, W.M., 1975, "Bubble growth rates in pure and binary systems: combined effect of relaxation and evaporation microlayers," Int. J. Heat Mass Transfer, Vol. 18, pp. 453-467.

Van Stralen, S.J.D., Cole, R., Sluyter, W.M. and Sohal, M.S., 1975, "Bubble growth rates in nucleate boiling of water at subatmospheric pressures," Int. J. Heat Mass Transfer, Vol. 18, pp. 655-669.

Westwater, J.W., 1963, "Things we don't know about boiling heat transfer," In Research in Heat Transfer, pp. 61-73, Pergamon Press, New York.

Wiebe, J.R. and Judd, R.L., 1971, " Superheat layer thickness measurements in saturated and subcooled nucleate boiling," J. Heat Transfer, Vol. 93 , pp. 455-461.

Zeng, L.Z., 1993, "The ebullition process in forced convection boiling," Ph.D. Diss., Mechanical Engineering, University of Florida, Gainesville.

Zeng, L.Z., Klausner, J.F., and Mei, R., 1993, "A unified model for the prediction of bubble detachment diameters in boiling systems, Part I: Pool boiling," Int. J. Heat Mass Transfer, Vol. 36, No. 9, pp. 2261-2270.

Zeng, L.Z., Klausner, J.F., Bernhard, D.M., and Mei, R., 1993, "A unified model for the prediction of bubble detachment diameters in boiling systems, Part II: Flow boiling," Int. J. Heat Mass Transfer., Vol. 36, No. 9, pp. 2271-2279.

Zuber, N., 1961, "The dynamics of vapor bubbles in nonuniform temperature fields," Int. J. Heat Mass Transfer, Vol. 2, pp. 83-98.

BIOGRAPHICAL SKETCH

Wen-Chin Chen was born on March 7, 1962, in Taiwan, Republic of China. He was enrolled in National Chung-Hsing University, in 1985. He majored in agricultural machinery engineering, and received his Bachelor of Science degree in 1987. He married Yi-Yu Chen in 1988. He came to the U.S.A. in 1989, and received his Master of Science degree from Florida Institute of Technology in 1991. He joined the Ph.D. Program in mechanical engineering at the University of Florida in August 1991. Since 1992 he has been working as a research and teaching assistant in the Department of Mechanical Engineering.

I certify that I have read this study and that in my opinion it conforms to acceptable standards of scholarly presentation and is fully adequate, in scope and quality, as a dissertation for the degree of Doctor of Philosophy.

James F. Klausner, Chair
Associate Professor of
Mechanical Engineering

I certify that I have read this study and that in my opinion it conforms to acceptable standards of scholarly presentation and is fully adequate, in scope and quality, as a dissertation for the degree of Doctor of Philosophy.

Renwei Mei, Cochair
Assistant Professor of
Aerospace Engineering,
Mechanics and Engineering
Science

I certify that I have read this study and that in my opinion it conforms to acceptable standards of scholarly presentation and is fully adequate, in scope and quality, as a dissertation for the degree of Doctor of Philosophy.

C.K. Hsieh
Professor of
Mechanical Engineering

I certify that I have read this study and that in my opinion it conforms to acceptable standards of scholarly presentation and is fully adequate, in scope and quality, as a dissertation for the degree of Doctor of Philosophy.

U.H. Kurzweg
Professor of Aerospace
Engineering, Mechanics and
Engineering Science

I certify that I have read this study and that in my opinion it conforms to acceptable standards of scholarly presentation and is fully adequate, in scope and quality, as a dissertation for the degree of Doctor of Philosophy.

S.A. Sherif
Associate Professor of
Mechanical Engineering

This dissertation was submitted to the Graduate Faculty of the College of Engineering and to the Graduate School and was accepted as partial fulfillment of the requirements for the degree of Doctor of Philosophy.

May, 1995

Winfred M. Phillips
Dean, College of Engineering

Karen A. Holbrook
Dean, Graduate School